

Ninth Japan-China Joint Seminar on Radiopharmaceutical Chemistry (JCSRC 2015)

**November 8 (Sun) – 9 (Mon), 2015
National Institute of Radiological Sciences
Chiba, JAPAN**

CHAIRPERSON:
Yasuhisa Fujibayashi (NIRS)

国立研究開発法人
放射線医学総合研究所

INTERNATIONAL ADVISORY COMMITTEE

Hideo Saji (Kyoto University)
Yasushi Arano (Chiba University)
Boli Liu (Beijing Normal University)
Zhifu Luo (China Institute of Atomic Energy)
Ming-Rong Zhang (NIRS)

LOCAL PROGRAM COMMITTEE

Ming-Rong Zhang (NIRS)
Tomoya Uehara (Chiba University)
Kazunori Kawamura (NIRS)
Kotaro Nagatsu (NIRS)
Lin Xie (NIRS)
Atsuo Waki (NIRS)

**For further information, please visit our web page:
http://www.nirs.go.jp/information/event/2015/11_08.shtml
Or contact to the secretariat: jcsrc2015@nirs.go.jp**

Welcome to

Ninth Japan-China Joint Seminar on Radiopharmaceutical Chemistry

JCSRC2015

November 8-9, Chiba, JAPAN

It is my pleasure to host the 9th Japan-China Joint Seminar on Radiopharmaceutical Chemistry (JCSRC) at National Institute of Radiological Sciences (NIRS), Chiba, JAPAN, from November 8th to 9th, 2015. Five years have already passed since the 8th JCSRC was held in Beijing in 2010. Traditionally, JCSRCs have been held every three years, but original plan for 2013 meeting has been suspended, because of some unexpected but big incidents. I offer my sincere apologies for this inconvenience.

With hindsight, however, two years extension brought us a big input from Korea. Professor Jae-Min Jeong, President of Korean Society of Radiopharmaceutical and Molecular Probes, expresses their willingness to be a member of our international seminar. After official acceptance at JCSRC2015, new structure as Japan-China-Korea Joint Seminar on Radiopharmaceutical Chemistry (JCKSRC) will be started.

JCSRC2015 is held in Chiba, an east wing of "Greater Tokyo Area". I hope you enjoy not only scientific discussion and communication at the meeting internationally, but traditional/new Japanese cultures in "a big melting pot with 37M population".

JCSRC2015 Chair



Yasuhisa Fujibayashi, Ph.D., D.Med.Sci.

Director, Molecular Imaging Center

National Institute of Radiological Sciences

4-9-1 Anagawa, Inage, Chiba 263-8555, Japan

Contents

Keynote Lecture

A General and Practical Method for Arene Radiofluorination with [^{18}F]fluoride and its Application to Clinical Use

Steven Liang, Ph.D

Oral Presentations

O-01 Radiosynthesis and evaluation of ^{18}F labeled mubritinib as a potential PET agent for HER2 positive breast cancer imaging

Tang, L., Li, Z., Zhang, X.

O-02 Preparation and preliminary biological evaluation of c-Gluc-Lys([Al^{18}F]NOTA)-TOCA

Guo, F.-H, Du, J., Wen, K., Shi, C.-Y.

O-03 Development of 5-amino-4-oxo-[$6\text{-}^{11}\text{C}$]hexanoic acid for estimation of tumor protoporphyrin IX accumulation induced by exogenous aminolevulinic acid

Suzuki, C., Tsuji, A.B, Kato, K., Kikuchi, T., Sudo, H., Okada, M., Sugyo, A., Magata, Y., Zhang, M.-R., Arano, Y., Saga, T.

O-04 Pd(0)-mediated [^{11}C]carbonylation of boronic acid esters with [^{11}C]carbon monoxide

Ishii, H., Minegishi, K., Nagatsu, K., Zhang, M.-R

O-05 Synthesis and evaluation of ^{18}F -labeled trimethoxyphenyl phosphonium cations as myocardial perfusion imaging agents

Chen, S., Zhao, Z., Lu, J.

O-06 Synthesis and evaluation of N-benzyl piperazine derivatives as selective SIGMA-1 receptor ligands

Ye, J., Chen, Y., Deuther-Conrad, W., Steinbach, J., Brust, P., Liu, B., Jia, H.

O-07 Novel production method of 4-borono-2- ^{18}F -fluorophenylalanine (^{18}F -FBPA) via ^{18}F -nucleophilic substitution

Tateishi, H., Takahashi, K., Arano, Y., Saga, T., Watanabe, Y.

O-08 Nimesulide analogs as brain cyclooxygenase-2 (COX-2)-targeted imaging agents: synthesis and in vitro evaluation

Yamamoto, Y., Hisa, T., Arai, J., Saito, Y., Mukai, T., Ohshima, T., Maeda, M., Yamamoto,

F.

O-09 Synthesis and evaluation of novel $^{99m}\text{Tc}(\text{CO})_3$ labelled glucose derivatives as potential tumor imaging agents

Liu, T. L., Gan, Q. Q., Zhang, J. B.

O-10 ^{99m}Tc -labeled 2-arylbenzothiazole derivatives as SPECT imaging probes targeting A β plaques

Zhang, X., Yu, P., Yang, Y., Peng, C., Liang, Z., Chen, B., Cui, M., Liu, B.

O-11 Development of radioiodinated pyrido[1,2-a]benzimidazole derivatives as novel tau imaging probes for SPECT

Watanabe, H., Ono, M., Kitada, A., Saji, H.

O-12 Development of fluorine-18 labeled 2-Arylquinoline derivatives for tau PET imaging in Alzheimer's disease

Tago, T., Furumoto, S., Okamura, N., Harada, R., Adachi, H., Ishikawa, Y., Yanai, K., Iwata, R., Kudo, Y.

O-13 ^{68}Ga -PSMA-11 micro PET-CT for evaluation of PSMA expression in animal model bearing with prostate cancer

Shao, G.-Q, Cui, C., Zang, S.-M, Luo, R., Yao, X.-C, Wang, F.

O-14 In vivo click reaction between TC- ^{99m}Tc -labeled azadibenzocyclooctyne-mama and 2-nitroimidazole-azide for tumor hypoxia targeting

Sun, W.-J, Chu, T.-W

O-15 Factors affecting radiochemical yields of isonitrile-based ^{99m}Tc -labeled trivalent probes for molecular imaging

Mizuno, Y., Jen, C.-W, Uehara, T., Arano, Y.

O-16 Radiolabeled immunoglobulin G visualizes active inflammation in atherosclerosis

Fukura, S., Shimizu, Y., Hanzawa, H., Nishijima, K., Sakamoto, T., Zhao, S., Ogawa, M., Kuge, Y.

O-17 Preparation and preliminary evaluation of a hybrid brachytherapy seed containing palladium-103 and iodine-125

Li, Z.-Y, Gao, H.-B, Zhang, W.-H, Cui, H.

O-18 Synthesis, characterization and in vivo evaluation of ^{64}Cu -DOTA-SPIONs-PEG-FA as a dual-modality PET/MRI agent

Sun, Y., Shen. Y, Liang. J, Chen. Y, Shen. L

O-19 Preclinical evaluation of a thymidine phosphorylase imaging probe, [¹²³I]IIMU: road to first-in-human clinical study

Nishijima, K., Zhao, J., Matsumoto, H., Akizawa, H., Ohkura, K., Shiga, T., Hirata, K., Watanabe, S., Okamoto, S., Tamaki, N., Kuge, Y.

O-20 Production of non-conventional radionuclides with emphasis on targetry system development

Nagatsu, K., Minegishi, K., Suzuki, H., Ohya, T., Fukada M., Hanyu. M, Kawamura. K, Zhang, M.-R.

Poster Presentations

P-01 A high yield automated synthesis of [¹⁸F]FMISO on PET-MF-2V-IT-I synthera with SPE purification

Zou, P., Wang, H.-Y, Xie, M.-H, Liu, Y.-L, Wu, J., Wu, H.

P-02 Preliminary evaluation of a novel ¹⁸F-labeled affibody for HER2 imaging

Yang, M., Xu, Y.-P, Bai, Z.-C, Zhang, P.-J, Pan, D.-H, Wang, L.-Z

P-03 A novel ¹⁸F-labeled phosphonium dication as a potential PET agent for tumor imaging

Li, H., Li, Z., Zhang, X.

P-04 Synthesis and evaluation of a novel progesterone receptor PET probe for breast cancer imaging

Wu, X. Li. Z, Zhang, X.

P-05 Click for PET: rapid and efficient 1,3-dipolar cycloadditions with 2-[¹⁸F]fluoroethylazide

Jia, L., Zhang, L.

P-06 Transport mechanism and androgen-stimulated uptake of the amino acid PET tracer [¹⁸F]fluciclovine (anti-[¹⁸F]FACBC) in primary and castration-resistant prostate cancer cells

Ono, M., Okudaira, H., Oka, S., Nakanishi, T., Mizokami, A., Kobayashi, M., Yoshimura, H., Kawai, K.

P-07 Development of a low cost multipurpose synthesis system for F-18 PET tracers

Mori, T., Kunieda, M., Fujibayashi, Y., Okazawa H., Kiyono, Y.

P-08 In vitro and in vivo characterization of [¹⁸F]interleukin-8 produced by a cell-free translation system and [¹⁸F]fluoro-L-proline

Harada, R., Furumoto, S., Testuro, T., Iwata, R., Yoshikawa, T., Okamura, N., Yanai, K.

- P-09 Carbon-11 formaldehyde: development of radiolabeling technique for carbon-11 labeled peptides**
Hanyu, M., Sugyou, A., Tsuji, A. B., Kawamura, K., Saga, T., Zhang, M.-R., Fukumura, T.
- P-10 Quantitative PET for monitoring blood–brain barrier opening induced by focused ultrasound by 2-amino-[3-¹¹C]isobutyric acid**
Okada, M., Kikuchi, T., Okamura, T., Tsuji, A. B., Wakizaka, H., Zhang, M.-R., Kato, K.
- P-11 Synthesis and PET studies of 2-amino-2-[¹¹C]methyl-butanoic acid for tumor imaging**
Kato, K., Suzuki, C., Tsuji, A. B., Sudo, H., Zhang, M.-R., Arano, Y., Saga, T.
- P-12 Radiosynthesis of [¹¹C]ADX88178 via direct [¹¹C]methylation as a novel radioligand for imaging of metabotropic glutamate receptor subtype 4**
Fujinaga, M., Yamasaki, T., Nengaki, N., Ogawa, M., Kumata, K., Shimoda, Y., Yui, J., Xie, L., Zhang, Y., Kawamura, K., Zhang, M.-R.
- P-13 Developments of new PET ligands based on 3-[5-(pyridine-2-yl)-2h-tetrazol-2-yl]-benzonitrile for metabotropic glutamate receptor 5 (mGluR5) imaging**
Shimoda, Y., Yamasaki, T., Fujinaga, M., Ogawa, M., Kurihara, Y., Nengaki, N., Kumata, K., Yui, J., Hatori, A., Xie, L., Zhang, Y., Kawamura, K., Zhang, M.-R.
- P-14 Small-animal PET study: [¹¹C]ITMM with ultra-high specific activity improved availability for metabotropic glutamate receptor subtype 1 (mGluR1)**
Yamasaki, T., Fujinaga, M., Yui, J., Wakizaka, H., Ohya, T., Nengaki, N., Zhang, M.-R.
- P-15 Development of a PET tracer for imaging of redox status in the brain**
Okamura, T., Okada, M., Kikuchi, T., Wakizaka, H., Zhang, M.-R.
- P-16 Proposal of (R)-[¹¹C]Emopamil as a novel tracer for imaging enhanced P-glycoprotein function**
Toyohara, J., Aramaki, H., Zaito, Y., Okamoto, M., Hosokawa, S., Shimizu, I., Ishiwata, K.
- P-17 Development of 1-N-[¹¹C]methyl-L- and -D-tryptophan for pharmacokinetic imaging of the immune checkpoint inhibitor 1-methyl-tryptophan**
Xie, L., Maeda, J., Kumata, K., Yui, J., Zhang, Y., Hatori, A., Nengaki, N., Wakizaka, H., Fujinaga, M., Zhang, M.-R.
- P-18 In vivo, in vitro, and in silico evaluation of radiometabolite of [¹¹C]PBB₃ as a**

clinically useful PET probe for imaging of tau pathology.

Hashimoto, H., Kawamura, K., Takei, M., Igarashi, N., Fujishiro, T., Shiomi, S., Watanabe, R., Muto, M., Furutsuka, K., Ito, T., Yamasaki, T., Yui, J., Nemoto, K., Kimura, Y., Higuchi, M., Zhang, M.-R.

P-19 **The primary research and development of iodine-125 brachytherapy seeds strand**
Zhang, W.-H.

P-20 **Preparation and preliminary biodistribution of no-carrier-added [¹²⁵I]MIBG**
Fan, C.-Y., Deng, X.-R., Liu, Z.-H., Li, F.-L., Chen, B.-J., Luo Z.-F.

P-21 **Preparation of [¹³¹I]-1H12 and its biological effects on A549 non-small cell lung cancer**
Du, M.

P-22 **Folic acid-conjugated BSA nanocapsule (n-BSA-FA) for cancer targeted radiotherapy and imaging**
Ma, Y., Liang, S., Guo, J., Wang, H.

P-23 **The establishment of sterile examination methods for technetium [^{99m}Tc] albumin aggregate (^{99m}Tc-MAA) injection**
Yu, J.-J., Du, J.-D., Zhang, X., Cui, H.

P-24 **Evaluation of the diagnostic value of ^{99m}Tc-MIBI SPECT positive tumor imaging and MRI in the recurrence or postoperative residual lesions of glioma**
Zhang, W., Liu, Y.

P-25 **In vitro and in vivo evaluation of technetium-99m-labeled propylene amine oxime complexes containing nitroimidazole and nitrotriazole groups as hypoxia markers**
Zhang, Q., Huang, H.-F., Chu, T.-W.

P-26 **Evidence-based radionuclide and radiopharmaceutical approaches of flow perfusion in hollow-fiber dialyzers.**
Weerakoon, B. S., Osuga, T.

P-27 **Imaging of osteolytic metastasis from breast cancer with new integrin $\alpha_v\beta_3$ receptor targeted radiotracer:[⁶⁸Ga]-DOTA-RGD₂**
Shao, G.-Q., Cui, C., Yao, X.-C., Luo, R., Zhou, Y., Liu, S., Wang, F.

P-28 **Development of radiogallium complex-conjugated multifunctional peptides for imaging of cancer**

Ogawa, K., Ishizaki, A., Yokokawa, M., Odani, A.

P-29 Evaluation of in vivo dynamics of the polymeric micelle by using two different radioisotope modification approaches

Makino, A., Tomoike, A., Ono, M., Kiyono, Y., Okazawa, H., Saji, H.

P-30 Versatile synthesis of C-functionalized polyaminocarboxylate bifunctional chelating agent with aromatic carboxylate

Suzuki, H., Kanai, A., Arano, Y.

P-31 Optically pure diphenoxy derivatives as more flexible probes for β -Amyloid plaques

Jia, J., Cui, M., Liu, B.

P-32 Synthesis and evaluation of novel near-infrared probes with side PEG chains for in vivo detection of A β plaques

Zhou, K., Fu, H., Cui, M., Liu, B.

P-33 Licochalcone A protect the heart from ischemia/reperfusion injury

Guo, W.-H., Jia, P., Feng, X.-F., Xu, S.-L., Jia, Z., Shen, J.-T., Xu, P.

Keynote Lecture

A GENERAL AND PRACTICAL METHOD FOR ARENE RADIOFLUORINATION WITH [¹⁸F]FLUORIDE AND ITS APPLICATION TO CLINICAL USE

Steven Liang, Ph.D.

Division of Nuclear Medicine and Molecular Imaging, Department of Radiology, Massachusetts General Hospital and Harvard Medical School, 55 Fruit St., Boston, MA 02114 USA

Introduction: Fluorine-18 (¹⁸F; *t*_{1/2} = 109.7 min) labelled compounds and radiopharmaceuticals are the mainstay of functional molecular imaging by positron emission tomography (PET) for a broad range of applications including clinical diagnosis and drug discovery. Consequently, there is a rapidly growing demand for new ¹⁸F-labeled agents to probe biological processes and targets in vivo by PET. Fluorine-18 is most readily prepared in high specific activity as no-carrier-added [¹⁸F]fluoride ion, by proton irradiation of [¹⁸O]H₂O (¹⁸O(p,n)¹⁸F nuclear reaction) in low energy (10-16 MeV) medical cyclotrons. Most ¹⁸F-labeling methodologies for aromatic nucleophilic substitution (S_NAr) reactions employ “naked” [¹⁸F]fluoride ion with appropriately activated (electron-deficient) aromatic / heteroaromatic substrates or electrophilic aromatic substitution reactions with [¹⁸F]F₂ and related reagents derived from elemental fluorine. However, radiofluorination of non-activated arenes from “naked” [¹⁸F]fluoride ion represents a major challenge in the field and there is an urgent need for a general and practical methodology that can introduce ¹⁸F into molecules which cannot be (easily) achieved using a conventional aromatic nucleophilic substitution (S_NAr) reaction or a low-specific-activity [¹⁸F]F₂ gas method.

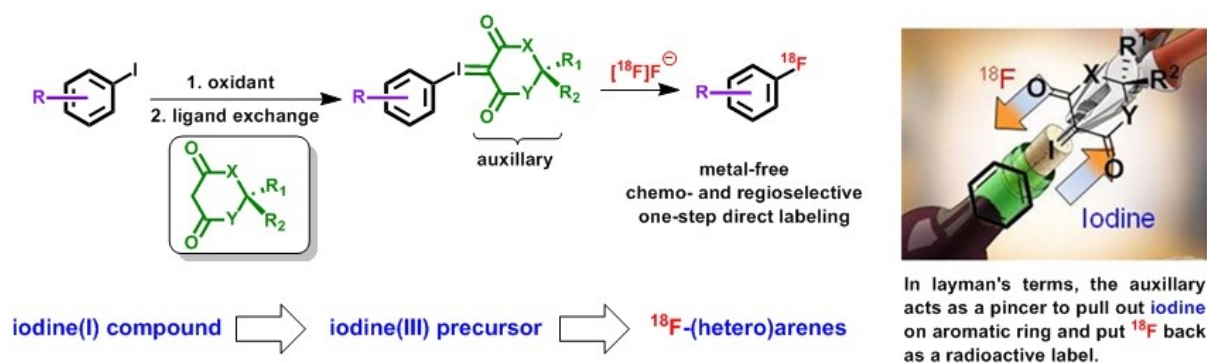


Figure 1. Technology overview

In 2014, we discovered a new method that is capable of regioselectively introducing ¹⁸F-fluoride ion into non-activated aromatic rings with very wide substrate scope under absolute metal-free conditions. We reported a novel spirocyclopentyl hypervalent iodine(III)-mediated radiofluorination strategy, based on iodonium ylides to afford ¹⁸F-aryl fluorides from “naked” [¹⁸F]fluoride in high radiochemical yields. The technique involves stable, easily purified precursors and is readily

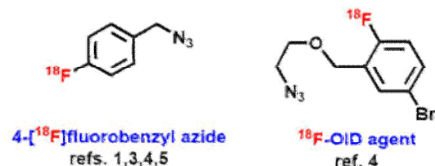
implemented with standard workup procedures and no metal was utilized during the preparation and radiosynthesis. The conceptual advantages of excellent regioselectivity and viability of incorporation of ^{18}F into a wide array of non-activated (hetero)arenes makes this methodology suitable for routine radiopharmaceutical production.

In the *Japan-China Joint Seminar on Radiopharmaceutical Chemistry 2015*, we aim to show the intricacies of developing PET radiopharmaceuticals from "bench to bedside", and cutting-edge translational chemical technologies for preclinical and clinical PET neuroimaging. The discovery from bioactive molecules to PET radiopharmaceuticals and our aspiration to work towards the ultimate, albeit impossible, goal in the field: to radiolabel virtually any target molecule for PET will be raised as points for discussion.

Radiolabeling of PET radiotracers and drug molecules/scaffolds



Application to bioconjugation reactions via 'clickable' agents



Translation to clinical production of radiopharmaceuticals

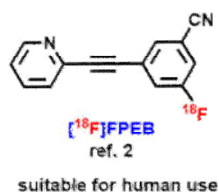


Figure 2. Application and Translation

References: 1) Rotstein B.H., et al. *Nat. Commun.* 2014, 5, 4365; 2) Stephenson N. A., et al. *J. Nucl. Med.* **2015**, 56, 489-492; 3) Calderwood, S., et al. *J. Fluorine Chem.* **2015**, 178, 249-253; 4) Wang, L. et al. *Angew. Chem. Int. Ed.* **2015**, DOI: 10.1002/anie.201505927 (in press); 5) Jacobson, O., et al. *J. Nucl. Med.* **2015**, DOI: 10.2967/jnumed.115.160960 (in press).

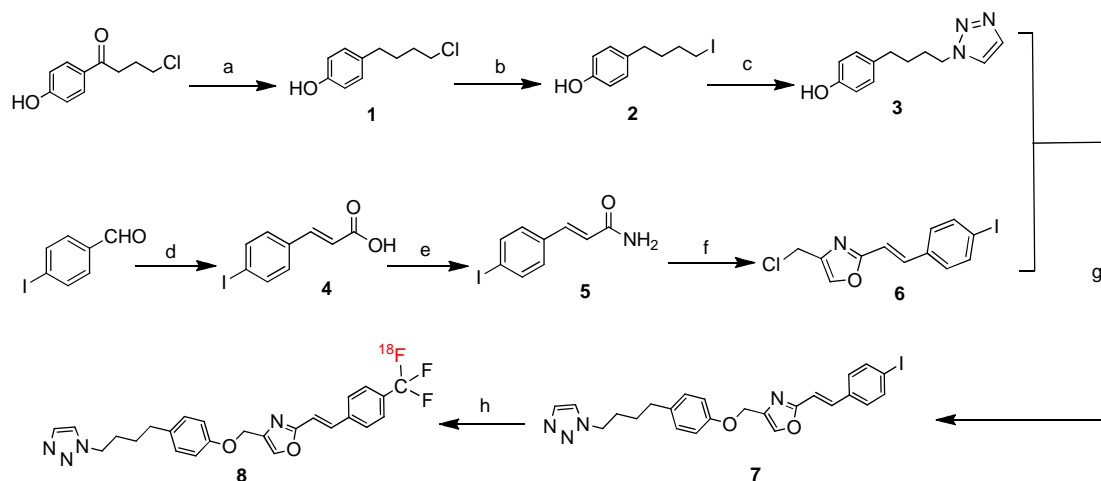
RADIOSYNTHESIS AND EVALUATION OF ^{18}F LABELED MUBRITINIB AS A POTENTIAL PET AGENT FOR HER2 POSITIVE BREAST CANCER IMAGING

Longguang Tang, Zijing Li*, Xianzhong Zhang*

Center for Molecular Imaging and Translational Medicine, School of Public Health, Xiamen University, Xiang'an South Rd, Xiamen, 361102, PR China

Objectives: Diverse phenotypes of breast cancer relate to molecular alterations driving cancer behavior. One of the most clinically relevant molecular aberrations in breast cancer is overexpression of the human epidermal growth factor receptor type 2 (HER2). HER2 overexpression occurs in 15 - 25 % of all invasive breast cancers with an intrinsic worse prognosis but good response to HER2 targeted therapies. Although there are already numerous literature data concerning peptide and protein drug targeting HER2 labeled with diagnostic and therapeutic radionuclides, no selective small molecular inhibitors of HER2 has been labeled as a PET agent for imaging of HER2 expression. Mubritinib (TAK-165), a potent and selective HER2 tyrosine kinase small molecular inhibitor ($\text{IC}_{50} = 6 \text{ nM}$) synthesized by Takeda Chemical Industries, is currently in phase I clinical trials in patients with advanced tumours that express HER2^[1]. In this ongoing study, we report the design, synthesis and labeling of ^{18}F CF₃-mubritinib without changing the chemical structure with aryl iodides to form Ar-CF₂- ^{18}F ^[2] as a new potential PET imaging agent for HER2 positive breast cancer for the first time.

Methods: The synthetic route of ^{18}F CF₃-mubritinib is shown in Scheme 1. The synthesized compounds were characterized by ^1H -NMR, ^{13}C -NMR, HRMS.



Scheme 1. Reagents and conditions: (a) Pd/C, H₂, r.t., overnight, 95 %; (b) NaI, CH₃CN, reflux, 20 h, 100 %; (c) 1H-1,2,3-triazole, K₂CO₃, DMF, 70 °C, 5 h, 85 %; (d) Piperidine, C₅H₅N, 6 h, reflux, 87 %; (e) NH₄Cl/SiO₂, TsCl, Et₃N, solvent-free, r.t., 80 %; (f) 1,3-Dibromoacetone, toluene, reflux, 75 %;

(g) K_2CO_3 , DMF, 60 °C, 24 h, 70 %; (h) $\text{ClCF}_2\text{CO}_2\text{Me}$, CuI, TMEDA, ^{18}F]KF/kryptofix, DMF, 150 °C, 20 min.

Results and Discussion: The precursor **7** were synthesized according to the reported procedures with modification. Yields of 85 % and 75 % for **3** and **6** were achieved, respectively. The precursor **7** was achieved by nucleophilic reaction between **3** and **6**, in 70 % yield. The chemical purity of the precursor **7** was > 95 %. The radiosynthesis of ^{18}F]CF₃-mubritinib is undergoing, which will be achieved by a newly reported strategy for the direct ^{18}F]trifluoromethylation of aryl iodide using methyl chlorodifluoroacetate and ^{18}F]fluoride through a copper-mediated cross-coupling reaction. In conclusion, a multi-step synthetic route with moderate to excellent yields to the precursor **7**, reference standard mubritinib and target tracer ^{18}F]CF₃-mubritinib has been developed. These results facilitate the potential preclinical and clinical PET studies of ^{18}F]CF₃-mubritinib as a new PET agent for imaging of HER2 signaling in animals and humans.

References: [1] Joji Nagasawa et al., *International Journal of Urology*, 2006, 13, 587–592; [2] Mickael Huiban et al., *Nat. Chem.*, 2013 Nov;5(11):941-4.

Preparation and preliminary biological evaluation of c-Gluc-Lys([Al¹⁸F]NOTA)-TOCA

F.-H. Guo^{1,2}, J Du^{1,3*}, K Wen², C.-Y. Shi²

1. Department of Isotope, China Institute of Atomic Energy, Beijing 102413, China;

2. Beijing Atom HighTech Co., Ltd., P. O. Box 275- 99, Beijing 102413, China;

3. China Isotope & Radiation Corporation, Beijing 100045, China

Objectives: Somatostatin analogues can specifically bind with Somatostatin receptor (SSTR) which is usually over-expressed on many tumor cells. So it may have important significance to use ¹⁸F labeled somatostatin analogues as the tumor probes for the diagnosis, the clinical staging and evaluation of therapeutic effect of SSTR positive tumor. The aims of this study were to design and synthesis Al¹⁸F radiolabeled glycosylated somatostatin analogues c-Gluc-Lys([Al¹⁸F]NOTA)-TOCA, to test it as a potential PET imaging agent for somatostatin receptor positive tumors, and to provide an experimental basis for further investigation of other peptides labeled with Al¹⁸F by same method.

Results and discussion:

1. The chemical purities of the synthetic somatostatin analogue c-Gluc-Lys(NOTA)-TOCA was more than 95%, and the synthetic yields was 11%. Under the optimum conditions, the labeling efficiency was approximately 73% within 25 min preparation time. The radiochemical purity was more than 95% after purification with HLB column.
2. The hydrophilicity of the labeled peptide c-Gluc-Lys([Al¹⁸F]NOTA)-TOCA was excellent with log*P* value of $-4.23 \pm 0.19 (n=3)$. The radiochemical purity of labeled peptide was not decreased significantly after incubation in the saline and the fetal bovine serum at 37 °C for 120 min. The labeled peptide was stable in vitro.
3. The biodistribution of the labeled peptide in normal mice showed that the labeled peptide can be fast cleared from blood with double exponential model after administered intravenously, and

mainly excreted through kidney. Radiolabeled metabolites were not emerged obviously in the urine within 120 min post injection. The liver uptake was low. The uptake in pancreas which contain SSTR was high with 2.59 ± 0.84 %ID/g at 120 min post injection.

4. The high tumor uptakes of c-Gluc-Lys([Al¹⁸F]NOTA)-TOCA in AR42J tumor bearing nude mice at 60 min post injection were found with 6.06 ± 1.42 %ID/g. T/NT values of tumor to heart, liver, muscle, blood were 48.06, 17.32, 54.29, and 42.02, respectively. After blocking with 600 times of c-Gluc-Lys(NOTA)-TOCA, the AR42J tumor uptake was reduced to 2.00 ± 0.65 %ID/g. This indicated that the uptake of c-Gluc-Lys([Al¹⁸F]NOTA)-TOCA in the tumor was receptor-mediated. The micro-PET scans of c-Gluc-Lys([Al¹⁸F]NOTA)-TOCA showed clear tumor delineation at 60 min post injection.

Conclusions: The Al¹⁸F labeled glycosylated somatostatin analogue c-Gluc-Lys([Al¹⁸F]NOTA)-TOCA shows promising p

Development of 5-amino-4-oxo-[6-¹¹C]hexanoic acid for estimation of tumor protoporphyrin IX accumulation induced by exogenous aminolevulinic acid

Suzuki, C.¹, Tsuji, A. B², Kato, K.^{2,3}, Kikuchi, T.², Sudo, H.², Okada, M.², Sugyo A.²,

Magata, Y.¹, Zhang, MR.², Arano, Y.⁴, Saga, T.²

¹ Medical Photonics Research Center, Hamamatsu University School of Medicine, Hamamatsu 431-3192, Japan; ² Molecular Imaging Center, National Institute of Radiological Sciences, Chiba 263-8555, Japan; ³ Department of Integrative Brain Imaging, National Center of Neurology and Psychiatry, Tokyo 187-5551, Japan; ⁴ Graduate School of Pharmaceutical Sciences, Chiba University, Chiba 260-8675, Japan.

Introduction: Fluorescence-guided resection (FGR), photodynamic therapy (PDT), and sonodynamic therapy (SDT) using tumor-specific accumulation of protoporphyrin IX (PpIX) induced by 5-aminolevulinic acid (ALA) administration are promising tumor therapeutic strategies. Pretreatment noninvasive imaging to estimate the quantity and spatial distribution of PpIX accumulation in tumors induced by ALA administration is expected to improve the efficacy of ALA-based FGR and PDT/SDT. PpIX synthesis from exogenous ALA has been reported to be regulated by ALA influx and/or ALA dehydratase (ALAD) activity, which catalyzes the first step of the synthesis of PpIX. In the present study, we designed, radiosynthesized, and evaluated a ¹¹C-labeled ALA analog, 5-amino-4-oxo-[6-¹¹C]hexanoic acid ([¹¹C]MALA), as a PET probe for estimating PpIX accumulation in tumor.

Methods: [¹¹C]MALA was radiosynthesized via ¹¹C-methylation of a Schiff-base-activated aminolevulinic acid derivative using [¹¹C]CH₃I, followed by the hydrolysis of ester and imine groups. *In vitro* cellular uptake of [¹¹C]MALA were determined in five tumor cell lines in the presence and absence of ALA and inhibitors of transporters, which are reported to transport ALA into cells. ALAD expression of each cell line was determined by western blot analysis. *In vivo* tumor accumulation of [¹¹C]MALA and [³H]ALA was determined in tumor-bearing mice. Dynamic PET studies were performed after intravenous injection of [¹¹C]MALA for 90 min. *In vitro* and *in vivo* ALA-induced PpIX accumulation was determined by measuring fluorescence in extracts of cells or tumors.

Results and Discussion:

1. Radiosynthesis of [¹¹C]MALA: [¹¹C]MALA was obtained using a remote-controlled synthesis module in a radiochemical yield (decay uncorrected, relative to [¹¹C]CO₂) of 4.4 ± 1.7 % and radiochemical purity of 97.5 ± 1.9 %.

2. In vitro cell uptake studies: [¹¹C]MALA uptake was dose-dependently inhibited by the addition of ALA and inhibitors of transporters, suggesting that [¹¹C]MALA is transported into tumor cells through transport systems similar to ALA. [¹¹C]MALA uptake was strongly correlated with ALAD expression and ALA-induced PpIX accumulation.

3. In vivo distribution and PET imaging: [¹¹C]MALA was rapidly transported into tumors and the tumor-to-muscle ratio of [¹¹C]MALA was higher in the tumor with higher tumor-to-muscle ratio of [³H]ALA at 1 min after injection of [¹¹C]MALA and [³H]ALA. Dynamic PET studies with [¹¹C]MALA showed that [¹¹C]MALA in tumors continuously decreased following initial uptake. The elimination rate of [¹¹C]MALA from AsPC-1 tumors with the highest ALAD expression level was slower compared with those from other tumors with lower expression levels. Since MALA is reported to bind to the catalytic center of ALAD, [¹¹C]MALA could be retained in the tumor cells with high ALAD expression levels through the formation of [¹¹C]MALA-ALAD complex. In the blocking studies, initial tumor uptake of [¹¹C]MALA was decreased and the elimination rate of [¹¹C]MALA from tumors was accelerated by the co-injection of excess unlabeled ALA, indicating that not only the influx of [¹¹C]MALA into cells but also the intracellular retention mechanism of [¹¹C]MALA is competitively inhibited by excess ALA. At 4 h post-injection of unlabeled ALA, AsPC-1 tumor showed the highest PpIX accumulation between the four tumors. Tumor accumulation of [¹¹C]MALA at the latter phase, which would reflect both the initial uptake and intracellular retention of [¹¹C]MALA, was strongly correlated with the PpIX accumulation. These findings suggesting that [¹¹C]MALA-PET could estimate the ALA-induced PpIX accumulation defined by the influx and metabolism of ALA.

Conclusions: [¹¹C]MALA-PET has the potential to noninvasively estimate tumor accumulation of exogenous ALA-induced PpIX.

Reference: Suzuki, C. *et al.* 1) *Bioorg. Med. Chem. Lett.* **23**: 4567-4570 (2013). 2) *J. Nucl. Med.* **55**: 1671-1677 (2014).

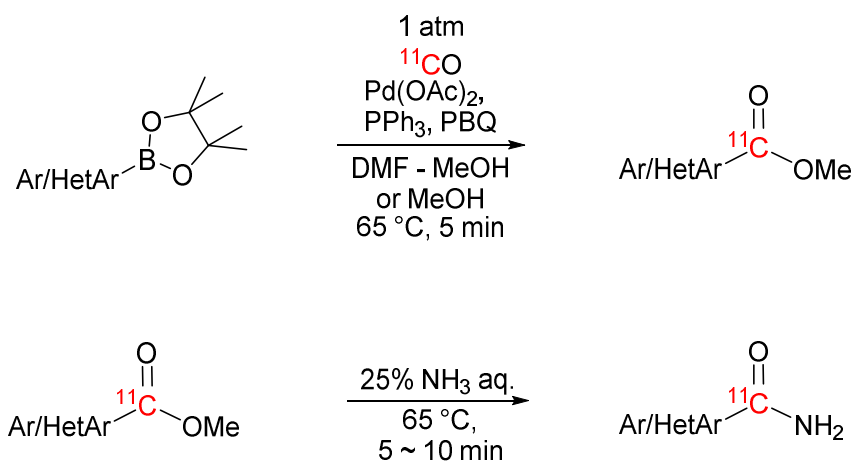
**Pd(0)-MEDIATED [^{11}C]CARBOXYLATION OF BORONIC ACID ESTERS
WITH [^{11}C]CARBON MONOXIDE**

H. Ishii^{1,*}, K. Minegishi¹, K. Nagatsu¹, M.-R. Zhang¹

¹ Molecular Imaging Center, National Institute of Radiological Science, Chiba 263-8555, Japan

Objectives: Introduction of carbonyl group into an aryl or heteroaryl groups is useful method for the construction of valuable pharmacologically active compounds. However typical carbonylation methods using [^{11}C]O generally requires high pressure and high temperature conditions. Therefore, the development of amenable method for the [^{11}C]carbonylation reaction is needed. Here we present the Pd(0)-mediated mild [^{11}C]carbonylation reaction using [^{11}C]O and boronic acid esters under atmospheric pressure.^{1,2}

Results and discussion: The carbonylation reaction was carried out using [^{11}C]O in the presence of aryl and heteroaryl boronic acid esters, paradium(II) acetate ($\text{Pd}(\text{OAc}_2)$), *p*-benzoquinone (PBQ) and triphenylphosphine (PPh_3) in MeOH or DMF-MeOH (v/v = 1:1). The reaction mixture was heated at 65 °C for 5 min under atmospheric pressure to give corresponding [*carbonyl*- ^{11}C]esters. Some of these [*carbonyl*- ^{11}C]esters were converted to corresponding [*carbonyl*- ^{11}C]amides by treating with 25% ammonia solution at 65 °C for 5 - 10 min. Using this methods, we have been succeeded the synthesis of various aryl/heteroaryl [*carbonyl*- ^{11}C]esters with decay-corrected radiochemical yield (RCY) in the range of 6-80%. The efficiency of the amidation was deeply affected by the structure of the substrate. Although [*carbonyl*- ^{11}C]salicylamide, nicotinamide, 3-quinolineamide, 4-isoquinolineamide and 4-hydroxybenzamide were obtained in good RCY from corresponding [*carbonyl*- ^{11}C]esters, the production of 4-benzyloxy[*carbonyl*- ^{11}C]benzamide was failed.



Conclusions: Pd(0)-mediated [^{11}C]carbonylation with aryl/heteroarylboronic acid pinacol esters and [^{11}C]O have been carried out successfully in MeOH or DMF-MeOH (v/v = 1:1) under atmospheric pressure at 65°C for 5 min and gave the corresponding [*carbonyl*- ^{11}C]esters in the range of 6-80% RCY. Some of these [*carbonyl*- ^{11}C]esters were converted to the corresponding [*carbonyl*- ^{11}C]amides by treating with 25% ammonia solution.

References: 1.) Takashima-Hirano, M.; Ishii, H.; Suzuki, M. *ACS Med. Chem. Lett.* **2012**, 3, 804.
2.) Ishii, H.; Minegishi, K.; Nagatsu, K.; Zhang, M.-R. *Tetrahedron*, **2015**, 71, 1588

Synthesis and evaluation of ^{18}F -labeled trimethoxyphenyl phosphonium cations as myocardial perfusion imaging agents

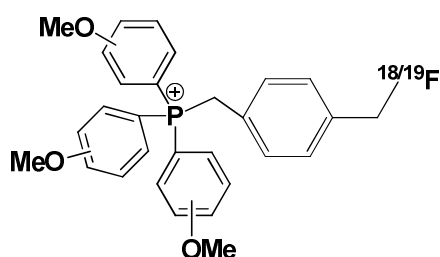
S. Chen¹, Z. Zhao², J. Lu^{1,*}

¹ Key Laboratory of Radiopharmaceuticals, Ministry of Education, College of Chemistry, Beijing Normal University, Beijing 100875, China; ² Department of Nuclear Medicine, Cardiovascular Institute and FuWai Hospital, Chinese Academy of Medical Sciences, Beijing 100037, China

Objectives: Mitochondria occupy approximately 30% of all myocardial tissues, which account for the enhanced negative transmembrane potential in myocardial cells reaching to 180 mV ^[1]. Thus, radiolabeled lipophilic phosphonium cations can accumulate in the mitochondria of heart as myocardial perfusion imaging (MPI) agents ^[2-4]. In this study, three ^{18}F -labeled trimethoxyphenyl phosphonium cations were prepared and their biological properties were also investigated.

Results and discussion:

1. The nonradioactive compounds (1a, 2a and 3a) were synthesized as standard references and characterized by ^1H -NMR, ^{19}F -NMR, ^{31}P -NMR and HRMS. The corresponding radiotracers (1b, 2b and 3b) were also prepared by the One-Pot method as previously reported ^[5] (Figure 1). The decay-corrected radiochemical yield of 1b, 2b and 3b were 20-25%, 50-55% and 30-35%, respectively. The $\log P$ values were 1.67 ± 0.01 ($n=3$), 1.53 ± 0.02 ($n=3$) and 1.54 ± 0.05 ($n=3$), respectively, suggesting that the three radiotracers were lipophilic. All their radiochemical purity (RCP) were $> 98\%$ determined with HPLC, and they were also stable after incubating both in saline at room temperature and in mouse serum at 37°C for 2 hours (RCP $> 95\%$). The result of paper electrophoresis experiment suggested that the three radiotracers were all positive charged.
2. The cell uptakes of three radiotracers were determined in rat embryonic cardiomyoblast cell line (H9c2, high transmembrane potential) and mouse normal fibroblast cell line (NIH/3T3, low transmembrane potential). Furthermore, carbonyl cyanide *m*-chlorophenylhydrazone (CCCP, $1\mu\text{M}$) was used as an inhibitor to mitochondria membrane potential in H9c2 cells. Taking of H9c2 (no CCCP treated) as 100% control, three radiotracers were only 20-45% cell uptake in NIH/3T3 cells, and 55-72% cell uptake in H9c2 cells treated with CCCP. These results demonstrated that the three novel ^{18}F -labeled phosphonium cations accumulated in the myocardial cells through the mitochondrial membrane potential.



- 1a: ^{19}F -tri(*para*-methoxy)phenyl phosphonium cation
 2a: ^{19}F -tri(*ortho*-methoxy)phenyl phosphonium cation
 3a: ^{19}F -tri(*meta*-methoxy)phenyl phosphonium cation
 1b: ^{18}F -tri(*para*-methoxy)phenyl phosphonium cation
 2b: ^{18}F -tri(*ortho*-methoxy)phenyl phosphonium cation
 3b: ^{18}F -tri(*meta*-methoxy)phenyl phosphonium cation

Figure 1. Structure of 1a, 2a, 3a and 1b, 2b, 3b.

3. The ex vivo biological distribution results in CD-1(ICR) female mice are shown in Table 1. All the three radiotracers have good heart uptake, retention, heart/liver ratio, heart/lung ratio and heart/blood ratio. Compared to [^{18}F]FMBTP^[5], 1b, 2b and 3b displayed a quicker liver clearance than [^{18}F]FMBTP (without MeO group on TPP; liver uptake: 14.93 ± 1.46 %ID/g at 5min, 5.16 ± 0.64 %ID/g at 30min). The initial heart uptake of 1b, 2b and 3b were 27.79 ± 1.59 , 19.4 ± 2.31 and 11.81 ± 3.84 %ID/g, respectively, decreasing with the change of methoxy position from *para*, *ortho* to *meta*. It was probably due to the strong electron-donating methoxy group, whose addition on the *para* and *ortho* position contributed to the resonance of triphenyl phosphonium core, and improved the heart uptake by negative transmembrane potential. Compared to 2b, 1b has higher initial heart uptake but also higher non-target organ uptake. Hence the heart/liver, heart/lung and heart/blood ratios of 1b are all lower than 2b.

Table 1. The biodistribution of [^{18}F]1b, 2b and 3b in mice. Expressed as % ID/g \pm SD, n = 4

	1b		2b		3b	
	5min	30min	5min	30min	5min	30min
Heart	27.79 ± 1.59	25.42 ± 5.60	19.4 ± 2.31	23.64 ± 2.91	11.81 ± 3.84	14.87 ± 2.85
Liver	35.19 ± 3.08	6.79 ± 0.68	9.48 ± 0.70	1.80 ± 0.19	13.09 ± 2.59	1.87 ± 0.30
spleen	17.42 ± 3.05	16.04 ± 4.46	7.21 ± 0.91	8.36 ± 2.04	6.84 ± 2.30	4.73 ± 0.53
Lung	23.59 ± 1.71	8.15 ± 1.40	12.28 ± 3.07	6.32 ± 1.28	14.52 ± 2.02	5.40 ± 1.99
kidneys	126.95 ± 13.78	71.39 ± 3.57	73.1 ± 2.25	84.26 ± 9.05	80.66 ± 26.18	35.82 ± 6.92
bone	16.53 ± 3.20	53.40 ± 9.33	5.00 ± 1.09	13.15 ± 6.47	5.56 ± 1.55	18.99 ± 3.13
muscle	7.18 ± 0.98	7.00 ± 3.75	4.20 ± 0.72	5.06 ± 0.22	3.82 ± 2.66	3.48 ± 1.17
blood	8.68 ± 0.48	2.70 ± 0.32	2.65 ± 1.85	1.23 ± 0.24	2.50 ± 0.47	0.71 ± 0.22
heart/liver	0.79	3.74	2.05	13.13	0.90	7.95
heart/lung	1.18	3.12	1.58	3.74	0.81	2.75
heart/blood	3.20	9.41	7.32	19.22	4.72	20.94

Conclusion: In this study, three ^{18}F -labeled trimethoxyphenyl phosphonium cations were synthesized and their biological properties were also investigated as myocardial perfusion imaging agents. All of these preliminary data suggested that 2b might be a potential MPI agent. Further researches such as MicroPET in rat are warranted.

Reference:

- [1] Dong-Yeon Kim, et al. *Bioconjugate Chem*, 21(3): 431–437 (2012).
- [2] Zhou Y, Liu S. *Bioconjug Chem*, 22:1459–72 (2011)
- [3] Dong-Yeon Kim, et al. *Nuclear Medicine and Biology*, 39:1093–1098 (2012)
- [4] Wang J, Liu S, et al. *J. Med. Chem*, 50: 5057-5069 (2007)
- [5] Zhao Z, et al. *Mol. Pharmaceutics*, 11: 3823–3831(2014)

SYNTHESIS AND EVALUATION OF *N*-BENZYL PIPERAZINE DERIVATIVES AS SELECTIVE SIGMA-1 RECEPTOR LIGANDS

Jiajun Ye¹, Yuanyuan Chen¹, Winnie Deuther-Conrad², Jörg Steinbach², Peter Brust², Boli Liu¹,
Hongmei Jia^{1,*}

¹Key Laboratory of Radiopharmaceuticals (Beijing Normal University), Ministry of Education, College of Chemistry, Beijing Normal University, Beijing 100875, China; ²Helmholtz-Zentrum Dresden-Rossendorf, Institute of Radiopharmaceutical Cancer Research, Department of Neuroradiopharmaceuticals, 04318 Leipzig, Germany.

Objectives: The σ_1 receptor functions as “ligand-operated receptor chaperone” and regulates various ion channels, lipids, G protein-coupled receptors, and other signaling proteins. Development of radiotracers with appropriate affinity and high selectivity for σ_1 receptors provide useful tools for investigation of diseases related to σ_1 receptors. In this study, several *N*-benzyl piperazine ligands were designed, synthesized and evaluated as σ_1 receptor ligands using 1-(4-benzylpiperazin-1-yl)-5-(1,2-dithiolan-3-yl)pentan-1-one as lead compound.¹

Methods: The synthetic routes of *N*-benzyl piperazine derivatives are illustrated in **Scheme 1**. The competition binding assays for σ_1 and σ_2 receptors of these compounds were performed as previously reported.² The binding assays used rat brain with (+)-[³H]pentazocine as radioligand for the σ_1 receptors, and rat liver membranes with [³H]DTG (in the presence of 10 μ M dextrallorphan) as radioligand for the σ_2 receptors. The results are shown in **Table 1**.

Results and Discussion: All the target compounds were characterized by ¹H NMR, ¹³C NMR and MS. The *in vitro* competition binding assays showed that these compounds possessed high affinity for σ_1 receptors ($K_i(\sigma_1) = 0.98\text{--}4.19$ nM) and high subtype selectivity ($K_i(\sigma_2) = 62.4\text{--}2500$ nM; $K_i(\sigma_2)/K_i(\sigma_1) = 50\text{--}1488$). In particular, compounds **9c** and **9d** had low nanomolar affinity for σ_1 receptors and excellent subtype selectivity. Reduction of amide group led to increased affinity for σ_2 receptors and thus significantly decreased the subtype selectivity (**9d** vs **10**).

Conclusions: The *N*-benzyl piperazine derivatives **9c** and **9d** possessed low nanomolar affinity for σ_1 receptors and very high selectivity. The synthesis and evaluation of the corresponding radiotracers are in progress.

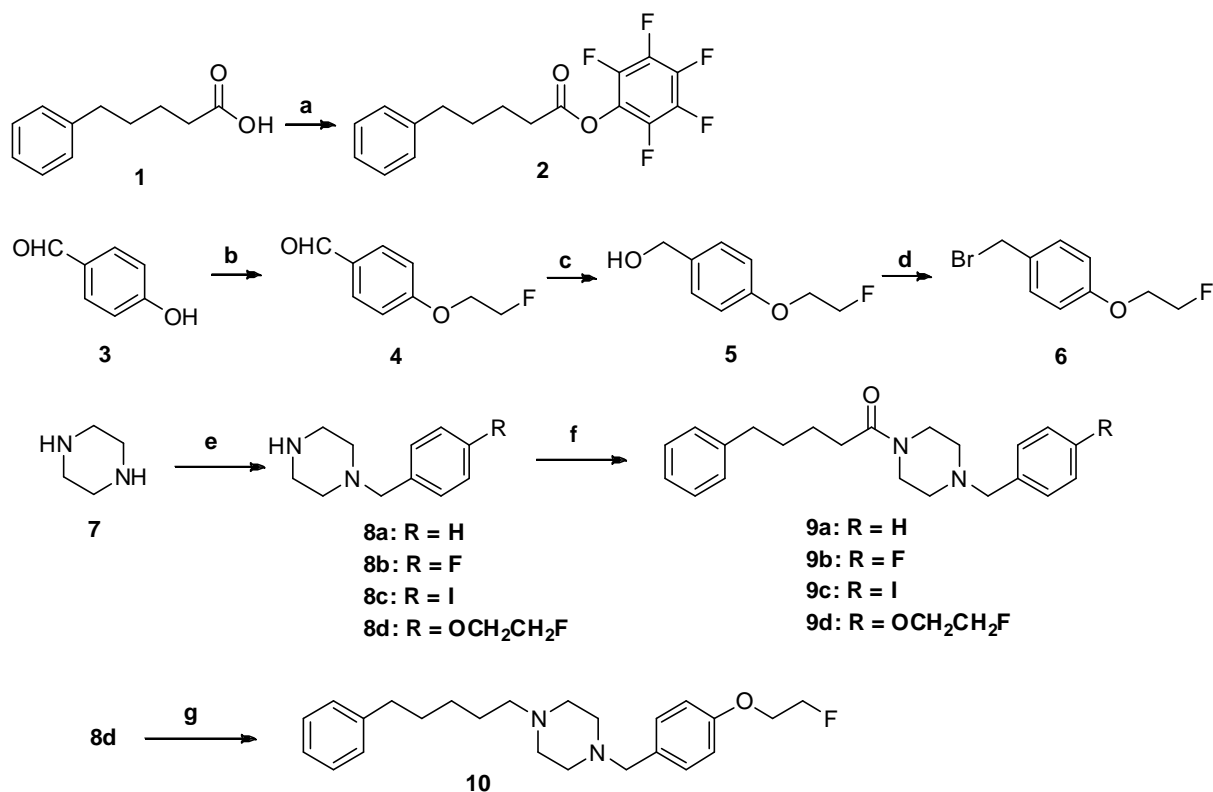
References: 1) Prezzavento, O., et al. *J. Med. Chem.* **56**: 2447-2455 (2013). 2) Fan, C., et al. *Science in China Series B* **49**: 169-176 (2006).

Acknowledgements: Supported by NSFC (21471019).

Table 1. Binding affinities of *N*-benzyl piperazine derivatives for σ_1 and σ_2 receptors.^a

Compound	$K_i(\sigma_1)$ (nM)	$K_i(\sigma_2)$ (nM)	$K_i(\sigma_2)/K_i(\sigma_1)$
9a	2.87 ± 0.49	2500 ± 707	871
9b	0.98 ± 0.18	99.6 ± 13.3	102
9c	1.46 ± 0.71	2173 ± 1393	1488
9d	4.19 ± 0.08	2000 ± 1414	477
10	1.24 ± 0.12	62.4 ± 8.6	50

^a Values are means \pm standard deviation (SD) of two experiments performed in triplicate.

Scheme 1. Synthetic routes of *N*-benzyl piperazine derivatives.

Reagents and conditions: (a) pentafluorophenyl trifluoroacetate, pyridine, DMF, 84%; (b) 1-bromo-2-fluoroethane, K₂CO₃, DMF, 100 °C, 99%; (c) ethanol, NaBH₄, 86%; (d) CH₂Cl₂, PBr₃, 0 °C, 92%; (e) acetonitrile, K₂CO₃, KI, 90 °C, for **8a**, benzyl bromide, 40%; for **8b**, 4-fluorobenzyl bromide, 75%; for **8c**, 4-iodobenzyl bromide, 95%; for **8d**, **6**, 23%; (f) **2**, trimethylamine, DMF, 42%, 55%,

55% and 52% for **5a**, **5b**, **5c** and **5d**, respectively; (g) (5-bromopentyl)benzene, acetonitrile, K_2CO_3 , KI, 90 °C, 48%.

Novel Production Method of 4-Borono-2-¹⁸F-Fluoro-Phenylalanine (¹⁸F-FBPA) via ¹⁸F⁻ Nucleophilic Substitution

Tateishi H.^{1,3}, Takahashi K.², Arano Y.³, Saga T.¹, Watanabe Y.²

¹Molecular Imaging Center, National Institute of Radiological Sciences, Chiba, Japan;

²RIKEN Center for Life Science Technologies, Kobe, Japan;

³Graduate School of Pharmaceutical Sciences, Chiba University, Chiba, Japan

Objectives: Boron neutron capture therapy (BNCT) is one of radiotherapies using alpha particle (⁴He) and recoiling lithium (⁷Li), which are produced by nuclear fission reaction of ¹⁰B with low energy thermal neutrons. Although BNCT has yielded good clinical outcomes in several types of cancer, it has not been widely used because nuclear power reactor is essential to obtain thermal neutrons. Recently, the neutrons are available from accelerator, therefore, BNCT is re-attracting attention to cancer therapists.

4-Borono-2-¹⁸F-fluoro-L-phenylalanine (¹⁸F-FBPA) is an ¹⁸F-labeled analog of 4-¹⁰B-borono-L-phenylalanine (¹⁰B-BPA), which is the most representative ¹⁰B carrier, and is used to predict ¹⁰B-BPA accumulation in tumors before BNCT. The routine production of ¹⁸F-FBPA has been conducted using an electrophilic substitution approach. However, this method has a limitation that one synthesis produces ¹⁸F-FBPA for only a few patients. Considering increased accelerator-based BNCT, we should synthesize ¹⁸F-FBPA using a nucleophilic substitution approach, which could produce larger radioactivities of ¹⁸F-FBPA than the conventional approach. Here, we designed and optimized a novel synthetic procedure of ¹⁸F-FBPA via an ¹⁸F⁻ nucleophilic substitution shown in Fig. 1.

Synthetic procedure: Our synthetic strategy is based on so-called “multi step phase transfer catalyst strategy” (ref 1)). As shown in Fig. 1, after ¹⁸F labeling, benzyl aldehyde **2** was converted to benzyl bromide **4**. **5** was synthesized using Maruoka catalyst and Schiff base. And then **6** was synthesized through Miyaura-borylation. After hydrolysis with HBr, **7** (¹⁸F-FBPA) was obtained.

Results and discussion: **1** was obtained in two steps synthesis from 4-bromo-2-fluorobenzaldehyde. **2** was obtained in high radiochemical yields of 72.4% for (a)-(1) and 71.0% for (a)-(2). **3** was obtained almost quantitatively by both two methods (b)-(1) and (b)-(2). **4** was most difficult to be obtained in our strategy. In our first plan, **4** could be obtained just through aqueous HBr to a Sep-Pak C18 column ((c)-(1)). We however were not able to obtain **4** because hydroxyl group in **3** might be difficult to be protonated in mild conditions. We therefore tried to synthesize **4** in the following stronger conditions (c)-(2) to (c)-(4). As a result, **4** was obtained in radiochemical yields of 45.3% for (c)-(2), 52.5% for (c)-(3), and 43.3% for (c)-(4). **5** and **6** were obtained almost quantitatively. After hydrolysis reaction (f), the object compound **7** (¹⁸F-FBPA) was confirmed by HPLC. The total synthesis time was approximately 100 min and the final radiochemical yield was 44.7% (decay corrected).

Conclusion: ¹⁸F-FBPA was successfully synthesized via an ¹⁸F⁻ nucleophilic substitution. Our method could produce larger amount of ¹⁸F-FBPA compared with the conventional procedure using an electrophilic substitution approach.

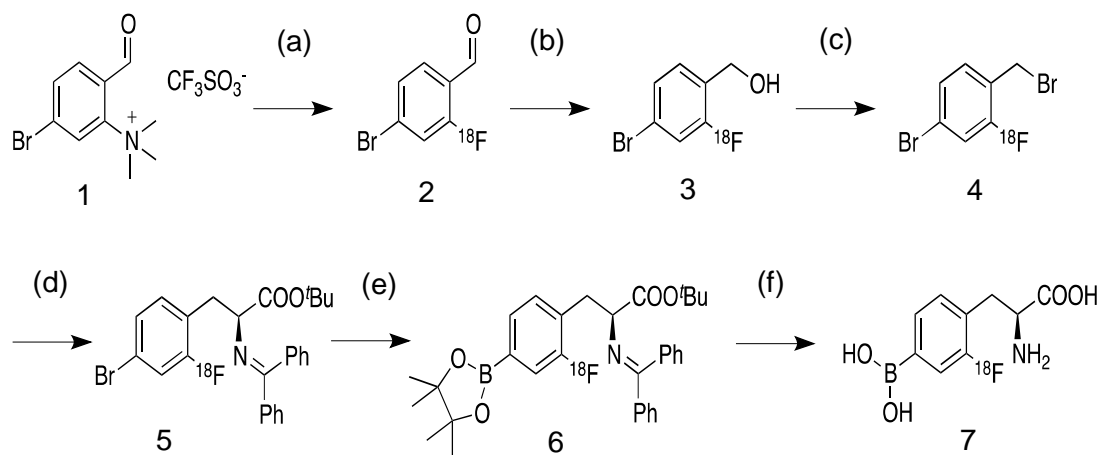


Fig.1 Synthesis of ^{18}F -FBPA. Reagents and conditions are shown as follows:

(a): $^{18}\text{F}^-$ source, (1) DMF or (2) MeCN

(b): (1) reaction on the solid support or (2) NaBH_4 (3 mg), MeOH

(c): (1) reaction on the solid support, (2) 1 mL of HBr, 90 $^\circ\text{C}$, 10 min, (3) 0.2 mL of PBr_3 , 150 $^\circ\text{C}$, 5 min or (4) 5 mg of PPh_3 , 6.3 mg of CBr_4 , 80 $^\circ\text{C}$, 10 min

(d): 3 mg of Maruoka cat, 25 mg of $\text{Ph}_2\text{=NCH}_2\text{COO}^t\text{Bu}$, Toluene/ 9M KOH, 0 $^\circ\text{C}$, 20 min

(e): 38.1 mg of B_2Pin_2 , 2.4 mg of $\text{Pd}_2(\text{dba})_3$, 2.4 mg of PCy_3 , 22.1 mg of AcOK in 1,4-dioxane, 100 $^\circ\text{C}$, 10 min

(f): HBr, 180 $^\circ\text{C}$, 15 min

Reference: 1) Lionel et al. *J.Nucl.Med*, 2013, vol.54, 1154-1161

Nimesulide Analogs as Brain Cyclooxygenase-2 (COX-2)-targeted Imaging Agents: Synthesis and *in Vitro* Evaluation

Yumi Yamamoto¹, Takuya Hisa¹, Jun Arai¹, Yohei Saito¹, Takahiro Mukai², Takashi Ohshima³, Minoru Maeda⁴, and Fumihiko Yamamoto¹

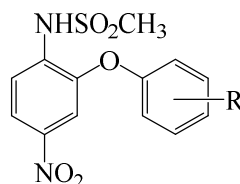
¹Tohoku Pharmaceutical University, Sendai 981-8558, Japan; ²Kobe Pharmaceutical University, Kobe 658-8558, Japan; ³Graduate School of Pharmaceutical Sciences, Kyushu University, Fukuoka 812-8582, Japan; ⁴Daiichi University of Pharmacy, Fukuoka 815-8511, Japan

Objectives: Cyclooxygenase (COX) is a critical enzyme that catalyzes the biosynthesis of prostaglandins from arachidonic acid. Two COX isoforms (COX-1 and COX-2) have been identified. COX-2 enzyme is expressed in response to inflammatory stimuli. While COX-2 was reported to regulate physiologic functions, its role in pathogenic mechanisms is largely unclear. In this study, to investigate the expression and activity of COX-2 in related disorders *in vivo*, we synthesized and evaluated isomeric methoxy/iodo analogs of nimesulide (a classical NSAID) as effective radioligand candidates for imaging brain COX-2 with PET or SPECT.

Results and Discussion:

1. Synthesis. To develop a radiolabeled molecule, we synthesized the target compound, nimesulide

1a and its analogs **1b-g**, each bearing a single methoxy/iodo substituent at the *ortho*-, *meta*-, or *para*-position of the phenyl ring, based on the copper-mediated arylation of phenols. All compounds, **1a-g** were obtained in satisfactory yields. (Figure)



a: R = H (nimesulide)
b: R = *o*-OCH₃ **e:** R = *o*-I
c: R = *m*-OCH₃ **f:** R = *m*-I
d: R = *p*-OCH₃ **g:** R = *p*-I

Figure Nimesulide methoxy/iodo derivatives (**1a-g**)

2. Acid dissociation constant (pKa) and lipophilicity. Lipophilicity is an important factor influencing the passive entry of intravenously administered compounds into the brain. The nimesulide molecule, **1a**, with a weakly acidic sulfonamide group, has a pKa value of 6.4-6.8; its lipophilicity is pH-dependent. In this study, we measured the pKa of compounds **1a-g** by spectrophotometric evaluation and determined their partition coefficients (log $P_{7.4}$) at pH 7.4, according to the OECD guidelines for testing of chemicals 117, using the reversed-phase HPLC method.

The experimental pKa and log $P_{7.4}$ of methoxy/iodo regioisomers **1b-g** were quite similar (pKa = 6.57-7.07 and log $P_{7.4}$ = 1.26-2.77) and were comparable to pKa and log $P_{7.4}$ of nimesulide (pKa = 6.57 and log $P_{7.4}$ = 1.61). Nimesulide was reported to possess brain-penetration activity, as evidenced from pharmacokinetic and tissue distribution studies after systemic administration in animals. Compounds **1b-g** were expected to display distribution properties similar to those of nimesulide.

3. *In vitro* COX-inhibitory potency. The selectivity and affinity toward COX-2 were considered the initial criteria for a prospective imaging agent. The inhibitory potency and selectivity of compounds

1a-g for the COX enzyme were determined *in vitro* using a colorimetric COX (ovine) inhibitor-screening assay.

As shown in Table 1, *para*-methoxy/iodo isomeric analogs **1d** and **1g** displayed inhibitory activity against COX-2, with IC₅₀ values of 2.31 and 0.47 μ M, respectively. In contrast, *ortho*- and *meta*-analogs **1b, c, e, and f** had poor inhibitory activity against COX-1 and COX-2 (>100 μ M, in all cases).

To further understand these results, we performed docking simulations using

Table 1 COX-inhibitory potency of compounds and celecoxib (as a reference drug)

Compounds	IC ₅₀ (μ M)		Selectivity
	COX-1	COX-2	
Nimesulide	>100	1.92	>52
(1a)			
<i>p</i> -OCH ₃ (1d)	>100	2.31	>43
<i>p</i> -I (1g)	>100	0.47	>213
Celecoxib	>100	0.56	>178

Discovery Studio 4.0 software program. The docking poses of the *para*-substituted analogs, **1d** and **1g**, were similar to that of nimesulide, especially in the context of active orientation of the COX-2 pharmacophore (NO₂, SO₂NH) on the nitrophenyl ring, while the *ortho*- and *meta*-substituted analogs were not positioned to accommodate the pharmacophore. In the case of **1g**, the iodo-substituent also interacted with Leu384 in the COX-2 active site. The higher selectivity of **1g** that is equipotent to celecoxib (a well-known COX-2 inhibitor) may be the cause of this interaction.

4. *In vitro* stability. To determine the stability of our compounds, we evaluated their *in vitro* stability using mouse plasma at 37°C. At 1, 10, 30, 60, and 120 minutes after incubation, nimesulide, **1a**, and iodo-analogs **1e-g** showed good stability, with >95% parent compound remaining even after 120-min incubation and no other metabolites were identified. Evaluations of the methoxy analogs are ongoing.

5. *In vitro* transport studies in Caco-2 cells. It is well established that the blood-brain barrier (BBB) contains efflux pumps, including P-gp, which acts as a main barrier for brain-targeted radioligands for *in vivo* imaging and pharmaceutical agents. In this study, the cellular transport of nimesulide, **1a**, and its regioisomeric methoxy/iodo analogs **1b-g** was evaluated in a Caco-2 cell culture model at pH 7.2 and 37°C.

Apparent bidirectional permeability (P_{app, A→B} and P_{app, B→A}) and efflux ratio (P_{app, B→A}/ P_{app, A→B}) were initially determined for all the compounds (**1a-g**) in the absence of a P-gp inhibitor. We observed slightly higher permeation coefficients in the apical-to-basolateral direction (P_{app, A→B} > P_{app, B→A}) than in the reverse direction for all test compounds, thus all efflux ratio values were <1.0. Further transport studies were done, using the same cells in the presence of the P-gp inhibitor verapamil (500 μ M). Compared to control, the addition of verapamil did not induce significant effect in the transport of compounds **1a-g** across the Caco-2 cell membranes. This observation might be beneficial for the development of a brain COX-2-targeted radioligand.

Conclusions: We designed and synthesized six isomeric methoxy/iodo-substituted analogs of nimesulide for the development of a brain COX-2-imaging radiotracer. *Para*-methoxy/iodo analogs **1d** and **1g** displayed an inhibitory potency and selectivity for the COX-2 enzyme. Transport studies using Caco-2 cells showed that P-gp was not involved in the cellular transport of *para*-methoxy/iodo

isomers **1d**, **1g**, or nimesulide, **1a**. Further investigations using the radiolabeled form of the para-methoxy/iodo substituted analogs are warranted for *in vivo* characterization.

Reference: Yamamoto Y. et al., *Chem. Pharm. Bull.*, **59**, 938. (2011)

SYNTHESIS AND EVALUATION OF NOVEL $^{99m}\text{Tc}(\text{CO})_3$ LABELLED GLUCOSE DERIVATIVES AS POTENTIAL TUMOR IMAGING AGENTS

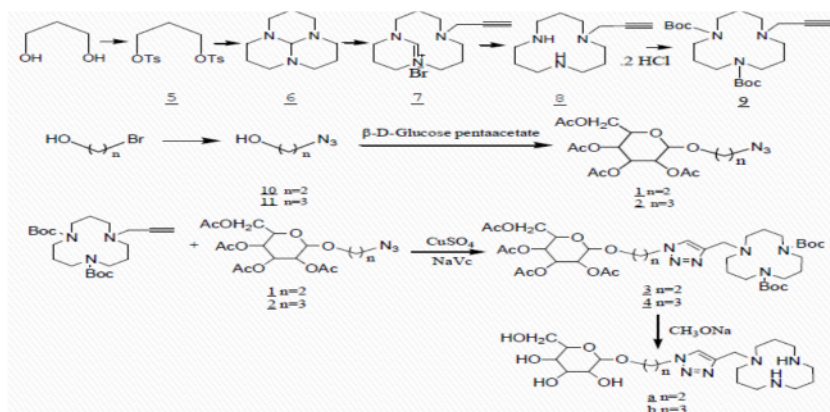
T.L. Liu, Q.Q. Gan, J.B. Zhang*

Key Laboratory of Radiopharmaceuticals, Ministry of Education; College of Chemistry, Beijing Normal University, Beijing, 100875.

Objectives: An enhanced glucose uptake and consumption is observed in tumor cells than in normal cells. [^{18}F]fluorodeoxyglucose (^{18}F -FDG) is the most widely used radiotracer for the diagnosis of tumor. However, the high costs related to its production and the necessary for a cyclotron nearby are realistic limitations. By comparison, technetium-99m has ideal physical and chemical characteristics, inexpensive cost and in-house availability. Therefore, development of ^{99m}Tc -labeled glucose derivatives for SPECT imaging is considered of great interest. The purpose of this study was to synthesize novel glucose derivatives by using the so-called ‘click chemistry’ and to evaluate the possibility of the corresponding $^{99m}\text{Tc}(\text{CO})_3$ complexes as potential tumor imaging agents.

Results and Discussion:

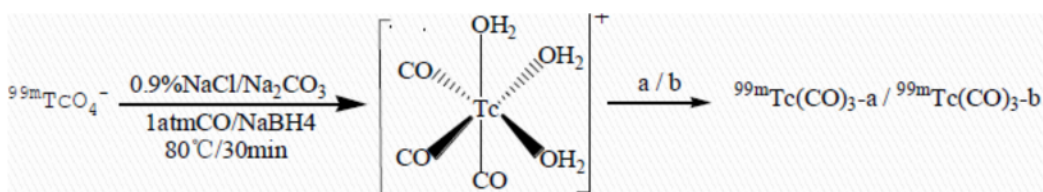
1. Synthesis of ligands: The ligands GEP12N3 (a) and GPP12N3 (b) were synthesized by reacting glucose-azide (complex 1 and 2) with alkyne-[12]aneN₃ (complex 9) by using ‘click chemistry’ (Scheme 1). The final ligands were characterized by IR, ^1H and ^{13}C NMR and MS.



Scheme 1. The synthesis routes of the ligands

2. Radiolabeling: The $^{99m}\text{Tc}(\text{CO})_3$ complexes ($^{99m}\text{Tc}(\text{CO})$ -a and $^{99m}\text{Tc}(\text{CO})$ -b) were achieved in aqueous solution at pH 7.4 by reaction of ligand a/b with $[\text{}^{99m}\text{Tc}(\text{H}_2\text{O})_3(\text{CO})_3]^+$ intermediate at

100 °C for 20 min (Scheme 2). The radiochemical purities of the corresponding $^{99m}\text{Tc}(\text{CO})_3$ complexes were over 95%, as measured by high performance liquid chromatography (HPLC). The HPLC results showed that the retention time of $^{99m}\text{TcO}_4^-$ was 4.361 min and $^{99m}\text{Tc}(\text{H}_2\text{O})_3(\text{CO})_3]^+$ was 12.114 min, while that of $^{99m}\text{Tc}(\text{CO})$ -a and $^{99m}\text{Tc}(\text{CO})$ -b were found to be 3.797 min and 3.806 min.



Scheme 2. Preparation procedures of the $^{99m}\text{Tc}(\text{CO})_3$ complexes

3. The partition coefficient: The partition coefficient (LogP) values of $^{99m}\text{Tc}(\text{CO})$ -a and $^{99m}\text{Tc}(\text{CO})$ -b were -1.370 ± 0.004 and -1.340 ± 0.002 , suggesting they were both hydrophilic.
4. The stability: The radiochemical purities of $^{99m}\text{Tc}(\text{CO})$ -a and $^{99m}\text{Tc}(\text{CO})$ -b were over 95 % in the reaction mixture at room temperature up to 6.0 h after preparation. On the other hand, no decomposition of the above complexes occurred over 6 h at 37 °C in the solution of murine plasma, suggesting they possessed great in vitro stability.
5. Biodistribution studies: The biodistribution results showed $^{99m}\text{Tc}(\text{CO})$ -a and $^{99m}\text{Tc}(\text{CO})$ -b exhibited high initial tumor uptake at 30 min post-injection (the ID%/g values were 3.28 ± 0.37 and 4.08 ± 0.37 , respectively). At 4 h post-injection, the tumor-to-muscle and tumor-to-blood ratios reached the highest. Especially for the tumor-to-muscle ratios, the values of $^{99m}\text{Tc}(\text{CO})$ -a and $^{99m}\text{Tc}(\text{CO})$ -b were 6.05 and 4.38, respectively.

Conclusions: The preliminary studies showed the $^{99m}\text{Tc}(\text{CO})_3$ complexes had the potential for tumor SPECT imaging and they should be further investigated.

Research support: Supported by a grant from NSFC (21171024).

References: Roger Alberto, Kirstin Ortner, Nigel Wheatley et al. J. Am. Chem. Soc., 2001, 123: 3135-3136.

^{99m}Tc-labeled 2-arylbenzothiazole derivatives as SPECT imaging probes targeting A β plaques

Xiaoyang Zhang¹, Pingrong Yu¹, Yanping Yang¹, Cheng Peng², Zhigang Liang², Baian Chen³,
Mengchao Cui^{1,*}, Boli Liu^{1,*}

¹Key Laboratory of Radiopharmaceuticals, Ministry of Education, Beijing Normal University, Beijing 100875, P. R. China. ²Department of Nuclear Medicine, Xuanwu Hospital, Capital Medical University, Beijing 100053, P. R. China. ³Department of Laboratory Animal Sciences, School of Basic Medical Sciences, Capital Medical University, Beijing 100069, P. R. China.

Objectives: According to the reported works^[1], it's difficult to keep the balance between high affinity and efficient brain uptake of ^{99m}Tc-labeled probes for β -amyloid plaques. In this work, we synthesized a series of ^{99m}Tc-labeled 2-arylbenzothiazole derivatives through conjugate approach, to screen potential imaging probes targeting A β plaques for SPECT with both potent binding affinities and favorable brain pharmacokinetics.

Methods: Competitive binding assay quantitatively evaluated the binding affinity of synthesized rhenium complexes. *In vitro* fluorescent staining on brain tissues of Tg mouse and AD patient was also performed. Radiolabelling was efficiently accomplished via ligand exchange approach with ^{99m}Tc-glucoheptonate (GH). *In vitro* autoradiography of Tg mouse brain sections and biodistribution in normal ICR mice were performed with purified ^{99m}Tc-labeled probes. The most potential probe was further evaluated by SPECT/CT imaging of an elder rhesus monkey (27-years old, female).

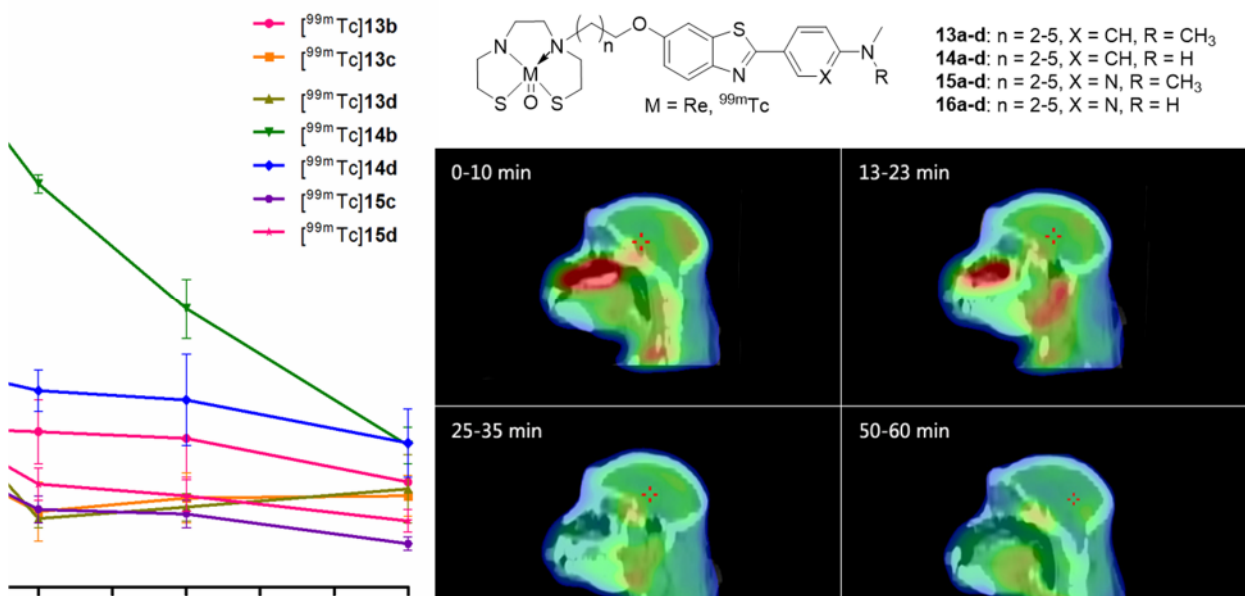


Figure 1. Chemical structure of synthesized probes (right top), brain pharmacokinetics in normal ICR mice of ^{99m}Tc -labeled probes (left) and SPECT/CT imaging of [^{99m}Tc]**14b** in rhesus monkey (right bottom).

Results: Seven rhenium complexes possessing potent binding affinity towards $A\beta_{1-42}$ peptides ($K_i < 50$ nM) were able to bind $A\beta$ plaques on brain tissues in fluorescent staining assay. After labeled by ^{99m}Tc and purification via HPLC, the selected probes also showed effective binding to $A\beta$ plaques in Tg mouse brain tissue in *in vitro* autoradiography studies. Moreover, [^{99m}Tc]**14b** exhibited outstanding brain pharmacokinetics in normal ICR mice (brain uptake $2.11 \pm 0.11\%$ ID/g at 2 min p.i. and $0.62 \pm 0.08\%$ ID/g at 60 min p.i.). Significant initial brain uptake (about 1.0% ID) of [^{99m}Tc]**14b** in an elder rhesus monkey was also observed by SPECT/CT imaging.

Conclusions: We report [^{99m}Tc]**14b** as a SPECT imaging probe targeting $A\beta$ plaques with potent *in vitro* binding affinity ($K_i = 8.8 \pm 1.8$ nM) and favorable brain pharmacokinetics in normal mice. The results from SPECT/CT imaging of rhesus monkey suggested [^{99m}Tc]**14b** to be a potential SPECT imaging probe for $A\beta$ plaques in AD brains.

Acknowledgements: National Science and Technology Major Projects for Major New Drugs Innovation and Development (No. 2014ZX09507007-002)

References: [1] Cui, M (2014) *Curr Med Chem*, 21, 82-112.

Corresponding Author: *Tel/Fax: +86-10-58808891. E-mail: cmc@bnu.edu.cn, liuboli@bnu.edu.cn

Development of radioiodinated pyrido[1,2-*a*]benzoimidazole derivatives as novel tau imaging probes for SPECT

H. Watanabe, M. Ono, A. Kitada, H Saji.

Graduate School of Pharmaceutical Sciences, Kyoto University, Kyoto, Japan.

Objectives: Alzheimer's disease (AD) is the most common form of dementia of the elderly. Neurofibrillary tangles composed of aggregates of hyperphosphorylated tau proteins are well known as one of the neuropathological hallmarks of AD. Since the accumulation of tau aggregates is well correlated with neurodegeneration and cognitive decline, *in vivo* imaging of the tau aggregates with PET or SPECT may be useful for diagnosis and monitoring of the progression of AD. In addition, tau imaging has a potential to allow facilitating research into causes of AD.¹⁾ Therefore, several PET probes, such as [¹⁸F]T807, [¹⁸F]THK-5117, [¹⁸F]THK-5351, and [¹¹C]PBB3, have been tested clinically and demonstrated their feasibility. In contrast, there have been no reports on the development of useful tau imaging probes for SPECT. Recently, we have reported [¹²⁵I](*E*)-6-iodo-2-styryl-1*H*-benzo[*d*]imidazole (SBI) as a new candidate tau imaging probe for SPECT.²⁾ However, the SBI derivatives showed nonspecific accumulation in the white matter of the AD brain section, while they displayed binding for tau aggregates. Therefore, we considered that it is necessary to develop more useful SPECT probes with highly selective binding affinity for tau aggregates. In this study, we newly designed and synthesized radioiodinated pyrido[1,2-*a*]benzoimidazole (PBI) derivatives, and evaluated their utility as novel SPECT probes for imaging tau aggregates in AD brains.

Methods: We synthesized several PBI derivatives. Radioiodinated PBI derivatives were prepared through an iododestannylation reaction from the tributyltin derivatives using hydrogen peroxide as an oxidant. Immunohistochemical staining and *in vitro* autoradiographic studies were performed using postmortem AD brain sections (frontal lobe and temporal lobe) to evaluate specific binding of these derivatives to tau aggregates. Brain uptake and clearance were measured in normal mice after injection of the PBI derivatives. In addition, we tested *in vitro* and *in vivo* stability in normal mice.

Results: Radioiodinated PBI derivatives were successfully prepared in high radiochemical yields and purities (>99%). In immunohistochemical staining using postmortem AD brains, tau aggregates were accumulated only temporal lobe, but β -amyloid plaques, another hallmark of AD, were deposited both temporal and frontal lobe. In *in vitro* autoradiographic studies, radioactivity of all PBI derivatives was highly accumulated in the temporal lobe. These labeling patterns were well correlated with immunohistochemical staining of tau (Figure 1A). Conversely, no marked accumulation was observed in the frontal lobe (Figure 1B). These results suggested that PBI derivatives bound to tau aggregates specifically in AD brain sections. In biodistribution studies in normal mice, all PBI derivatives showed high brain uptake at 2 min postinjection and rapid clearance with time. In addition, these compounds were stable in *in vitro* and *in vivo* in normal mice.

Conclusion: The findings in the present study suggested that radioiodinated PBI derivatives may be useful SPECT probes for *in vivo* imaging of tau aggregates in AD brains.

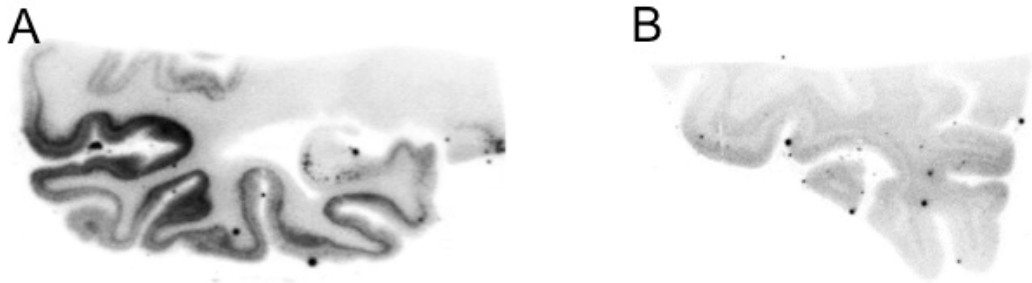


Figure 1. Typical autoradiographic images of PBI derivatives in temporal lobe (A) and frontal lobe (B).

References: 1) Villemagne V L, et al. (2015) *Lancet Neurol.*, 14, 114-124.
2) Matsumura K, et al. (2015) *J. Med. Chem.*, 58, 7241-7257.

Development of Fluorine-18 Labeled 2-Arylquinoline Derivatives for Tau PET Imaging in Alzheimer's Disease

Tetsuro Tago^{1,2}, Shozo Furumoto^{1,2*}, Nobuyuki Okamura³, Ryuichi Harada⁴, Hajime Adachi^{1,2},

Yoichi Ishikawa¹, Kazuhiko Yanai^{1,3}, Ren Iwata¹, and Yukitsuka Kudo⁴

¹Division of Radiopharmaceutical Chemistry, Cyclotron and Radioisotope Center, Tohoku University, Sendai, Japan; ²Department of Radiopharmaceutical Chemistry, Graduate School of Pharmaceutical Sciences, Tohoku University, Sendai, Japan; ³Department of Pharmacology, Tohoku University School of Medicine, Sendai, Japan; ⁴Division of Neuro-Imaging, Institute of Development, Aging and Cancer, Sendai, Japan

Objectives: Pathological hallmarks of Alzheimer's disease (AD) are senile plaques and neurofibrillary tangles composed of amyloid- β and hyperphosphorylated tau proteins, respectively. It is known that the accumulation of these pathologies in the brain starts before the onset of clinical symptoms of AD. Therefore, noninvasive imaging of them would enable preclinical diagnosis of AD and monitoring of the pathological progression. Recently, we have reported ¹⁸F-labeled 2-arylquinoline (2-AQ) derivatives for imaging of tau pathology by positron emission tomography (PET) (1,2). In the present study, we performed structure-activity relationship study of 2-AQ derivatives for further structural optimization of our tau radiotracers.

Methods: Radiosyntheses of 2-AQ derivatives were achieved by a conventional nucleophilic substitution of tosylate precursor using ¹⁸F-fluoride activated with Kryptfix. Binding properties of the derivatives were assessed by autoradiography (ARG) with AD brain sections. In vitro binding assays were performed to determine the affinity for AD brain homogenate. Blood-brain barrier permeability was determined by biodistribution assay with ICR mice. Metabolism analysis was also performed in mice.

Results: We prepared fifteen 2-AQ derivatives (Fig 1) in this study. In vitro ARG and binding assays suggested that 6-substituted quinoline derivatives had higher binding affinity for AD tau aggregates compared with other compounds. Biodistribution studies in mice demonstrated that the

structure of ^{18}F -labeling side-chain has a considerable effect on the pharmacokinetics of radiotracers, and (3-fluoro-2-hydroxy)-1-propoxyl side-chain was superior to others in clearance from blood and tolerance to defluorination. Among the tested compounds, [^{18}F]THK-5151, a 2-(pyridin-5-yl)quinoline derivative, was the most promising candidate for tau imaging radiotracer. Furthermore, we evaluated effects of chirality of THK-5151 on its biological properties. As a result, (*S*)-enantiomer was revealed to have more favorable properties of pharmacokinetics in mice as a tau imaging agent than (*R*)-enantiomer.

Conclusion: The structure-activity relationship study of 2-AQ derivatives revealed the appropriate structural features such as ^{18}F -labeling side-chain and fundamental framework for PET tau tracers. Altogether, (*S*)-enantiomer of [^{18}F]THK-5151 (now called [^{18}F]THK-5351) showed outstanding binding properties and pharmacokinetics in mice. Clinical PET studies in AD patients are now underway for evaluation of the usefulness as a tau imaging agent.

References: 1) Fodero-Tavoletti et al. *Brain* 2011; 134: 1089. 2) Okamura et al. *J Nucl Med* 2013; 54: 1420.

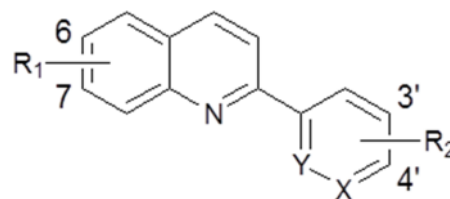


FIGURE 1. Fundamental structure of 2-AQ derivatives

⁶⁸Ga-PSMA-11 micro PET-CT for evaluation of PSMA expression in animal model bearing with prostate cancer

G-Q. SHAO¹, C. CUI¹, S-M ZANG, R. LUO¹, X-C. YAO¹, F. WANG^{1,*}

¹Department of Nuclear Medicine, Nanjing Medical University Affiliated Nanjing Hospital,
Nanjing, 210006, China

Objective: ¹⁸F-fluorodeoxyglucose (FDG) PET-CT imaging is of limited value for diagnosis of prostate cancer. Prostate-specific membrane antigen (PSMA) was highly expressed in prostate cancers and served as specific and ideal molecular target for diagnosis and therapy. In patients with metastatic castration resistant prostate cancer (mCRPC), PSMA was significantly upregulated, which might further promote multiple lymph node and bone metastasis. PSMA targeted theranostics has been hot spot in the management of mCRPC, and referred as “new century molecule”. PSMA-11 (Glu-urea-lys-HBED-CC), containing a HBED-chelator and binding with high affinity to PSMA, showed better bio-distribution profile and kinetics profile. The aim of this study was to prepare and synthesize ⁶⁸Ga-PSMA-11 with automated module, evaluate the affinity to prostate cancer and quantitation of PSMA expression in nude mice tumor model with ⁶⁸Ga-PSMA-11 micro PET-CT, this study might pave the way for PSMA targeted theranostics in prostate cancer.

Results and Discussion

1. Preparation and Radiochemical Stability of ⁶⁸Ga-PSMA-11 and Quality Control. ⁶⁸Ga-PSMA-11 was prepared with automated module (ITG company, Germany). The synthesis protocol was as follows, add 100 μ L PSMA-11 (10 μ g in 0.1 M HEPES buffer, pH = 7.5) into a mixture of 1 ml of ⁶⁸GaCl₃ eluate (185-370 MBq), 250 μ L HEPES (1 M in H₂O, PH: 4) in reaction vials, the reaction system was incubated in room temperature for 20 minutes. The radiochemical yield (RCY) was determined via analytical RP-HPLC and its radiochemical stability was determined by incubating in phosphate buffered saline (PBS). It was stable in vitro and its radiochemical purity was as high as (95.8 \pm 3.6)% and (92.5 \pm 4.1) 3h, 24h after radiolabeling.

2. **Cell Binding and Internalisation.** 22RV1 prostate cancer cells were cultured in RPMI medium, supplemented with 10% fetal calf serum. Tumor cells (10^5 per well) were incubated with ^{68}Ga -PSMA-11 in the presence of 12 different concentrations of analyte (0–5000 nM, 100 μL /well, ^{68}Ga -labelled Glu-urea-Lys(Ahx)-HBED-CC). The 50% inhibitory concentration (IC_{50}) was 26.8 ± 1.7 nM. The specific cell uptake and internalisation of ^{68}Ga -PSMA-11 in prostate cancer cell (C2212) was determined in cell-based assay. Specific cell uptake was determined by competitive blockade with 500 μM of the PSMA inhibitor 2-PMPA. The surface-bound fraction and the intra-cellular binding fraction were measured respectively and tumor uptake per cent of Initially Applied radioactivity bound to 10^6 cells [$\% \text{IA}/10^6$ cells] was (3.6 ± 1.01) and (0.92 ± 0.23) .

3. **Biodistribution study.** Nude mice (Male, 6-8w, 20-22g) bearing prostate cancer xenograft (22RV1:tumor volume of 100–400 mm^3) was selected for biodistribution studies and was euthanized at 5min, 15min, 30min, 60min, 2h, 4h after tail vein injection of ^{68}Ga -PSMA-11. Blood elimination of ^{68}Ga -PSMA-11 was fast while its uptake by the liver and kidneys were relatively low, tumor uptake ($\% \text{ID/g}$) of ^{68}Ga -PSMA-11 reached peak (10.14 ± 1.82) at 60min. Binding specificity of ^{68}Ga -PSMA-11 with PSMA was confirmed via block study (pre-injection of high dose of ^{68}Ga -labelled Glu-urea-Lys(Ahx)-HBED-CC). Prostate cancer xenograft bearing nude mice (PC-3, PSMA negative) was served as control group and tumor uptake ($\% \text{ID/g}$) was (1.05 ± 0.69) , significantly lower than that of 22RV1.

4. **MicroPET-CT imaging.** BALB/c-nude mice bearing prostate cancer (22RV1 group and PC-3 group, $n=4$) accepted microPET-CT imaging respectively one hour after tail vein injection of 3.7MBq(0.1ml) ^{68}Ga -PSMA-11. VOI(volume of interest) of the tumor was drawn on PET-CT fusion imaging slice by slice and radiotracer uptake (SUV_{max}) was calculated. 22RV1 prostate cancer showed significant higher radiouptake (SUV_{max} being 10.32 ± 1.08) than PC3 (SUV_{max} being 1.23 ± 0.34 , $p < 0.05$). Correlation was found between tumor uptake of ^{68}Ga -PSMA-11 and PSMA expression ($r = 0.89$, $p < 0.05$). ^{68}Ga -PSMA-11 micro PET-CT could quantitate PSMA expression in tumor tissue, which may have great potential for PSMA targeted theranostics in prostate cancer.

Conclusion: ^{68}Ga -PSMA-11, as new PSMA targeted small molecule showed high affinity to PSMA positive tumors. ^{68}Ga -PSMA-11 PET-CT imaging may have great potential for PSMA targeted theranostics and be of great value in the clinical management of prostate cancer.

IN VIVO CLICK REACTION BETWEEN TC-99M-LABELED AZADIBENZOCYCLOOCTYNE-MAMA AND 2-NITROIMIDAZOLE-AZIDE FOR TUMOR HYPOXIA TARGETING

W.-J. Sun, T.-W. Chu*

Beijing National Laboratory for Molecular Sciences, Radiochemistry and Radiation Chemistry Key
Laboratory of Fundamental Science, College of Chemistry and Molecular Engineering, Peking
University, Beijing 100871, P. R. China

Objectives: Tumor hypoxia plays an important role in tumor propagation as hypoxic cells could cause resistance to radio- and chemo-therapy. The hypoxia detection is necessary for tumor prognosis and treatment. Nuclear medical imaging based on single photon emission computed tomography (SPECT) and positron emission tomography (PET) is a noninvasive method to detect hypoxia. ^{99m}Tc -labeled 2-nitroimidazole which is of bioreductivity and hypoxia-selectivity, is commonly used as the hypoxia-imaging agent for mapping the tumor hypoxia. They are generally gained from the coordination of ^{99m}Tc -core with organic ligand conjugated with nitroimidazole. The large ligand and nuclide may disturb the bioactivity of nitroimidazole. Pretargeting strategy has the potential to overcome this problem. It is based on the tumor hypoxia-binding of 2-nitroimidazole tagged with a reporter and the subsequent binding of radiolabeled effector to the prelocalized 2-nitroimidazole after a suitable interval, resulting in superior tumor-to-nontumor ratios. This strategy has been increasingly used in tumor radioimmuno-detection and radioimmunotherapy. The strain-promoted cyclooctyne-azide cycloaddition (SPAAC) is a rapid, efficient and catalyst-free *in vivo* click reaction with high specificity and versatility under mild conditions. Azide is small and stable in biological systems and will make less interference to the pharmacophore. In recent years, the SPAAC has been widely used into tracking glycans metabolically labeled with azides in living systems. Its application for pretargeted tumor hypoxia-imaging has remained unexplored so far. Herein, we applied the SPAAC in hypoxia-pretargeting *in vivo* and envisioned that it would protect the bioreductivity of nitroimidazole.

Results and Discussion:

1. Chemistry: Azadibenzocyclooctyne, which is of favorable kinetics, was synthesized and coupled with monoamine-monoamide-dithiol (MAMA) ligand for ^{99m}Tc -labeling. 2-nitroimidazole tagged with azide (2NIM-Az) was synthesized for hypoxia-binding. The molecular structures are shown in Figure 1. The *in vitro* SPAAC reaction shows appropriate reaction kinetics (rate constant is $0.98 \text{ M}^{-1}\text{s}^{-1}$). All the MAMA-ligands were labeled with ^{99m}Tc . The RP-HPLC chromatogram of AM, 2NIM-Az and MAMA-triazole-2NIM were measured by RP-HPLC analysis. The characteristic retention time of AM, 2NIM-Az and MAMA-triazole-2NIM are 26.4 min, 6.4 min and double peaks of 9.3 min and 9.7 min respectively. The radiochemical purities are over 95%.

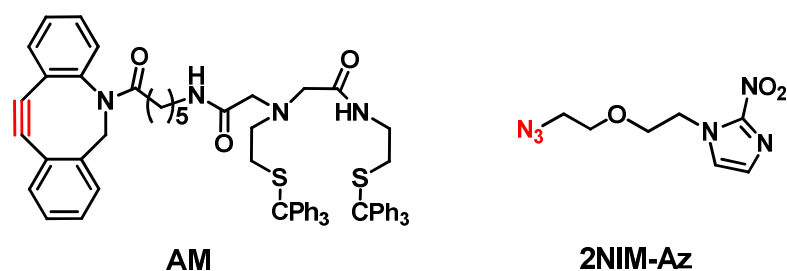


Figure 1. Azadibenzocyclooctyne-MAMA (**AM**) and 2-nitroimidazole-azide (**2NIM-Az**)

2. Biodistribution study: The biodistribution studies of ^{99m}Tc -AM and ^{99m}Tc -triazole-2NIM, which were used as blank control and conventional hypoxia-imaging agent control respectively, were performed in tumor bearing male Kunming mice. As shown in Tables 1 and 2, compared with the other two intervals, the hypoxia-pretargeting experiment after interval of 5 h shows better uptake in tumor and T/M and T/B than the controls. As a potential conventional hypoxia imaging agent, ^{99m}Tc -triazole-2NIM shows higher uptake and better retention in tumor than the blank control (^{99m}Tc -AM). The pretargeting experiment shows similar uptake in tumor with ^{99m}Tc -triazole-2NIM. And both of them show good uptakes in tumor, which are twice as much as that of blank control. However, ^{99m}Tc -triazole-2NIM shows poor T/M which is even lower than ^{99m}Tc -AM. The pretargeting strategy shows highest T/M which is twice as much as that of ^{99m}Tc -AM, and shows similar T/B with ^{99m}Tc -triazole-2NIM at 8 h post-injection.

Table 1. The uptake in tumor and T/M and T/B of the control experiments in mice bearing S180 tumor.

	Time post-injection of radiolabeled compound			
	1 h	2 h	4 h	8 h
^{99m}Tc-AM				
Tumor (%ID/g)	0.29 ± 0.04	0.27 ± 0.04	0.28 ± 0.03	0.25 ± 0.03
T/M	3.37 ± 0.40	4.13 ± 0.19	4.89 ± 0.26	5.01 ± 0.08
T/B	0.46 ± 0.07	0.53 ± 0.04	0.80 ± 0.10	0.77 ± 0.12
^{99m}Tc-triazole-2NIM				
Tumor (%ID/g)	0.42 ± 0.05	0.54 ± 0.10	0.71 ± 0.14	0.54 ± 0.12
T/M	1.38 ± 0.13	0.83 ± 0.21	1.83 ± 0.31	0.72 ± 0.10
T/B	1.48 ± 0.16	1.81 ± 0.16	2.02 ± 0.37	1.42 ± 0.24

Table 2. The uptake in tumor and T/M and T/B of pretargeting experiment in mice bearing S180 tumor after an interval (2, 5 or 12 h) for hypoxia pretargeting.

	Time post-injection of radiolabeled compound			
	1 h	2 h	4 h	8 h
2 h				
Tumor (%ID/g)	0.47 ± 0.15	0.31 ± 0.09	0.44 ± 0.10	0.73 ± 0.14
T/M	2.03 ± 0.37	1.48 ± 0.18	1.92 ± 0.27	2.47 ± 0.26
T/B	0.94 ± 0.10	0.80 ± 0.11	1.09 ± 0.08	2.18 ± 0.37

5 h				
Tumor (%ID/g)	0.58 ± 0.05	0.58 ± 0.05	0.52 ± 0.09	0.70 ± 0.09
T/M	3.91 ± 0.73	4.33 ± 0.66	6.35 ± 0.73	8.55 ± 0.57
T/ B	0.67 ± 0.06	0.70 ± 0.10	1.08 ± 0.14	1.44 ± 0.06
12 h				
Tumor (%ID/g)	0.66 ± 0.11	0.99 ± 0.12	0.23 ± 0.04	0.35 ± 0.07
T/M	2.41 ± 0.31	2.63 ± 0.09	1.98 ± 0.13	1.65 ± 0.12
T/ B	0.86 ± 0.11	1.44 ± 0.04	1.58 ± 0.01	1.10 ± 0.07

Conclusion: In a word, pretargeting based on strain-promoted cyclooctyne-azide cycloaddition (SPAAC) may protect the bioactivity of nitroimidazole, and it may provide an innovative approach for developing the tumor hypoxia-SPECT imaging agents.

Factors affecting radiochemical yields of isonitrile-based $^{99\text{m}}\text{Tc}$ -labeled trivalent probes for molecular imaging

Yuki Mizuno[†], Chun-Wei Jen[†], Tomoya Uehara[†], and Yasushi Arano[†]

[†]Department of Molecular Imaging and Radiotherapy, Graduate School of Pharmaceutical Sciences,
Chiba University, 1-8-1 Inohana, Chuo-ku, Chiba 260-8675 Japan

An isonitrile group (CN-R) is an excellent monodentate ligand to certain low oxidation state metals such as $^{99\text{m}}\text{Tc}(\text{I})$ and $\text{Re}(\text{I})$. We recently developed a new chemical design to prepare $^{99\text{m}}\text{Tc}$ -labeled trivalent probes by reacting a monovalent CN-containing ligand with $[\text{}^{99\text{m}}\text{Tc}(\text{CO})_3(\text{OH}_2)_3]^+$ precursor. The resulting $[\text{}^{99\text{m}}\text{Tc}(\text{CO})_3(\text{CN-R})_3]^+$ compound would possess much higher binding affinity than its free ligand (CN-R) due to the formation of the trivalent targeting molecule upon complexation. Indeed, we synthesized an isonitrile ligand L1 that possesses a monovalent RGD peptide as a targeting vector ($\text{L1} = \text{CN-}\beta\text{Ala-GG-RGD}$), and L1 produced a stable mixed ligand $^{99\text{m}}\text{Tc}$ -labeled trivalent RGD probe ($[\text{}^{99\text{m}}\text{Tc}(\text{CO})_3(\text{L1})_3]^+$) upon the complexation with $[\text{}^{99\text{m}}\text{Tc}(\text{CO})_3]^+$ core. The $^{99\text{m}}\text{Tc}$ -labeled trivalent probe demonstrated higher *in vivo* target uptake in a nude mouse model without removing the excess unlabeled ligand. These findings indicate that the meal coordination-mediated synthesis of trivalent $^{99\text{m}}\text{Tc}$ -labeled probes using monovalent CN-R ligands would constitute a useful approach to synthesize ready-to-use $^{99\text{m}}\text{Tc}$ -labeled molecular imaging probes as well as $^{186/188}\text{Re}$ -labeled therapeutic radiopharmaceuticals.

However, the radiolabeling efficiency needs to be improved since relatively high ligand concentration (150 μM) was required to prepare the objective $^{99\text{m}}\text{Tc}$ -labeled probe in high radiochemical yields. Since isonitrile groups are more likely to be converted to formyl groups under acidic conditions, the complexation reaction at basic reaction conditions is preferred to acidic ones. To our surprise, higher radiochemical yields were achieved at slightly acidic conditions (pH 6.0) than basic ones (pH 8.0).

The reaction at basic conditions produced multiples side products, which significantly reduced the radiochemical yields.

This study was undertaken to investigate the formation mechanism of the side products observed at basic conditions for better understanding the complexation ability of $[^{99m}\text{Tc}(\text{CO})_3(\text{OH}_2)_3]^+$ or $[\text{Re}(\text{CO})_3(\text{OH}_2)_3]^+$ with isonitrile ligands. We prepared a monovalent ligand L1' (CN- β Ala-GG-CONH-Bn) as a model for simplicity. The non-radioactive $^{185/187}\text{Re}$ was also used to characterize the reaction products by MS and NMR.

The reaction of L1' with $[^{99m}\text{Tc}(\text{CO})_3(\text{OH}_2)_3]^+$ at basic conditions generated multiple peaks in HPLC analysis as also observed with the reaction between L1 and $[^{99m}\text{Tc}(\text{CO})_3(\text{OH}_2)_3]^+$. The generation of similar side products was observed by the reaction of L1' with $[^{99m}\text{Tc}(\text{CO})_3(\text{OH}_2)_3]^+$ and $[\text{Re}(\text{CO})_3(\text{OH}_2)_3]^+$. $[^{99m}\text{Tc}(\text{CO})_3(\text{L1}')_3]^+$ and $[\text{Re}(\text{CO})_3(\text{L1}')_3]^+$ were then isolated by HPLC and reconstituted in a buffered-solution at pH 8.0. When the solution was treated at 100°C for 30 min, the side products were generated from both ^{99m}Tc and Re compounds. The NMR and MS analyses using Re-complexes revealed that these side products were produced by the reaction similar to the bimolecular elimination reaction described below (Fig. 1).

We hypothesized that the key step of this reaction was the abstraction of 2-proton in L1' by a base since the acidity of this proton is relatively high due to the electron withdrawing effect of its neighboring carbonyl group. This in turn suggested that lowering the acidity of 2-proton in a monovalent ligand would reduce the generation of the side products. We thereby synthesized L2' (CN-GABA-GG-CONH-Bn) where β Ala in L1' was replaced with γ -amino butyric acid (GABA) to lower the acidity of 2-proton by keeping it away from the carbonyl group. The reaction of L2' with $[^{99m}\text{Tc}(\text{CO})_3(\text{OH}_2)_3]^+$ at basic conditions significantly reduced the side products.

These findings indicate the importance of the acidity of 2-proton coupled to an isonitrile moiety for the stability of the resulting ^{99m}Tc -labeled compounds. The present results would provide a good basis for increasing the radiochemical yields of isonitrile-based ligands and developing ready-to-use ^{99m}Tc -labeled probes.

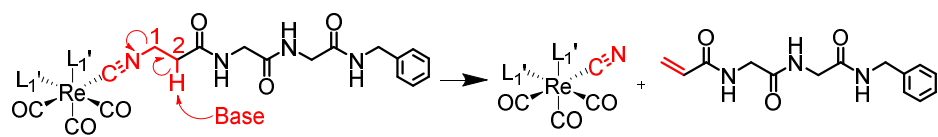


Figure 1. The mechanism for generating side products at basic conditions. The 2-proton in a ligand is abstracted by a base, resulting in the elimination of an isocyanide from L1' to form alkyne.

Radiolabeled immunoglobulin G visualizes active inflammation in atherosclerosis

Sagiri Fukura¹, Yoichi Shimizu², Hiroko Hanzawa³, Ken-ichi Nishijima^{1,4}, Takeshi Sakamoto³, Songji Zhao¹, Mikako Ogawa², Yuji Kuge^{1,4}

¹Graduate School of Medicine, Hokkaido University, Sapporo 060-8638, Japan. ²Faculty of Pharmaceutical Science, Hokkaido University, Sapporo 060-0812, Japan. ³Center for Exploratory Research, Research & Development Group, Hitachi, Ltd., Hatoyama 350-0395, Japan. ⁴Central Institute of Isotope Science, Hokkaido University, Sapporo 060-0812, Japan.

Objectives :

Atherosclerotic plaque formation and following plaque rupture cause fatal diseases such as acute coronary syndrome and cerebral infarction. Macrophage infiltration is characteristic for vulnerable plaques, and it is well known that macrophages express Fc receptors to recognize immunoglobulin G (IgG). In this study, we explored usefulness of a radiolabeled IgG (^{99m}Tc-IgG) for detecting of atherosclerotic lesions.

Methods :

Mouse IgG_{2b} without specificity to any biomolecules was used. The IgG was labeled with ^{99m}Tc via 6-hydrazinonicotinate to yield ^{99m}Tc-IgG. ApoE^{-/-} or wild-type (C57BL/6J) mice were intravenously injected with ^{99m}Tc-IgG, and the aortas were excised at 24 h after the injection. After radioactivity measurement, autoradiography (ARG) and histologic studies were performed with the serial aortic sections. RAW264.7 mouse macrophages were polarized into M1 or M2 cells by incubating with LPS and IFN γ or IL-4 for 48 h, then treated with ^{99m}Tc-IgG, and the radioactivity in the cells was measured after the 1-hour incubation. The M1 polarized macrophages were also used to assess the effects of pretreatment with anti-Fc gamma receptor antibody on the ^{99m}Tc-IgG accumulation level. The expression levels of Fc gamma receptors (CD64 and CD32) in the cells were measured by Western blot analysis.

Results & Discussion :

^{99m}Tc-IgG accumulation levels in the aortas of apoE^{-/-} mice were significantly higher than those of wild-type mice (5.1 ± 1.4 vs. 2.8 ± 0.5 %ID/g, $p < 0.05$), and the accumulation areas were highly correlated with the macrophage infiltration areas. In the atherosclerotic region, there are two types of macrophages, that is, M1 (classically activated macrophage) and M2 (alternatively activated macrophage). Then, we evaluated ^{99m}Tc-IgG accumulation levels in those macrophages. M1 polarized macrophages showed significantly higher levels of ^{99m}Tc-IgG compared with M2 and M0 (non-polarized) macrophages (2.2 ± 0.3 (M1) vs. 0.5 ± 0.1 (M2), 0.4 ± 0.1 (M0) %ID/mg protein, $p < 0.01$), and showed higher expression levels of CD32 and CD64 than M2 and M0 macrophages. Furthermore, the cellular uptake of ^{99m}Tc-IgG in M1 polarized macrophages was significantly suppressed by the pretreatment with anti-Fc gamma receptor antibody (2.2 ± 0.3 (non-pretreatment) vs. 1.2 ± 0.2

(pretreatment) %ID/mg protein, $p < 0.01$). These results suggest that ^{99m}Tc -IgG was accumulated in M1 polarized macrophage via Fc gamma receptors.

Conclusions :

^{99m}Tc -IgG was accumulated in pro-inflammatory M1 polarized macrophages in atherosclerotic lesions. Therefore, radiolabeled IgG should visualize active inflammation sites in atherosclerotic lesions.

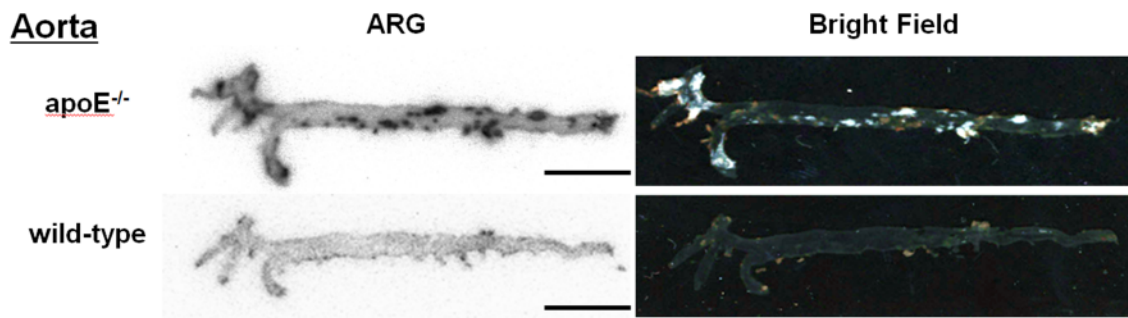


Figure 1. Autoradiography (ARG) and bright field images of the aorta of $\text{apoE}^{-/-}$ and wild-type mice at 24 hour after administration of ^{99m}Tc -IgG. Accumulation of ^{99m}Tc -IgG in the atherosclerotic lesions was found in $\text{apoE}^{-/-}$ mouse.

PREPARATION AND PRELIMINARY EVALUATION OF A HYBRID BRACHYTHERAPY SEED CONTAINING PALLADIUM-103 AND IODINE-125

Zhong-Yong Li ^{1,2}, Hui-Bo Gao ¹, Wen-Hui Zhang ¹, Hai-ping Cui^{1,2,*}

¹ Atom High Tech Co. Ltd., Beijing 102413, China; ² China Institute of Atomic Energy, Beijing
102413, China

Objectives: It has been confirmed in clinic that ^{103}Pd and ^{125}I are effective in brachytherapy treatment of tumors, with short and long doubling time, respectively. However, for treatment of tumors composed of cells with different doubling time, a brachytherapy source with a mixture of ^{103}Pd and ^{125}I radioisotopes might be more desirable. The aim of this work was to design a new ^{103}Pd and ^{125}I hybrid seed and establish the preparation method. To evaluate the inhibitory effect of the hybrid seed preliminarily, pulmonary adenocarcinoma of GLC-82 cells ($T_p=17\text{d}$) and pulmonary large cell carcinoma of H460 cells ($T_p=5\text{d}$) were cultured and used to test in vitro killing effect of radiation, and the models of mice transplanted GLC-82 and H460 were established and used to observe in vivo radiotherapeutic effect of radiation.

Results and discussion:

1. Design of a new ^{103}Pd and ^{125}I hybrid seed: The hybrid seed consisted of a carbon bar with a multi-coating containing ^{103}Pd and ^{125}I on the surface as source core and a sealed titanium tube as source capsule. Both ^{103}Pd and ^{125}I were distributed evenly on the core.
2. Preparation of the ^{103}Pd and ^{125}I hybrid seed: The process for preparation of the hybrid seeds consisted of five steps: 1) Nano palladium crystallites were uniformly seeded on the surface of a batch of carbon bars by put them into a PdCl_2 solution and a $\text{N}_2\text{H}_4\cdot\text{H}_2\text{O}$ solution successively, 2) ^{103}Pd was deposited on the carbon bars by electroless plating in a solution consisting of PdCl_2 , Na_2EDTA , NH_4OH , $\text{N}_2\text{H}_4\cdot\text{H}_2\text{O}$ and ^{103}Pd , 3) Silver was deposited on the carbon bars by electroless plating in a solution consisting of AgNO_3 , Na_2EDTA , NH_4OH and $\text{N}_2\text{H}_4\cdot\text{H}_2\text{O}$, 4) ^{125}I was adsorbed on the carbon bars as Ag^{125}I by iodinating the silver-coating in a solution consisting of NaBr , NaI , NaOH , $\text{K}_3[\text{Fe}(\text{CN})_6]$ and ^{125}I , 5) each carbon bar with ^{103}Pd and Ag^{125}I was sealed in a titanium capsule.

In this process, about 98 percent of ^{103}Pd and 99 percent of ^{125}I were deposited on the carbon bars uniformly. But a portion of the energy of ^{103}Pd and ^{125}I would be shielded by the core and the titanium capsule, the self-shielding were close to 52 percent and 26 percent, respectively. So the total utilization

for ^{103}Pd and ^{125}I were about 47 percent and 72 percent, respectively. The apparent activities of ^{103}Pd and ^{125}I could be flexibly determined.

3. In vitro killing effect: GLC-82 cells and H460 cells were cultured in vitro. Then they were exposed directly to the hybrid seeds (^{103}Pd : ^{125}I =25.9MBq:18.5MBq), ^{103}Pd seeds (44.4MBq) and ^{125}I seeds (29.6MBq) for 48 hours to test the killing effect.

The GLC-82 cells around the hybrid seeds, ^{125}I seeds and ^{103}Pd seeds were all inhibited and became swollen and transfiguring. The H460 cells around ^{125}I seeds showed no obvious abnormality while those around the hybrid seeds and ^{103}Pd seeds were damaged and became sparse.

4. In vivo radiotherapeutic effect: GLC-82 and H460 tumor models were established and 20 mice were chosen randomly for each model. For each model, they were divided into four groups (n=5). Then the hybrid seeds (^{103}Pd : ^{125}I =25.9MBq:18.5MBq), ^{103}Pd seeds (44.4MBq), ^{125}I seeds (29.6MBq) and nonradioactive seeds were implanted into the tumors for 60 days to observe the radiotherapeutic effect.

The radioactive seeds could inhibit the tumors growth. For the same seed, the inhibitory effect to GLC-82 was better than that to H460. For the same model, the hybrid seeds had the best radiotherapeutic effects, ^{103}Pd seeds and ^{125}I seeds were similar and took the second place, and nonradioactive seeds showed the worst.

Conclusions: A novel hybrid brachytherapy seed containing ^{103}Pd and ^{125}I was designed and prepared. The design was simple in structure, and the preparation method was reliably and effectively and easily used in manufacturing. The results showed that the inhibition of the hybrid seed for tumors was more effective than the seed with a single radioisotope. Although it is still followed by many problems, it is believed that the ^{103}Pd and ^{125}I hybrid seed has bright prospects in clinical application.

References: 1) Ling CC. Int J Radiat Oncol Biol Phys 23(1): 81-87 (1992). 2) S Nag, et al. Endocuriether Hypertherm Oncol 12(1): 119-124 (1996). 3) Wen-Jiang S. Chin J Min Inv Surg 7(2): 118-119 (2007). 4) Chen Z, et al. Int J Radiat Oncol Biol Phys 55(3): 825-834 (2003). 5) Harder GF, et al. US 20080249398 (2008).

Synthesis, Characterization and *in vivo* Evaluation of ^{64}Cu -DOTA-SPIONs-PEG-FA as a Dual-Modality PET/MRI Agent

Yu-lin Sun^{1,2}, Yi-ming Shen^{1,2}, Ji-xin Liang², Yu-qing Chen^{1,2}, Lang-tao Shen^{1,2,*}

¹HTA Co. Ltd., Beijing 102413, China; ²China Institute of Atomic Energy, Beijing 102413, China.

Objectives: The folate receptor (FR) is over-expressed on many tumor types, such as tumors of the ovary, cervix, endometrium, lung, kidney, breast, colon, and brain. The aim of the study was to develop a novel nanoparticle-based dual-modality PET/MRI probe for imaging folate receptor-positive tumours. This probe was composed of a superparamagnetic iron oxide nanoparticles (SPIONs) coated with the biocompatible polymer poly (ethylene glycol)(PEG), the components of folic acid (FA), 1,4,7,10-tetraazacyclododecane- 1,4,7,10-tetraacetic acid (DOTA) and copper-64 (Figure 1). The bio-distribution and PET imaging of ^{64}Cu -DOTA-SPIONs-PEG-FA on the model mice were studied.

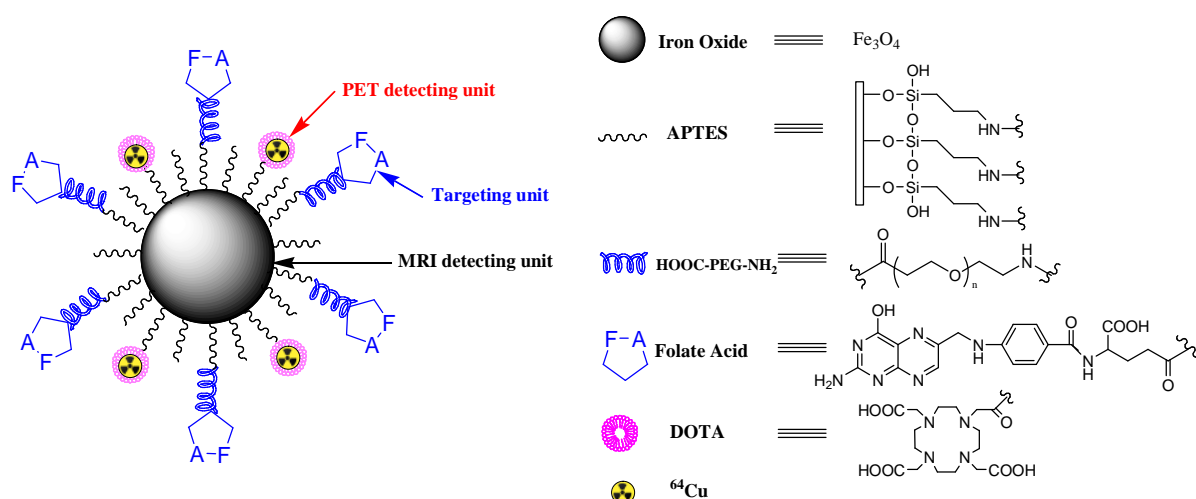


Figure 1. ^{64}Cu -DOTA-SPIONs-PEG-FA

Results and discussion:

1. Syntheses and Characterization of DOTA-SPIONs-PEG-FA: Firstly, SPIONs were prepared by the method of co-precipitation. Then, the SPIONs were attached to APTES. In the next step, the fragments of PEG-FA were conjugated to SPIONs *via* APTES. Finally, DOTA was bound to the nanoparticles. The shape and size distributions of SPIONs and SPIONs-PEG-FA were examined by Transmission Electron Microscope (TEM) and dynamic light scattering (DLS), respectively. The mean size of SPIONs-PEG-FA is about 60 nm. DLS revealed that SPIONs-PEG-FA had slight broader distribution with mean sizes 134 nm. The saturation magnetization (Ms) of SPIONs and

DOTA-SPIONs-PEG-FA are 35.6 emu/g and 7.9 emu/g. The preparation of SPIONs-PEG-FA was further confirmed by FT-IR. The peaks at 582.5, 1109.0, 1631.7 and 3431.3 cm^{-1} are assigned to the Fe-O of SPIONs, CH_2 bending of PEG, C=O stretching of the amide bond and N-H stretching of the amide bond, respectively. The r_2 relaxivity of DOTA-SPIONs-PEG-FA is $55.9 \text{ mM}^{-1}\text{s}^{-1}$.

2. ^{64}Cu -Radiolabeling of DOTA-SPIONs-PEG-FA: Labeling of DOTA-SPIONs-PEG-FA was conducted by incubation with $^{64}\text{CuCl}_2$ at 60°C for 45 min in 0.1 M ammonium acetate buffer (pH 6.5). It was found that DOTA-SPIONs-PEG-FA could be labeled at least 2-3 $\mu\text{Ci}/\mu\text{g}$ with a yield of 40%. The non-specific-bound ^{64}Cu was complexed with EDTA after the labeling reaction. Then, ^{64}Cu -EDTA was separated from ^{64}Cu -DOTA-SPIONs-PEG-FA by using a Vivaspin 500 filter with 10 KDa molecular weight cut off membrane. Incubation at 37°C for 4 h in human serum, the radiochemical purity of the ^{64}Cu -DOTA-SPIONs-PEG-FA remained between 98% to 93%. It indicated a good *in vitro* stability of this ^{64}Cu radiolabel.

3. Biodistribution studies: The biodistribution of ^{64}Cu radiolabel was investigated on the mice bearing with KB cells tumor. At 1 h post-injection, the liver and spleen showed a high accumulation of 27.4 ± 6.11 and $16.2 \pm 9.9\%$ ID/g, respectively. Kidney uptake remained relatively constant (3-4% ID/g). Other organs (blood, muscle) showed low uptake. The activity of ^{64}Cu -DOTA-SPIONs-PEG-FA was $9.7 \pm 5.2\%$ ID/g in KB cells tumor, compared to that of ^{64}Cu -DOTA-SPIONs-PEG-OH was $1.4 \pm 0.3\%$ ID/g. This result showed that ^{64}Cu -DOTA-SPIONs-PEG-FA was targeted to the tumor.

4. PET and MR imaging: Tumor-bearing Balb/c mouse was administered 500 μCi of ^{64}Cu -DOTA-SPIONs-PEG-FA (2 mg Fe/kg body weight) *via* tail vein injection and imaged at 4 h post-injection by using of MicroPET/CT. T2-weight MR image was taken from a mouse which was injected with DOTA-SPIONs-PEG-FA (2 mg Fe/kg body weight). The MR signal intensity of the entire tumor decreased from pre-injection to post-injection. The PET image showed the accumulation of ^{64}Cu -DOTA-SPIONs-PEG-FA in the tumor.

Conclusion: ^{64}Cu -DOTA-SPIONs-PEG-FA as a novel dual-modality PET/MRI imaging probe was prepared and investigated. This probe seems to be promising to image human nasopharyngeal epidermoid carcinoma on the mouse in both modes of PET and MRI.

References: 1) Yoo Mi-Kyong, et al. *Acta Biomaterialia* **8**:3005-3013 (2012). 2) Charles

Glaus., et al. *Bioconjugate Chem* **21**:715-722 (2010). 3) Rosales R. T. M., et al. *J. Label. Compd. Radiopharm.* **57**:298-303(2014).

PRECLINICAL EVALUATION OF A THYMIDINE PHOSPHORYLASE IMAGING PROBE, [¹²³I]IIMU: ROAD TO FIRST-IN-HUMAN CLINICAL STUDY

Ken-ichi Nishijima¹, Sonji Zhao¹, Hiroki Matsumoto², Hiromichi Akizawa³,
Kazue Ohkura⁴, Toru Shiga¹, Kenji Hirata¹, Shiro Watanabe¹, Shozo Okamoto¹,
Nagara Tamaki¹ and Yuji Kuge¹.

¹ Hokkaido University, Sapporo, Japan, ² Nihon Medi-Physics Co. Ltd., Sodegaura, Japan, ³ Showa
Pharmaceutical University, Machida, Japan, ⁴ Faculty of Pharmaceutical Sciences, Health Sciences
University of Hokkaido, Japan

Objectives: Thymidine phosphorylase (TP) catalyzes the reversible phosphorolysis of thymidine to thymine and 2-deoxyribose-1-phosphate. TP expression correlates well with tumor malignancy, including infiltration metastasis, and overall poor survival. Moreover, TP is essential for the bioactivation of 5-fluorouracil and its prodrugs, including doxifluridine and capecitabine. Accordingly, *in vivo* imaging of TP activity would contribute not only to the estimation of tumor malignancy but also to the prediction of prognosis after treatment with the fluoropyrimidine-based anticancer drugs. We previously reported a radiolabeled uracil derivative, I-123-labeled 5-iodo-6-[(2-iminoimidazolidinyl)methyl]uracil ([¹²³I]IIMU) as a novel SPECT probe for TP. A clinical study to verify the safety of [¹²³I]IIMU injection was approved by the Institutional Review Board of Hokkaido University Hospital for Clinical Research, and the first-in-human (FIH) clinical study on healthy adults was started. In this seminar, we would like to introduce our researches, including the synthesis of [¹²³I]IIMU [1, 2] and the efficacy [3-5] and safety evaluation, toward the FIH clinical study, and also our preliminary results on the FIH clinical study.

Methods, Results and Discussion:

1. Radiosynthesis of [¹²³I]IIMU [1]: [¹²³I]IIMU was synthesized according to a method previously reported [2]. Briefly, [¹²³I]IIMU synthesis was achieved by radioiodination of the precursor, 6-[(2-iminoimidazolidinyl)methyl]uracil (HIMU-TFA) at the C-5 position with *N*-chlorosuccinimide / [¹²³I]NaI. The crude product was purified by RP-HPLC using a solvent system containing HCl, to obtain [¹²³I]IIMU-HCl. The radioactive fraction was sterilized through a 0.22 µm membrane filter. The radiochemical purity of [¹²³I]IIMU was determined with HPLC. Sterility tests and bacterial endotoxins tests were also performed. [¹²³I]IIMU for intravenous injection was prepared in 2.5 h with a yield of 205 ± 24 MBq (n=3). The radiochemical purities of [¹²³I]IIMU were found to be more than 99%. Sterility tests and bacterial endotoxins tests showed negative results. Thus, we successfully prepared [¹²³I]IIMU for intravenous injection with high purity. Results of quality control tests demonstrated that the [¹²³I]IIMU preparations were suitable for clinical studies.

2. *In vitro*, *in vivo* and SPECT/CT imaging studies [1, 3]: In *in vitro* and *in vivo* studies using [¹²⁵I]IIMU, high accumulation levels of radioactivity were observed in the tumor cells/tissues with high TP expression levels (A431), and low accumulation levels were observed in the tumor cells/tissues with low TP expression levels (AZ521). In SPECT/CT imaging studies, A431

tumors were clearly visualized 3 h after the injection of [^{123}I]IIMU. Furthermore, to assess whether IIMU imaging could predict the efficacy of capecitabine, we examined the correlation among TP expression levels, sensitivity to capecitabine, and accumulation levels of [^{123}I]IIMU in human colorectal cancer cell lines with different TP expression levels. The *in vitro* and *in vivo* studies showed that the accumulation levels of [^{123}I]IIMU in the tumor cells/tissues were correlated with TP expression levels, and effects of capecitabine were higher in the tumor with a high TP-expression than that with a low TP-expression. These results showed that [^{123}I]IIMU could be used not only as a SPECT probe estimating tumor malignancy, but also as an *in vivo* companion diagnostic agent for predicting the efficacy of capecitabine treatment.

3. Safety assessment: The human radiation absorbed dose was estimated as 17 $\mu\text{Sv}/\text{MBq}$ on the basis of the biodistribution data of [^{125}I]IIMU in normal mice. The no observed adverse effect level (NOAEL) for intravenous administration of non-radiolabeled IIMU to mice was higher than 1.8 mg/kg. The bacterial reverse mutation assay showed negative results. These results showed that [^{123}I]IIMU is an acceptable dosimetry and pharmacological safety at the dose required for SPECT imaging.

4. FIH clinical study: Healthy male volunteers were recruited for the FIH study and a subject (age: 20 years) was injected with 55 MBq of [^{123}I]IIMU. Whole-body planar images were acquired 1, 3, 6, 24 and 48 hr after the injection. Adverse events were not observed. The effective dose equivalent was estimated as 13 $\mu\text{Sv}/\text{MBq}$ with the highest radiation dose to the thyroid, followed by the liver.

Conclusions: Our findings indicate that [^{123}I]IIMU is desired to be developed as a diagnostic agent for imaging TP-expressing tumors. It was shown that [^{123}I]IIMU injection can be safely administered in clinical studies. Nuclear imaging with [^{123}I]IIMU is expected to provide useful information, such as estimation/determination of therapeutic effects of anticancer drugs, decision-making for a treatment plan, prognostic prediction, understanding of disease stages, and malignancy assessment, which is difficult to obtain by other conventional methods.

References: 1) Nishijima K., et al. *J Lablled Compd Radiopharm* **56S1**: S349 (2013). 2) Takahashi M., et al. *J Lablled Compd Radiopharm* **51**: 384-387 (2008). 3) Akizawa H., et al. *Nucl Med Biol* **37**:427-432 (2010). 4) Li H., et al. *Nucl Med Commun* **32**: 1211-1215 (2011). 5) Zhao S., et al. *Ann Nucl Med* **29**: 582-587 (2015)

PRODUCTION OF NON-CONVENTIONAL RADIONUCLIDES WITH EMPHASIS ON TARGETRY SYSTEM DEVELOPMENT

K. Nagatsu^{1,*}, K. Minegishi^{1,2}, H. Suzuki¹, T. Ohya¹, M. Fukada¹, M. Hanyu¹,
K. Kawamura¹ and M-R. Zhang¹

¹ Molecular Imaging Center, National Institute of Radiological Institute, Chiba 263-8555, JAPAN

² Neos Tech Co., Ltd., Chiba 260-0027, JAPAN

Objectives: Radio-metals and radio-halogens in conjunction with specifically functionalized agents play prominent roles in both fields of diagnostic imaging (PET, SPECT) and targeted radionuclide therapy (TRT). Due to the shelf-life issue, radionuclides with relatively longer half-lives are only available commercially, and a number of them is unfortunately limited. However, the demands of clinically important or specifically interested nuclides, for example, ¹²⁴I, ⁶⁴Cu, ⁸⁹Zr, or ²¹¹At, are high and emerging. Thus, we have promoted to establish the efficient production method including targetry development for providing these non-conventional radionuclides routinely.

To carry out robust activation, the target material should be placed on the beam trajectory with keeping its thickness during the bombardment. However, in a conventional system where the beam is provided horizontally, targets with physical property of low melting point or thermally sensitive ones are frequently deformed or lost their position when bombarded at relatively higher beam intensity. Consequently, the production results may be unstable or decrease in their yields. In order to increase production reliability, we thus developed a vertical irradiation system, where any forms of target including easily deforming solid targets can be irradiated under desired condition by the aid of gravity.

Methods: The vertical beam station was installed on the basement floor, and the beam extracted from cyclotron was provided vertically by using a 90°-bending magnet placed on the ground level. The beam station, which can hold up to four different targets on a turn-around table, is operated remotely. We have designed two types of target holder, namely a capsulated crucible made of inert metals and a vertically-oriented vessel made of ceramics [1–3]. The difference between two holders is derived from the way of recovery for individual radionuclides interested. The former is designed as small as possible in its volume that is favorable scale for the recovery of volatile nuclides, e.g., ¹²⁴I, ⁷⁶Br, or ²¹¹At, by dry-distillation method. Meanwhile, the ceramic-vessel is intended to produce radiometals remotely from solid targets. The function expected to the ceramic-vessel is not only to hold the solid target literary, but also as a dissolving vessel being capable of corrosive solutions. Owing to chemical resistance of ceramics, the target in the vessel can be dissolved *in-situ* by introducing proper solutions directly. Consequently, we can obtain radioactive solution from immobile solid target without ionic contaminants eluted from the target vessel itself. Then, the solution is transferred easily to hotcell through a tubing without using any remote-handling or logistic systems.

We evaluated the feasibility of this concept through the productions of ⁸⁹Zr, ^{99m}Tc, ⁴³Sc, ⁶⁸Ge and ¹⁸⁶Re from their respective target materials, namely ^{nat}Y powder, ¹⁰⁰Mo powder, ^{nat}CaO powder, ^{nat}Ga piece, and ¹⁸⁶W powder.

Results and Discussion: Table 1 shows a part of radionuclides available in our institute. The produced radionuclides dissolved in suitable media were recovered to hotcell remotely, and purified to nearly 100% in both radiochemical and radionuclidic purity by automated apparatus developed by ourselves. The target yield for each production was well agreed with the value of theoretically estimated, and the efficiency of purification was also acceptable, likely 70% to 90%, within several hours of processing from the end of bombardment in many cases.

These radionuclides in suitable formulation have been successfully provided for wide applications, for instance, radiochemical studies, preclinical studies, and educational purpose [4].

Table 1 Available radionuclides produced by the vertical irradiation method

Nuclide	T _{1/2}	Decay	Route/ Energy/ Target	Target yield at EOB	
¹²⁴ I	100 h	β ⁺	¹²⁴ Te(p,n)/ 14 MeV/ ¹²⁴ TeO ₂ matrix	0.2 mCi/μAh	Capsulated
⁷⁶ Br	16 h	β ⁺	⁷⁶ Se(p,n)/ 14 MeV/ ⁷⁶ Ag ₂ Se matrix	2.0 mCi/μAh	Capsulated
²¹¹ At	7.2 h	α/EC	²⁰⁹ Bi(α,2n)/ 34 MeV/ ^{nat} Bi shots	0.6 mCi/μAh	Capsulated
⁸⁹ Zr	78 h	β ⁺	⁸⁹ Y(p,n)/ 15 MeV/ ^{nat} Y powder	1.5 mCi/μAh	Ceramic
^{99m} Tc	6.0 h	IT	¹⁰⁰ Mo(p,2n)/ 18 MeV/ ¹⁰⁰ Mo powder	6.0 mCi/μAh	Ceramic
⁴³ Sc	3.9 h	β ⁺	⁴⁰ Ca(α,x)/ 34 MeV/ ^{nat} CaO powder	1.4 mCi/μAh	Ceramic
⁶⁸ Ge	288 d	EC	⁶⁹ Ga(p,2n)/ 30 MeV/ ^{nat} Ga piece	0.03 mCi/μAh	Ceramic
¹⁸⁶ Re	3.7 d	β ⁺	¹⁸⁶ W(d,2n)/ 20 MeV/ ¹⁸⁶ W powder	0.1 mCi/μAh	Ceramic

Conclusion: The targetry system developed in this study and the subsequent purification systems showed good performance, and we have easily carried out the routine productions with less effort. Based on these results, we believe that the system described here has a great potential to produce other useful tracers. We will keep on not only producing the above nuclides routinely, but also developing the novel ways of production for upcoming ones. That would contribute toward our ultimate goal, establishment of the robust library of useful radionuclides.

References: [1] Nagatsu, K., et al. *Appl. Radiat. Isot.* **69**: 146–157 (2011); [2] Nagatsu, K., et al. *Nucl. Med. Biol.* **39**: 1281–1285 (2012); [3] Nagatsu, K., et al. *Appl. Radiat. Isot.* **94**: 363–371 (2014); [4] Washiyama, K., et al. *Japanese J. Radiol. Tech.* in press (2015)

Poster Presentations

P-01

A High Yield Automated Synthesis of [^{18}F] FMISO on PET-MF-2V-IT-I Synthera with SPE Purification

P. Zou, H. -Y. Wang, M. -H. Xie, Y. -L. Liu, J. Wu, H. Wu

Key Laboratory of Nuclear Medicine, Ministry of Health, Jiangsu Key Laboratory of Molecular Nuclear Medicine, Jiangsu Institute of Nuclear Medicine, Wuxi 214063, China

Objective: [^{18}F]FMISO (Fluoromisonidazole) is currently the most widely studied and validated PET (Positron Emission Tomography) radiotracer has been used for investigating tumor hypoxia. Due to favourable in vivo characteristics, its high specificity and the longer half-life of ^{18}F (109.8 min) allowing for remote-site delivery, [^{18}F]FMISO has gained increased importance for molecular imaging of tumors. An automated and optimized synthesis of [^{18}F]FMISO has been developed on the PET-MF-2V-IT-I synthera (PET CO.,LTD., China), utilizing purification with solid phase extraction (SPE) cartridges. The suggested SPE purification using the reverse phase or strong cation exchange cartridges provided [^{18}F]FMISO in high purity and radiochemical yield.

Method:

2'-Nitro-1'-imidazolyl)-2-O-acetyl-3-O-tosylpropanol (NITTP, the precursor for [^{18}F]FMISO synthesis) was synthesized according to the method of Cherif et al. [^{18}F]Fluoride (352MBq) was trapped on a QMA cartridge and eluted with $\text{K}_2\text{S}_2\text{O}_8/\text{K}_2\text{CO}_3$ solution. The eluted ^{18}F solution in dry acetonitrile at 120°C for 5min under a flow of nitrogen. To the dried complex, the precursor NITTP in acetonitrile was added and the reaction mixture heated at 100°C for 10 min. Hydrochloric acid (1 M) was thereafter added and hydrolysis of the labelled product was conducted at 105°C for 2 min. Then, sodium hydroxide (1 M) was added, stirred, neutralized. After synthesis, the mixture containing the labelled product was then passed over the Alumina N cartridges. The reaction mixture was diluted with H_2O (20 mL) and transferred to (1) a Sep-Pak C18 cartridge, (2) a Sep-Pak Silica cartridge, (3) a Sep-Pak CM cartridge, or (4) a Sep-Pak PS-2 cartridge to trap [^{18}F]FMISO. Next, the amount of radioactivity deposited on the different cartridges was compared to calculate the trapping efficiency. The [^{18}F]FMISO was eluted with ethanol solution (2 mL) and a sterile filter into the product vial, respectively.

Result and Discussion:

[¹⁸F]FMISO was prepared starting from the precursor NITTP, the PET-MF-2V-IT-I synthera was used with the only change of content of reagent vials and cartridges for purification. In this method, only 5 mg NITTP was used, but it give a high yied of [¹⁸F]FMISO and low amount of by-products. In other reports, 10 mg of the precursor NITTP was used.

Four Sep-Pak cartridges (C18, CM, Silica, PS-2) were tested for purification in these experiments, the automated synthesis of [¹⁸F]FMISO results in a synthesis yield of 23%, 52%, 38% and 16% (EOS), respectively. The radiochemical purity was $\geq 98\%$. The total synthesis time was 25min by using only cartridge purification, and no subsequent HPLC purification as previously reported. The CM cartridge was shown to be the most useful in this application.

Conclusion:

We have developed an automated robotic method of synthesis of [¹⁸F]FMISO with high radiochemical yield and a low amount of the precursor. The use of PET-MF-2V-IT-I synthera and cartridge purification simplifies the handling ant shortens the total synthesis time.

Preliminary Evaluation of a Novel ^{18}F -labeled affibody for HER2 Imaging

M. Yang^{1,2,3*}, Y. -P. Xu¹, Z.-C. Bai², P.-J. Zhang³, D.-H. Pan¹, L.-Z. Wang¹

¹ Key Laboratory of Nuclear Medicine, Ministry of Health, Jiangsu Key Laboratory of Molecular Nuclear Medicine, Jiangsu Institute of Nuclear Medicine, 20 Qianrong Road, Wuxi 214063, China

² Department of Radiation Oncology, The First Affiliated Hospital of Nanjing Medical University, 300 Guangzhou Road, Nanjing 210029, China

³ School of Pharmaceutical Science, Zhengzhou University, Zhengzhou 450000, China

Objective: Human epidermal growth factor receptor 2 (HER2) is a potential target for diagnosis and therapy of the tumor. An affibody protein with strong binding affinity for HER2, ZHER_{2:342}, has been reported. Previous study showed that ^{18}F -FBEM labeled ZHER_{2:342}-Cys was a promising PET imaging probe for targeting HER2, however, the time-consuming synthetic procedure and unfavourable abdominal background may hamper the translation of the probe. GGGRDN is a new hydrophilic linker and improve the pharmacokinetic quality of peptides. In this study, ZHER_{2:342}-NDRGGG-Cys (denoted as MZHER) was designed and the HER2 targeting potential of ^{18}F labeled NOTA-MAL-MZHER was evaluated.

Results and Discussion

1. Synthesis of NOTA-MAL-MZHER

MZHER was conjugated with MAL-NOTA under standard reaction conditions as previously described. The desired fractions were combined and lyophilized to afford the final product as a white powder. NOTA-MAL-MZHER was obtained in 40 % yield and confirmed by MS.

2 Preparation of ^{18}F -Al-NOTA-MAL- MZHER

NOTA-MAL- MZHER was labeled by ^{18}F -Al in one-step method within 20 min with a yield about 10%. The radiochemical purity was > 95%. Compared with ^{18}F -FBEM- ZHER_{2:342} -Cys, the procedures of labeling was greatly simplified and the yields was improved (10% vs 6.5%).

3. PET Imaging

The HER2 targeting of ^{18}F -Al-NOTA-MAL- MZHER was assessed in Balb/c nude mice bearing HER2 positive expressing Hela tumors and HER2 negative expressing MCF-7 tumors. Hela tumors were clearly visualized with good contrast to background through microPET. On the contrast, MCF-7 xenografts were barely visible by microPET. At 60 min postinjection, the average tumor uptakes of ^{18}F -Al-NOTA-MAL- MZHER in Hela and MCF-7 tumors were $4.19 \pm 1.43\% \text{ID/g}$ and $0.56 \pm 0.31\% \text{ID/g}$ respectively. It preliminarily proved the specificity of ^{18}F -Al-NOTA-MAL- MZHER towards HER2.

At 60 min postinjection, the liver uptakes were $3.53 \pm 0.59 \% \text{ID/g}$ and $1.80 \pm 0.63 \% \text{ID/g}$ respectively, which were significantly lower than those of ^{18}F -FBEM- ZHER_{2:342} -Cys ($5.04 \pm 0.69\% \text{ID/g}$). ROI analysis also showed that the kidneys uptakes of ^{18}F -Al-NOTA-MAL- MZHER was greatly higher than those of ^{18}F -FBEM- ZHER_{2:342} -Cys ($185.89 \pm 39.53\% \text{ID/g}$, $120.69 \pm 32.03\% \text{ID/g}$ vs $14.08 \pm 0.05 \% \text{ID/g}$). It suggested that ^{18}F -Al-NOTA-MAL- MZHER may own better pharmacokinetic than those of ^{18}F -FBEM- ZHER_{2:342} -Cys, which may be benefit for tumor diagnosis.

Conclusion

^{18}F -Al-NOTA-MAL-MZHER appears to be a promising candidate for HER2-positive tumor imaging with favorable preclinical results.

Acknowledgements

This work was supported by National Natural Science Foundation (81171399, 51473071, 81101077, 21401084, 81401450 and 81472749), Jiangsu Province Foundation (BE2014609, BE2012622, BL2012031 and BM2012066) and Wuxi Foundation (CSZ0N1320).

Reference:

- 1) Xu YP et al, *Mol Imaging Biol* **16**:578-585(2014);
- 2) Yang M et al, *Theranostics* **1**:220-229(2011);
- 3) Kramer-Marek G et al, *Eur J Nucl Med Mol Imaging* **35**:1008-1018.

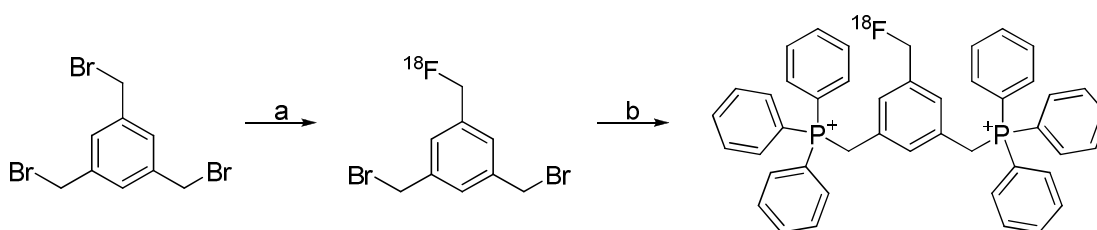
A NOVEL ^{18}F -LABELED PHOSPHONIUM DICATION AS A POTENTIAL PET AGENT FOR TUMOR IMAGING

Hua Li, Zijong Li*, Xianzhong Zhang*

Center for Molecular Imaging and Translational Medicine, School of Public Health, Xiamen University, Xiang'an South Rd, Xiamen, 361102, PR China

Objectives: The mitochondrial transmembrane potential in carcinoma cells is significantly higher than normal epithelial cells, which could be considered as an important characteristic to detect carcinoma cells and image tumors. Since plasma and mitochondrial potentials are negative, delocalized organic cations could be electrophoretically driven through these membranes, and localize in the energized mitochondria of tumor cells. However, diagnostic and prognostic values of most of the cationic molecular probes reported until now are often limited due to their insufficient tumor localization (low radiotracer tumor uptake) and high radioactivity accumulation in the chest and abdominal regions (low tumor selectivity)^[1]. To conquering those shortcomings, we designed and synthesized the ^{18}F -labeled molecules with two phosphonium cations, which had a higher affinity to mitochondria than that with one cation.

Methods: All the synthesized compounds were characterized by ^1H -NMR, ^{13}C -NMR, HRMS. The ^{18}F labelled intermediate was synthesized according to the reported procedures^[2] with a little modification. The log D value of the ligand was determined at pH 7.4. *In vivo* biodistribution studies were performed in female ICR mice.



Scheme 1. ^{18}F labeling route: a. K^{18}F , K_{222} , CH_3CN , $100\text{ }^\circ\text{C}$, 6 min, purified with HPLC; b. triphenylphosphine, CH_3CN , $90\text{ }^\circ\text{C}$, 15 min, purified with HPLC.

Results and Discussion: The ^{18}F labeled phosphonium dication probe has been successfully prepared without time and energy consuming precursor synthesis in this study, with the log D value determined to be 0.5. In conclusion, a two-step synthetic route with excellent yields to the ^{18}F labeled phosphonium dication has been developed. Further evaluations of this dication supposed to have higher tumor uptakes and selectivity for tumors is undergoing.

Reference: [1] Chang-Tong Yang et al., *Bioconjugate Chem.* 2008, 19, 2008–2022; [2] Zuoquan Zhao et al., *Mol. Pharmaceutics* 2014, 11, 3823–3831.

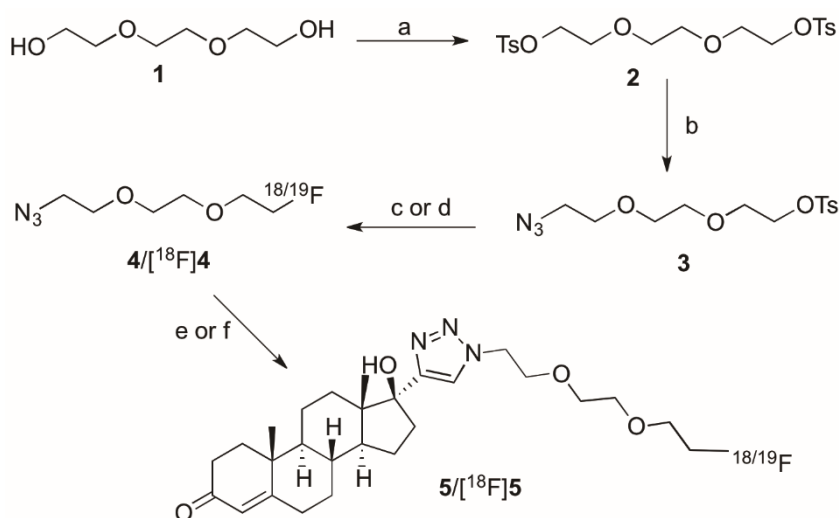
SYNTHESIS AND EVALUATION OF A NOVEL PROGESTERONE RECEPTOR PET PROBE FOR BREAST CANCER IMAGING

Xiaowei Wu, Zijing Li*, Xianzhong Zhang*

Center for Molecular Imaging and Translational Medicine, School of Public Health, Xiamen University, Xiang'an South Rd, Xiamen, 361102, PR China

Objectives: The breast cancer is a serious threat to women's health, and its early diagnosis can effectively reduce the mortality rate of the patients. However, the high heterogeneity of breast cancer, as well as its many kinds of tissue subtypes demands different clinical manifestations, therapeutic response and prognosis. Molecular typing of tumor through comprehensive molecular techniques will provide key information for the classification of tumors, and make tumor classification based on morphological steering on molecular characteristics^[1]. In this study, we designed a novel probe based on the ethisterone structure targeting progesterone receptor (PR) to discover breast cancer in the early stage and supply useful information for breast cancer subtyping.

Methods: The synthetic routes of the reference compound **5** and the ¹⁸F labeled [¹⁸F]**5** are shown in Scheme 1. All the synthesized compounds were characterized by ¹H-NMR, ¹³C-NMR and MS.



Scheme 1. Reagents and conditions: a. TsCl, CH₂Cl₂, NaOH, r.t. b. NaN₃, ACN, 3 h, r.t. c. KF, K₂₂₂, ACN, 80 °C, overnight. d. K¹⁸F, K₂₂₂, ACN, 80 °C, 20 min. e. CuI, DIPEA, THF, 60 °C, 3 h. f. CuI, DIPEA, THF, 60 °C, 20 min.

Results and Discussion: Yields of 85 % and 90 % for **3** and **4** were achieved, respectively. The [¹⁸F]**5** were synthesized according to the reported procedures^[2] with a little modification, and [¹⁸F]**5** was achieved by reaction between [¹⁸F]**4** and ethisterone in 55 % yield. These early stage results indicate the synthesis and labeling of this new potential PET agent is successful. The imaging on the PR positive animals is undergoing.

References: [1] Achim T. Reibel et al., *Biomacromolecules* 2015, 16, 842–851; [2] Suping Bai et al., *J. Med. Chem.* 2014, 57, 4239–4251

CLICK FOR PET: RAPID AND EFFICIENT 1,3-DIPOLAR CYCLOADDITIONS WITH 2-¹⁸F]FLUOROETHYL AZIDE

Lina Jia¹, Lan Zhang^{1,*}

¹Department of Radiochemistry and Engineering, Shanghai Institute of Applied Physics, Chinese Academy of Sciences (CAS), Shanghai 201800, China.

Introduction: The copper (I) catalyzed 1,3-dipolar cycloaddition between azides and alkynes (CuAAC) to form 1,2,3-triazoles is the most well-known ‘click reaction’ and nearly became synonymous with the concept of click chemistry. The click reaction meets the need for requirements in the preparation of radiopharmaceuticals, especially for radiopharmaceuticals with short half-life nuclides (e.g. PET probes) because of its mild reaction conditions, tolerance of solvents and pH, high chemoselectivity and perfect regioselectivity. Besides, many click synthons have been developed, especially 2-¹⁸F]Fluoroethylazide ([¹⁸F]FEA). It can be extensively used because of short radiolabeling time, high labeling and distillation efficiency, and simple structure. Therefore, this reaction was introduced into the field of ¹⁸F- radiopharmaceutical preparation and achieved great success.

The work of our group aimed for radiolabeling of target molecules with the advantages of click reaction and developing simple and efficient preparation techniques of PET probes (Figure 1). Furthermore, the screening of PET probes was conducted through biological evaluation for the investigation of their clinical value.

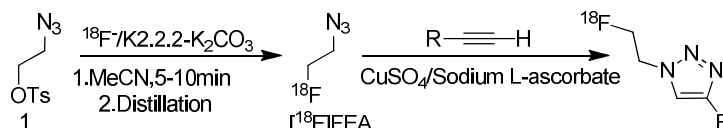


Figure 1. Radiosynthesis of [¹⁸F]FEA and [¹⁸F]-1,2,3-triazole with CuAAC reaction.

1. Click Radiolabeling of RGD Peptide and Biological Evaluation in Mice Bearing U87MG Tumors

The terminal alkynyl modified propioloyl RGDfK was labeled with [¹⁸F]FEA. [¹⁸F]FEA was prepared by nucleophilic radiofluorination of 2-azidoethyl 4-toluenesulfonate (1) with radiochemical yield of $71 \pm 4\%$ ($n = 5$, decay-corrected). We assessed the conditions of the CuAAC reaction which included peptide concentration, reaction time, temperature and catalyst dosage. The ¹⁸F-labeled-RGD peptide ([¹⁸F]F-RGDfK) could be obtained in 60 min with total radiochemical yield of $60 \pm 2\%$ ($n = 3$, decay-corrected). [¹⁸F]F-RGDfK showed high stability in phosphate buffered saline and new-born calf serum. Micro-PET imaging at 1 h post injection of [¹⁸F]F-RGDfK showed medium concentration of radioactivity in tumors while much decreased concentration in tumors in the blocking group. These results showed that [¹⁸F]F-RGDfK obtained by click chemistry maintained the affinity and specificity

of the RGDfK peptide to integrin $\alpha v\beta 3$. This study provided useful information for peptide radiofluorination with click chemistry.

2. Click Radiolabeling and Preliminary Evaluation of Bile Acid Compounds

Bile acids serve as signaling molecules and are recognized by many receptors, including the G-protein-coupled receptor (GPCR, also known as TGR5), farnesoid-X-receptor (FXR, NR1H4), which closely associated with the occurrence and development of certain diseases. Therefore, the PET probes ^{18}F -CDCA targeting FXR and ^{18}F -LCA targeting TGR5 were synthesized with CuAAC.

^{18}F -CDCA was prepared with a high decay-corrected radiochemical yield ($74\pm 2\%$), high radiochemical purity ($>99\%$), and high specific activity ($>320\text{ GBq}/\mu\text{mol}$) and the overall synthesis time, including HPLC purification, was 70-80 min. ^{18}F -CDCA had a high metabolic stability in vitro and in vivo. PET imaging studies in nude mice indicated a rapid uptake of ^{18}F -CDCA into liver tissue with uniform distribution of radioactivity and a suitable clearance time in the liver which was beneficial for PET imaging in the liver. Thus, it is potential for early detection of abnormalities in the liver and staging of neoplasms with ^{18}F -CDCA.

^{18}F -LCA was also obtained with a high radiochemical yield ($66\sim 74\%$), high radiochemical purity ($>99\%$), and high specific activity ($>300\text{ GBq}/\mu\text{mol}$). ^{18}F -LCA had a similar lipophilicity to the parental bile acid lithocholic acid and a high metabolic stability in vitro. This work made a solid foundation for further study the ^{18}F -LCA as the PET probe for the tumors of TGR5-overexpression.

3. Multi-click in One Pot for ^{18}F -Labeling of Small Molecules

A novel strategy for labeling multiple ^{18}F -PET probes in one pot has been developed for PET probes screening and preclinical studies (Figure 2). In this study, $[^{18}\text{F}]\text{FEA}$ was selected as the prosthetic group, $\text{CuSO}_4/\text{Sodium L-ascorbate}$ was selected as the catalytic system. It simply requires the addition of equal amount of multiple terminal alkynyl precursors to the click reaction system, and then multiple PET probes could be prepared in one pot under mild reaction conditions after separation with appropriate HPLC gradients in a single run. If combined with high throughput screening, the discovery of high-efficiency PET probes may be accelerated.

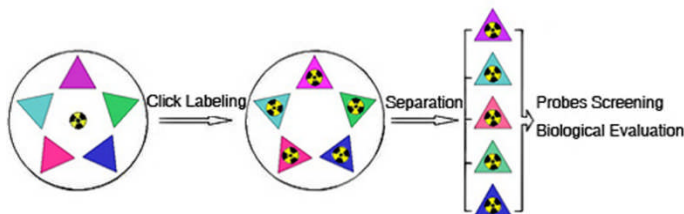


Figure 2. ‘One pot method’ strategy for labeling multiple probes.

Conclusion: In this line, click chemistry was shown to be a powerful labeling tool for radio-probe synthesis. Our group has taken full advantage of this reaction for developing new PET probes and labeling strategy, and obtained achievement in the radiolabeling of peptide and small molecules. Click

chemistry would allow the chemoselective radiolabeling under mild conditions of a broad range of appropriately functionalized compounds in a very versatile and flexible way which will make it has a wider application prospects.

References: Meldal M., et al. 1) Chem Rev 108: 2952-3015 (2008). Li J., et al. 2) Bioorg Med Chem 20: 3850-3855 (2012). Jia L., et al. 3) Nucl Med Biol 41: 495-500 (2014). Jia L., et al. 4) Appl Radiat Isot 75: 64-70 (2013).

Transport mechanism and androgen-stimulated uptake of the amino acid PET tracer [¹⁸F]fluciclovine (anti-[¹⁸F]FACBC) in primary and castration-resistant prostate cancer cells

Ono M^{1,2}, Okudaira H¹, Oka S¹, Nakanishi T³, Mizokami A⁴, Kobayashi M⁵, Yoshimura H¹, Kawai K²

¹Research Center, Nihon Medi-Physics Co., Ltd., Chiba, Japan; ²Division of Health Sciences, Graduate School of Medical Sciences, Kanazawa University, Ishikawa, Japan; ³Department of Membrane Transport and Biopharmaceutics, Faculty of Pharmaceutical Sciences, Kanazawa University, Ishikawa, Japan; ⁴Department of Integrative Cancer Therapy and Urology, Graduate School of Medical Sciences, Kanazawa University, Ishikawa, Japan; ⁵Wellness Promotion Science Center, Institute of Medical, Pharmaceutical and Health Science, Kanazawa University, Ishikawa, Japan

Abstract

Objectives: Positron emission tomography (PET) enables the non-invasive detection of lesion localization and therapy evaluation in patients with prostate cancer (PCa). Androgens are key regulators in PCa progression, and chemical castration therapy is often used clinically. However, more than half of patients with PCa develop castration-resistant prostate cancer (CRPC), which has a poor prognosis, within several years following castration treatment. In addition, androgen-related signaling is thought to be maintained after PCa converts to CRPC. Here, we investigated the transport mechanism and effect of androgen treatment in vitro to assess the potential clinical utility of the amino acid PET tracer [¹⁸F]fluciclovine (also known as anti-[¹⁸F]FACBC) in CRPC diagnosis.

Methods: [¹⁴C]fluciclovine was used in this study as a surrogate for [¹⁸F]fluciclovine because the half-life of ¹⁴C (5700 years) is longer than that of ¹⁸F (110 min), making it more convenient for in vitro experiments. We investigated amino acid-transporter expression and [¹⁴C]fluciclovine uptake in the androgen receptor-positive PCa cell line LNCaP and in CRPC cells cultured in the presence or absence of the androgen (5 α -dihydrotestosterone; DHT).

Results: Ion-dependency and inhibition studies showed that the Na⁺-dependent amino acid transporter ASCT2 mediated intracellular [¹⁴C]fluciclovine uptake in both cell types. We then confirmed that ASCT2 was expressed in both cell types and showed that it mediated [¹⁴C]fluciclovine uptake. Furthermore, DHT stimulated ASCT2 expression and [¹⁴C]fluciclovine uptake, especially in LNCaP cells.

Conclusions: We conclude that ASCT2 can play a major role in [¹⁴C]fluciclovine uptake in androgen-dependent PCa and CRPC cells regardless of androgen dependency, suggesting that [¹⁸F]fluciclovine-PET may be applicable for the detection of primary PCa and CRPC. Further clinical studies are needed to assess the efficacy of [¹⁸F]fluciclovine-PET for CRPC diagnosis.

DEVELOPMENT OF A LOW COST MULTIPURPOSE SYNTHESIS SYSTEM FOR F-18 PET TRACERS

Tetsuya Mori¹, Masaki Kunieda², Yasuhisa Fujibayashi³, Hidehiko Okazawa¹, Yasushi Kiyono¹

¹ Biomedical Imaging Research Center, University of Fukui, Fukui 910-1193, Japan

² Department of Nuclear Power and Energy Safety Engineering, School of Engineering, University of Fukui, Fukui 910-8507, Japan

³ Molecular Imaging Center, National Institute of Radiological Sciences, Chiba 263-8555, Japan

Objectives: Automated synthesizer is necessary for translational research of PET tracers because it has advantages such as reproducibility production and workers exposure reduction. Most of the synthesizers for clinical use have a high performance, but are expensive. Therefore, we have designed a flexible module system at low cost for preclinical studies using commercially available servomotors for hobby robot kits. The system was realized to control plastic three-way valves, plastic syringes and I/O units for external devices. In order to enhance the usefulness of the system, we designed a F-18 labeling module and a purification module using solid phase extraction. In this study, we optimized the synthesis of 16 β -[¹⁸F]fluoro-5 α -dihydrotestosterone (FDHT) and 16 α -[¹⁸F]fluoro-17 β -estradiol (FES) and [¹⁸F]fluoroacetate (FA) as examples.

Results and Discussion:

Modules: The labeling module was consisted of a 10 mL plastic syringe, seven plastic three-way valves and a heater unit. The additional unit was included two valves. The purification module was consisted of one syringe unit and six valve units. The reactor was used a standard 10 mL vial and all wetted parts were utilized medical devices and disposable sterile materials.

Radiosynthesis of FDHT: The FDHT synthesis was started from 2 mg of 16 β -[[(trifluoromethyl)sulfonyl]oxy]-3,3-(ethylenedioxy) androstan-17-one in acetonitrile and it was labeled with purified F-18 in K₂CO₃/kryptofix 222 mixture at 110°C for 8 min. Then 1.5 mg of NaBH₄ in ethanol was added to the reacted solution and the hydrolysis was carried out using HCl at 95°C for 5 min.

The reduction using NaBH₄ was completed in less than 10 min. The hydrolysis was inadequacy using 0.1M HCl but it was accomplished using 1 M HCl. The labeling yield was 27% (decay corrected) in analytical HPLC.

Radiosynthesis of FES: The FES synthesis was started from 1 mg of 3-O-Methoxymethyl-16,17-O-sulfuryl-16-epistriol in acetonitrile and it was labeled with dried [¹⁸F]KF at 110°C for 8 min. Added 0.2N hydrochloric acid in 90% acetonitrile (2 mL) and heated at 95°C for 5 min. The labeling yield was 43% (decay corrected) in analytical HPLC. The yield using this module was comparable to the yield using a clinical synthesizer.

Radiosynthesis of FA: The FA synthesis was started from 5 mg of O-mesyl glycolate in acetonitrile and it was labeled with purified F-18 in K_2CO_3 /kryptofix 222 mixture at 110°C for 5 min. The intermediate compound, ethyl [^{18}F]FA, was hydrolysis with 1N NaOH on Oasis HLB cartridges for 7 min and then eluted to a final vial.

In the labeling process, the amount of K_2CO_3 had a remarkable influence on the yield of ethyl [^{18}F]FA and smaller amount of K_2CO_3 was suitable. The optimized procedure was achieved with a high and reproducible radiochemical yield was 53% (decay corrected) within 55 min. The radiochemical purity of the product was greater than 95%.

Conclusions: The system helped the study of the optimum conditions for the synthesis and realized multi probe synthesis. Therefore, the convenient system may help the research of the PET tracer development.

IN VITRO AND IN VIVO CHARACTERIZATION OF [¹⁸F]INTERLEUKIN-8 PRODUCED BY A CELL-FREE TRANSLATION SYSTEM AND [¹⁸F]FLUORO-L-PROLINE

Ryuichi Harada¹, Shozo Furumoto², Tago Tetsuro², Ren Iwata², Takeo Yoshikawa¹, Nobuyuki Okamura¹, Kazuhiko Yanai^{1, 2}

¹Department of Pharmacology, Tohoku University Graduate School of Medicine, Sendai, 980-8575, Japan, ²Cyclotron and Radioisotope Center, Tohoku University, Sendai Japan

Objectives: Recent advances in the development of biopharmaceutical products enable the specific target engagement, resulting in increasing interest for use of them as PET tracers. We previously proposed a novel strategy for preparing of proteins labeled with carbon-11 using a cell free translation system with [¹¹C]methionine. However, macromolecules tend to show slower kinetics *in vivo*, requiring a longer scanning time to acquire high contrast image. Therefore, fluorine-18, having a longer half-life than carbon-11, would be more useful as a nuclide for radiolabeling of the macromolecules. In this study, we applied the cell-free translation system to radiosynthesis of [¹⁸F]interleukin-8 ([¹⁸F]IL-8) with 4-[¹⁸F]fluoro-L-proline (FPro) to proof the utility of the system as a novel method for labeling proteins with ¹⁸F.

Results and Discussion:

1. Synthesis of IL-8 containing FPro by using a cell-free translation system

We investigated some fluorinated amino acids that can be incorporated into proteins and easily labeled with fluorine-18 because non-natural amino acids are generally not incorporated into proteins. The reaction mixture containing template DNA, a commercial available cell-free translation system PURExpress® reagents, and FPro instead of natural L-proline was reacted at 37 °C for 120 min. Western blot analysis using anti-IL-8 antibody demonstrated a 10 kDa band was observed, which corresponds to the molecular weight of IL-8. In addition, the incorporation of FPro into IL-8 was confirmed by MALDI-TOF mass spectrometry.

2. Radiosynthesis of *trans*-4-[¹⁸F]fluoro-L-proline

Trans-4-[¹⁸F]FPro was radiosynthesized using the corresponding tosylate precursor (3 mg). Aqueous ¹⁸F⁻ contained in K₂CO₃ solution (1.0–1.5 GBq, 0.5 mL) and Kryptofix222 (16 mg) were placed in a vial. After drying by azeotropic evaporation with acetonitrile, the activated [¹⁸F]KF/Kryptofix222 was reacted with the precursor (3 mg) in DMSO (0.7 mL) at 110°C for 10 min. After deprotection and purification by semi-preparative HPLC, *trans*-4-[¹⁸F]FPro was obtained with radiochemical purity of >95% and the decay-corrected radiochemical yield of 30-40%.

3. Radiosynthesis of [¹⁸F]interleukin-8

As described above, the reaction mixture was reacted in the addition of [¹⁸F]FPro instead of unlabeled FPro at 37 °C for 15, 30, 60, 90, 120 min. Gel-ARG analysis demonstrated that a radioactive band at

10kDa of [^{18}F]IL-8 increased in time-dependent manner, but not saturate within 120 min, providing the low radiochemical yield (the decay-corrected radiochemical yield was less than 1.5%). A possible reason for the slow reaction is considered to be simply unreacted [^{18}F]FPro due to non-natural amino acids.

4. In vitro binding of [^{18}F]interleukin-8 to IL-8 receptor

After purification using conventional ion exchange spin column, we evaluated the binding nature of synthesized [^{18}F]IL-8 to IL-8 receptor *in vitro*. [^{18}F]IL-8 specifically bound to IL-8 receptor expressing CHO cells, but not control CHO cells. *In vitro* competitive binding analysis using [^{125}I]IL-8 indicated that K_i value of IL-8 FPro variant was less than 10 nM. These results demonstrated that the synthesized [^{18}F]IL-8 by this method was biologically active.

5. IL-8 receptor imaging in xenograft-bearing mice

To evaluate whether synthesized [^{18}F]IL-8 works *in vivo*, small animal PET imaging was conducted and compared with *trans*-4-[^{18}F]FPro for imaging of IL-8 receptor. [^{18}F]IL-8 showed largest uptake in the kidneys and then gradually accumulated in the bladder. [^{18}F]IL-8 showed specific uptake in IL-8 receptor xenograft, which was clearly visualized by PET as a high contrast image, whereas *trans*-4-[^{18}F]FPro showed no specific uptake in the IL-8 receptor xenograft.

Conclusion: [^{18}F]IL-8 produced by this method bound to IL-8 receptors *in vitro* and specifically accumulated in xenograft expressing IL-8 receptors *in vivo*. This technique may be a useful tool for labeling macromolecule and preclinical evaluation of interesting proteins *in vitro* and *in vivo*.

References: Harada R et al., Nucl Med Biol **39**: 155-160 (2012)

Carbon-11 Formaldehyde: Development of radiolabeling technique for carbon-11 labeled peptides

Masayuki Hanyu¹, Aya Sugyou², Atsushi B Tsuji², Kazunori Kawamura¹, Tsuneo Saga², Ming-Rong Zhang¹ and Toshimitsu Fukumura¹

¹Molecular Probe Program, ²Diagnostic Imaging Program, Molecular Imaging Center, National Institute of Radiological Science, 4-9-1 Anagawa, Inage-ku, Chiba 263-8555, Japan

Objectives

Some low molecular weight oligopeptides have been considered as potential imaging agents because they possessed good permeability properties that could permit rapid access to the target tissues. Radiolabeled peptides are becoming increasingly important in nuclear oncology, where they are used in the diagnosis and treatment of several different cancers. One of the main challenges of PET for radiochemists is the development of rapid synthetic methods for the introduction of short-lived positron-emitting radionuclides into the peptide of interest.

[¹¹C]Formaldehyde has been used as a carbon-11 labeling agent for compounds required in PET studies. Several methods have been reported for the preparation of [¹¹C]formaldehyde from [¹¹C]MeOH by metal catalysis. For the reasons, the use of [¹¹C]formaldehyde has not been developed to any great extent because the current labeling approaches using [¹¹C]formaldehyde are generally inaccessible. Hooker *et al.* [1] recently reported the development of a facile method for the preparation of [¹¹C]formaldehyde. Furthermore, the treatment of tryptamine with [¹¹C]formaldehyde under acidic conditions provided [¹¹C]2,3,4,9-tetrahydro-1H- β -carboline in a good radiochemical yield. We envisaged that the treatment of Trp or Cys with [¹¹C]formaldehyde under acidic conditions would provide [1-¹¹C]1,2,3,4-tetrahydro- β -carboline-3-carboxylic acid ([1-¹¹C]Tpi, [¹¹C]**1**) or [2-¹¹C]ThioPro [¹¹C]**2** as well as several related analogues, respectively. Herein, we report the synthesis of carbon-11 radiolabeled oligopeptides via a cyclic reaction using [¹¹C]formaldehyde [2, 3].

Results and Discussion

The synthesis of [¹¹C]**1** was initially examined under the traditional acid catalyzed Pictet-Spengler conditions (cyclic reaction) using Trp and a solution of [¹¹C]formaldehyde in DMF. The radiosynthesis of [¹¹C]**1** was conducted by mixing a solution of [¹¹C]formaldehyde in DMF with a solution TsOH in DMF, and using Trp instead of tryptamine according to the previously described method [1]. The desired product was obtained with a moderate radiochemical conversion (RCC: 42.3 \pm 3.2%). Next, we proceeded to evaluate the Pictet-Spengler reaction using 1 mol/L HCl as the reaction solvent. Under these reaction conditions, the RCC of [¹¹C]**1** was found to be similar to those reported above. Interestingly, the Pictet-Spengler reaction was found to proceed smoothly when an aqueous solution of Trp•HCl was used without the addition of an acid catalyst to give the desired product in a 45.2% RCC. In the current study, the Pictet-Spengler reaction between [¹¹C]formaldehyde and Trp•HCl was

found to proceed in the absence of an additional acid catalyst when the materials were heated in aqueous DMF.

The radiosynthesis of [^{11}C]**2** was conducted by mixing a solution of [^{11}C]formaldehyde in DMF with Cys•HCl aqueous solution. The desired product was obtained with a RCC ($73.4\pm 4.6\%$). Thus, when Cys•HCl was used, it effectively provided the acid catalyst under trace amounts of [^{11}C]formaldehyde. This procedure represents an effective radiolabeling method because it requires particularly mild conditions.

Cyclic RGD peptides, such as cyclo[Arg-Gly-Asp-D-Tyr-Lys], are potent antagonists for the $\alpha\text{v}\beta 3$ integrin receptor. A variety of different cyclic RGD peptides conjugated to a radioactive tracer have been reported for the PET imaging of tumors that over-express the $\alpha\text{v}\beta 3$ integrin receptor. With this in mind and to establish further potential uses for our new labeling method, we investigated the application of our direct labeling method using [^{11}C]formaldehyde to the model cyclic RGD peptide cyclo[Arg-Gly-Asp-D-Tyr-Lys(Trp)] •HCl (**3**). The reaction of compound **3** with [^{11}C]formaldehyde under the conventional manual synthetic procedure proceeded smoothly to give the desired product cyclo[Arg-Gly-Asp-D-Tyr-Lys(1- ^{11}C Tpi)] ([^{11}C]**4**) with a RCC of $22.3\pm 4.3\%$. Interestingly, the guanidino, phenolic hydroxy, carboxylic acid and amide groups of cyclic RGD peptide remained intact under the reaction conditions. Although this method needs an oligopeptide having Trp residue on the terminal site except for the C-terminal side, a Trp residue can be easily introduced to the epsilon amino group of Lys residue or N-terminal amino acid residue. Based on this result, it is therefore clear that this procedure could be particularly effective for the direct formation of cyclic C-C bonds for the radiolabeling of oligopeptides. Further details about studies by remote-controlled radiosynthesis and PET will be reported.

We have successfully achieved the preparation of [^{11}C]**4** via a Pictet-Spengler reaction. This labeling reaction was completed under mild reaction conditions over a short reaction time in only one step using the HCl salt of the precursor without the need for a protecting group.

Reference

- [1] Hooker J. M. *et al. Angew. Chem. Int. Ed.* 2008; **47**: 5989-5992.
- [2] Hanyu, M. *et al. J. Pep. Sci.* 2013; **19**, 663-668. [3] *Peptide Science* 2013, 2014;181-182.

Quantitative PET for monitoring blood–brain barrier opening induced by focused ultrasound by 2-amino-[3-¹¹C]isobutyric acid

M. Okada¹, T. Kikuchi¹, T. Okamura¹, A. B Tsuji¹, H. Wakizaka¹, M.-R. Zhang¹, K. Kato²

¹Molecular Imaging Center, National Institute of Radiological Sciences, Chiba 263-8555, Japan;

²Department of Integrative Brain Imaging, National Center of Neurology and Psychiatry, Tokyo 187-8551, Japan

Objectives: The blood-brain barrier (BBB) plays an important role in protecting the central nervous system by restricting the entry of substances, and it also prevents the transport of therapeutic agencies. Several BBB-opening operation methods have been developed to improve the chemotherapeutic efficacy of cerebral diseases such as brain tumors. It is needed to monitor the BBB condition noninvasively, high sensitively and quantitatively and repeatedly to optimize the BBB-opening operation for effective chemotherapeutic strategies. We recently developed an efficient method for preparing ¹¹C-labeled 2-aminoisobutyric acid AIB ([3-¹¹C]AIB) ¹⁾, and we also reported that *in vivo* [3-¹¹C]AIB PET in rats opened BBB by focused ultrasound (FUS) and microbubbles visualized BBB-opened region ²⁾. In the present study, we evaluated the effect of FUS intensity on BBB permeability by *in vivo* [3-¹¹C]AIB PET.

Results and Discussion: The PET studies of [3-¹¹C]AIB in rats were conducted at 5 min after operation of BBB by 1-MHz FUS (0.33 and 0.49 MPa) with microbubbles. The uptake of [3-¹¹C]AIB in both 0.33- and 0.49-MPa-FUS-sonicated sides were significantly higher than that in each contralateral side and increased with time. The 0.49-MPa-FUS sonication resulted in higher uptake of [3-¹¹C]AIB than the 0.33-MPa-FUS sonication. The blood-to-brain influx rate constants (K_i) values were estimated from Patlak plots with the data of arterial plasma analysis and PET. The arterial plasma [3-¹¹C]AIB radioactivity rapidly decreased by 10 min, and then approximately 0.5% of injected dose per mL of radioactivity remained from 20 min to 60 min ²⁾. The K_i values of FUS-sonicated sides were significantly higher (4.1 and 7.3 $\mu\text{L/g/min}$ at 0.33 and 0.49 MPa, respectively) than those of the corresponding contralateral sides (1.7 and 1.8 $\mu\text{L/g/min}$ at 0.33 and 0.49 MPa, respectively). The BBB permeability status is affected by various FUS and microbubble condition such as FUS intensity, sonication duration, and concentration of microbubbles and moreover, these effects of FUS also differ among patients. Therefore, quantitative K_i value obtained by [3-¹¹C]AIB PET could be a useful indicator for optimizing the BBB-opening operation by FUS.

Conclusions: [3-¹¹C]AIB PET visualized the BBB-opened area noninvasively, high sensitively and quantitatively and could determine the quantitative K_i value as an indicator of BBB permeability.

Therefore, PET imaging with [3-¹¹C]AIB is a promising method for quantitative BBB permeability measurements.

References: 1) Kato K., *et al.* Bioorg Med Chem Lett **21**(8): 2437-40 (2011). 2) Okada M., *et al.* Nucl Med Commun *in press* (2015)

Synthesis and PET studies of 2-amino-2-[¹¹C]methyl-butanoic acid for tumor imaging

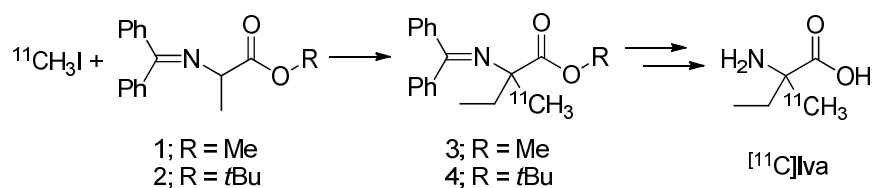
Kato Koichi^{1,2}, Suzuki Chie^{1,3}, Tsuji Atsushi B.¹, Sudo Hitomi¹, Zhang Ming-Rong¹, Arano Yasushi³, Saga Tsuneo¹ *1Molecular Imaging Center, National Institute of Radiological Sciences, Chiba, Japan; 2Department of Integrative Brain Imaging, National Center of Neurology and Psychiatry, Tokyo, Japan; 3Graduate School of Pharmaceutical Sciences, Chiba University, Chiba, Japan.*

Objectives: Isovaline (Iva) is an α,α -dialkylated unnatural amino acid and its ¹⁴C-labeled analog ([¹⁴C]Iva) shows high tumor uptake. The incorporation of carbon-11 into Iva structure would provide a promising PET probe for tumor-seeking however there was no report about ¹¹C-labeling synthesis of Iva. In this study, we synthesized 2-amino-2-[¹¹C]methyl-butanoic acid ([¹¹C]Iva) and evaluated its potential for a tumor imaging PET probe.

Results and discussion: ¹¹C-Methylation of benzophenone imine analog of 2-amino butyrate **1** and **2** using iodo[¹¹C]methane and subsequent hydrolyses were employed for the synthesis of [¹¹C]Iva (Scheme 1). We investigated the base-promoted ¹¹C-methylation reactions of **1** and **2** which were carried out at room temperature for 90 s. As seen in table 1 (entry 4), KO^tBu was effective for the methylation of **1**. We also investigated the additive effect of electron transfer inhibitor (TMB), radical scavenger (TEMPO), and organocatalyst for electron transfer (*o*-phen) for the ¹¹C-methylation to evaluate the electron transfer process which was frequently discussed in the reactions using KO^tBu. In the present case, the use TMB and TEMPO gave **3** in higher radiochemical conversions (entries 7 and 8), suggesting that the inhibition of radical generation induced by KO^tBu improved the ¹¹C-methylation of **1**. After several investigation for the subsequent hydrolyses, we chose **2** for the precursor of automated synthesis of [¹¹C]Iva. Replacement of methyl ester to corresponding *tert*-butyl analog realized simultaneous deprotection of imine and ester groups under the acidic condition, resulting in shorter total synthesis time and simple reaction operations. The hydrolyses of **4** with 2 M aqueous solution of HCl proceeded quantitatively at 100 °C for 5 min and the automated synthesis of [¹¹C]Iva was optimized. The total time of automated synthesis including the purification and formulation of [¹¹C]Iva was approximately 40 min. The radioactivity of [¹¹C]Iva was in the range 1.88–2.55 GBq, and radiochemical yield was in 10.3 ± 1.2% (decay uncorrected, relative to the calculated [¹¹C]carbon dioxide) when the synthesis was started from 18.5 to 22.2 GBq of [¹¹C]carbon dioxide at the end of bombardment. *In vitro* cell uptake of [¹¹C]Iva with and without several inhibitors of amino acid transporters was determined in SY cells at 37 °C. The uptake of [¹¹C]Iva into SY cells was increased time dependently and was almost completely inhibited by an inhibitor of system L-amino acid transporters (2-amino-2-norbornanecarboxylic acid) and a LAT1 inhibitor (2-methyl-*L*-tylosine) but not by inhibitors of system A (2-aminomethyl-isobutyric acid) and ASC (a mixture of alanine, serine, and cysteine). These results suggest that [¹¹C]Iva would be transported into cells mainly via LAT1,

which is a system L amino acid transporter and overexpresses widely in various types of tumors. Dynamic PET scan was performed for 90 min just after injection of [^{11}C]Iva into SY tumor bearing mice. PET results represented that [^{11}C]Iva was highly accumulated in SY tumors and the accumulation in non-tumor tissue except for pancreas, kidney, and bladder was much lower than tumor.

Conclusions: [^{11}C]Iva was synthesized with high radiochemical yield via ^{11}C -methylation assisted with KO t Bu and TMB or TEMPO. [^{11}C]Iva was a substrate for L-type amino acid transporters. [^{11}C]Iva has the potential for tumor imaging with high tumor-to-tissue contrast.



Scheme 1

Table 1. α - ^{11}C -Methylation of imine precursors

Entry	Precursor	Base (μmol)	Solvent	Additive (μmol)	RCC
1	1	TBAF (20)	DMSO	none	nd
2	1	TBAF (20)	THF	none	nd
3	1	TEA (10)	DMSO	none	nd
4	1	DBU (10)	DMSO	none	nd
5	1	KO t Bu (10)	DMSO	none	15.3 ± 4.9
6	1	KO t Bu (10)	THF	none	54.3 ± 6.9
7	1	KO t Bu (10)	THF	TMB (10)	80.6 ± 7.6
8	1	KO t Bu (10)	THF	TEMPO (10)	79.4 ± 5.0
9	1	KO t Bu (10)	THF	o -Phen (10)	1.2 ± 1.0
10	2	KO t Bu (10)	THF	TEMPO (10)	91.2 ± 5.1

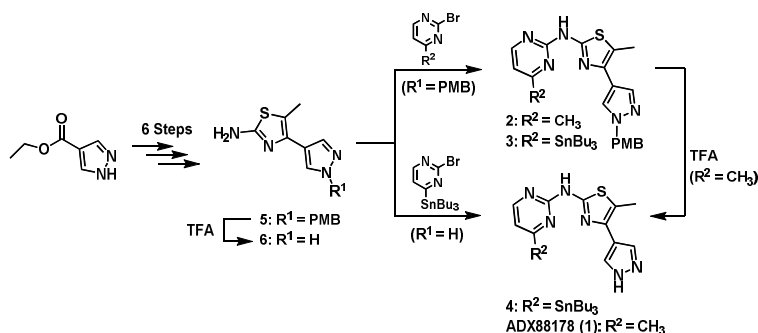
Radiosynthesis of [¹¹C]ADX88178 via direct [¹¹C]methylation as a novel radioligand for imaging of metabotropic glutamate receptor subtype 4

M. Fujinaga¹, T. Yamasaki¹, N. Nengaki^{1,2}, M. Ogawa^{1,2}, K. Kumata¹, Y. Shimoda¹, J. Yui¹, L. Xie¹,
Y. Zhang¹, K. Kawamura¹, M.-R. Zhang¹

¹Molecular Imaging Center, National Institute of Radiological Sciences, Chiba 263-
8555, Japan, ²SHI Accelerator Service Co. Ltd., Tokyo 141-8686, Japan

Objectives: Metabotropic glutamate receptors (mGluRs) are one of the G protein-coupled receptor families, which regulate excitatory neurotransmissions on the central nerves system (CNS). Of these, mGluR4 has received particular attention because of the potential therapeutic effect by mGluR4 activation in several CNS disorders. For example, several pharmaceuticals for mGluR4 were reported to show neuroprotective activity in models of Parkinson's disease, a degenerative disorder of dopaminergic neurons in the basal ganglia. However, to-date no appropriate mGluR4 PET ligand has been employed. Recently, ADX88178 (**1**) has been developed as a selective and potent positive allosteric modulator for metabotropic glutamate receptor 4¹⁾. To the best of our knowledge, [¹¹C]methylation of pyrimidine ring at 4- or 6-position has not been previously reported. The aim of this study was to challenge the introduction of [¹¹C]methyl group into pyrimidine ring and develop [¹¹C]**1** as a novel PET ligand for mGluR4.

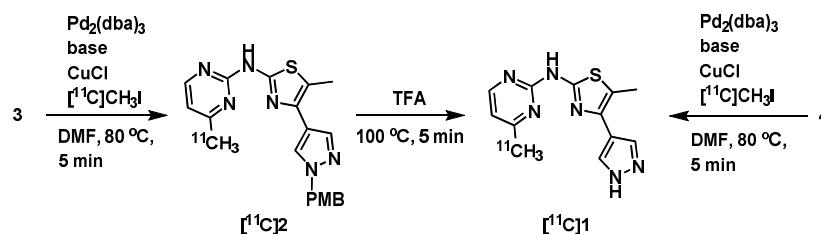
Results and Discussion: Compound **5** was prepared from ethyl 4-pyrazolecarboxylate at 6 steps as described previously²⁾. After deprotection of **5** with TFA, *N*-arylation reaction of thiazole derivatives **5** or **6** with 2-bromo-4-substituted pyrimidines in the presence of Pd(OAc)₂/Xanthophos afforded **2**, **3**, or **4** in moderate yields. Compound **1** was synthesized by debenzylation of **2** with TFA.



Scheme 1. Synthesis of ADX88178 (**1**), precursor **3** and **4** for mGluR4

Synthesis of [¹¹C]**1** was performed via C-[¹¹C]methylation reaction by using of two precursor. Firstly, C-[¹¹C]methylation of heteroarylstannane **4** was performed with [¹¹C]CH₃I in the presence of Pd₂(dba)₃, P(*o*-tol)₃, CuCl, and base at 80 °C for 5 min. When K₂CO₃ or CsF were used as a base, only trace [¹¹C]**1** was produced and unreacted [¹¹C]CH₃I was mainly observed. On the other hand, when C-

$[^{11}\text{C}]$ methylation of heteroarylstannane **3** was smoothly proceeded in the presence of CsF as a base. However, the following deletion of the PMB group in $[^{11}\text{C}]\mathbf{2}$ did not proceed by addition of TFA to the reaction mixture in DMF. When DMF was partly removed after $[^{11}\text{C}]$ -methylation, the deprotection with TFA produced a mixture of $[^{11}\text{C}]\mathbf{1}$ and $[^{11}\text{C}]\mathbf{2}$. To accomplish efficient deprotection of PMB in $[^{11}\text{C}]\mathbf{2}$, DMF was completely removed under reduced pressure after the C- ^{11}C coupling reaction. Finally, cleavage of the PMB group in $[^{11}\text{C}]\mathbf{2}$ proceeded efficiently in TFA at 100 °C for 5 min. Purification for the reaction mixtures using reversed phase semi-preparative HPLC gave $[^{11}\text{C}]\mathbf{1}$ in $16 \pm 6\%$ ($n = 5$) radiochemical yield at 2 steps (based on the total $[^{11}\text{C}]\text{CO}_2$, corrected for decay). Starting from 22 GBq of $[^{11}\text{C}]\text{CO}_2$, 0.54–1.10 GBq of $[^{11}\text{C}]\mathbf{1}$ was produced within 45 min of synthesis time from EOB. In the final product solutions, the radiochemical purity of $[^{11}\text{C}]\mathbf{1}$ was high than 98% and the purity remained >95% after 90 min.



Scheme 2. Synthesis of $[^{11}\text{C}]\mathbf{1}$ by 2 routes

In vitro autoradiography was performed with $[^{11}\text{C}]\mathbf{1}$ using rat brain sections. In the control section, radioactivity signals were detected in the cerebellum, striatum, thalamus, cerebral cortex, and medulla oblongata. In addition, the radioactivity expression was decreased by treatment with unlabeled **1**; a decrease of 12.3% for the cerebellum, 13.8% for the thalamus, 12.5% for the medulla oblongata, and 15.8% for the striatum. These distribution patterns of radioactivity in the control section were similar to the reported biological distribution pattern of mGluR4 in the rat brain. However, radioactivity was also seen in some mGluR4-negligible regions, such as the cerebral cortex and midbrain, suggesting that specific binding of $[^{11}\text{C}]\mathbf{1}$ may contain binding to other receptors.

Conclusions: We successfully synthesized $[^{11}\text{C}]\mathbf{1}$ as a novel radioligand for mGluR4 by 2 step reaction with C- $[^{11}\text{C}]$ methylation and debenzylation reaction. This labeling technique enables synthesis of PET ligands including electron-deficient $[^{11}\text{C}]$ methylpyrimidine or pyridine moieties. $[^{11}\text{C}]\mathbf{1}$ showed specific binding for mGluR4 in the in vitro autoradiogram of rat brain, although the specific binding of $[^{11}\text{C}]\mathbf{1}$ was not so high. Therefore, development of new candidates with higher binding affinity to mGluR4 than **1** is required.

References: 1) Emmanuel L. P, *et al*, *J. Pharm. Exp. Ther.*, **2012**, 343, 167-177.

2) Borea, C. WO 2010/079239.

DEVELOPMENTS OF NEW PET LIGANDS BASED ON 3-[5-(PYRIDINE-2-YL)-2H-TETRAZOL-2-YL]BENZONITRILE FOR METABOTROPIC GLUTAMATE RECEPTOR 5 (mGluR5) IMAGING

Y. Shimoda^{1,*}, T. Yamasaki¹, M. Fujinaga¹, M. Ogawa^{1,2}, Y. Kurihara^{1,2}, N. Nengaki^{1,2}, K. Kumata¹, J. Yui¹, A. Hatori¹, L. Xie¹, Y. Zhang¹, K. Kawamura¹, M. -R. Zhang¹

¹Molecular Imaging Center, National Institute of Radiological Science, Chiba 263-8555, Japan;

²SHI Accelerator Service Co Ltd., Tokyo 141-8686, Japan

Objectives: Metabotropic glutamate receptor 5 (mGluR5) is characterized as a G protein coupled receptor and is known as one of regulators for excitatory neurotransmission, which is involved in central nervous system (CNS) disorders, such as fragile X syndrome, Parkinson's disease, and depression. Therefore, mGluR5 is an important target for development of new pharmaceuticals against these CNS disorders. Recently, 3-[5-(pyridine-2-yl)2H-tetrazol-2-yl]benzonitrile (**1**) has been reported as a potential compound for mGluR5 ($K_i = 190$ nM).^{1,2} In this study, we attempt to develop a novel PET ligand for mGluR5 using **1** as a lead compound.

Results and Discussions:

1. In vitro binding assay: Five new analogs of **1** were designed and synthesized (Figure 1). Their affinity for mGluR5 was estimated using a binding assay with the mGluR5-selective radioligand (*E*)-[¹¹C]ABP688 in rat brain homogenate. Of these analogs, compounds **2a** and **2b** showed relatively high affinity (**2a**: $K_i = 10.8$ nM; **2b**: $K_i = 9.4$ nM) for mGluR5.

2. Radiochemistry: [¹¹C]**2a** and [¹¹C]**2b** were synthesized by reacting desmethyl or arylstannyl precursor with [¹¹C]CH₃I. Starting from 14.8–22.2 GBq [¹¹C]CO₂, 0.58–0.91 GBq [¹¹C]**2a** was produced with $14 \pm 4\%$ ($n = 3$) radiochemical yield at 32 min after the end of bombardment

(EOB). Starting from 22.2–28.1 GBq [¹¹C]CO₂, 0.86–2.99 GBq [¹¹C]**2b** was acquired with $25 \pm 14\%$ ($n = 11$) radiochemical yield at 32 min after EOB. In the final product solution, the specific activity of [¹¹C]**2a** and [¹¹C]**2b** was 57–71 and 52–190 GBq/μmol, respectively. Radiochemical purity of both ligands was higher than 98% at the end of synthesis.

3. In vitro Autoradiography: In vitro autoradiography with [¹¹C]**2a** or [¹¹C]**2b** was performed using rat brain sections. In the control sections, distribution pattern of both radioligands was heterogeneously exhibited, which corresponded with the biological localization of mGluR5. In blocking study, co-incubation with mGluR5-selective MPEP (1.0 μM) dramatically diminished the accumulations of

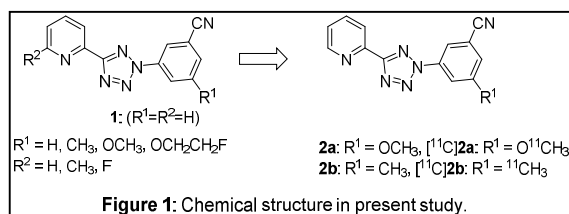
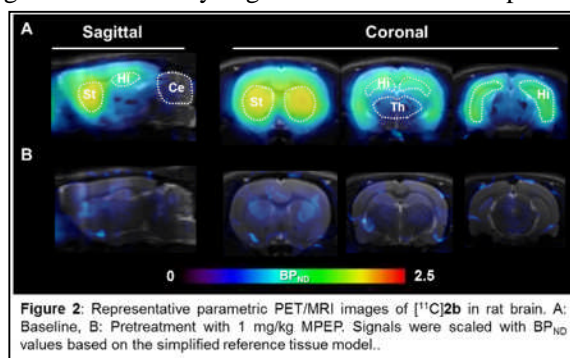


Figure 1: Chemical structure in present study.

radioactivity. The specific binding of [^{11}C]**2b** was slightly higher than that of [^{11}C]**2a**. Therefore, we decided to perform further evaluation of [^{11}C]**2b** using PET assessment.

4. Small-animal PET study: In control rats, the uptake of [^{11}C]**2b** immediately reached maximum levels in the brain regions after injection and quickly decreased after that. The uptake ratio of each region against cerebellum, a reference region for mGluR5, under the equilibrium state was 3.0 ± 0.1 in the striatum, 2.4 ± 0.1 in the hippocampus, 2.3 ± 0.1 in the frontal cortex, and 2.0 ± 0.1 in the thalamus, respectively. By treatment with MPEP, these ratio reduced by 1.3–1.6 in each brain region. As shown in Figure 2, the parametric PET images could identify regional differences in specific binding to mGluR5, demonstrating that PET with [^{11}C]**2b** could provide significant signal for mGluR5 in brain regions.

Conclusions: We have found out compound **2b** as a promising PET ligand candidate for mGluR5 by in vitro binding assay and subsequently synthesized [^{11}C]**2b**. PET study with [^{11}C]**2b** in rat brain was possible to visualize regional distribution of mGluR5. [^{11}C]**2b** is a potential PET ligand for imaging of mGluR5 in brain.



References:

- 1) *J. Med. Chem.* **2004**, 47, 4645–4648, 2) *Bioorg. Med. Chem. Lett.* **2005**, 15, 5061–5064

SMALL-ANIMAL PET STUDY: [¹¹C]ITMM WITH ULTRA-HIGH SPECIFIC ACTIVITY IMPROVED AVAILABILITY FOR METABOTROPIC GLUTAMATE RECEPTOR SUBTYPE 1 (mGluR1)

T. Yamasaki^{1,*}, M. Fujinaga¹, J. Yui¹, H. Wakizaka¹, T. Ohya¹, N. Nengaki^{1,2}, M.-R. Zhang¹

¹Molecular Imaging Center, National Institute of Radiological Sciences, Chiba 263-8555, Japan;

²SHI Accelerator Service Co Ltd., Tokyo 141-8686, Japan.

Objectives: Metabotropic glutamate receptor subtype 1 (mGluR1) is a crucial target in the developments of new pharmaceuticals to treat central nervous system (CNS) disorders, such as Parkinson's disease, stroke, and epilepsy. We recently developed *N*-[4-[6-(isopropylamino)pyrimidin-4-yl]-1,3-thiazol-2-yl-4-[¹¹C]methoxy-*N*-methylbenzamide ([¹¹C]ITMM) as a potential PET probe for mGluR1 imaging. The aim of this study was to improve visualization and specific binding for mGluR1 using [¹¹C]ITMM with ultra-high specific activity (SA) in small-animal PET studies.

Results and Discussion:

1. Radiosynthesis of [¹¹C]ITMM: Radiosynthesis for [¹¹C]ITMM, with either conventional or ultra-high SA, was performed by reacting a phenol precursor with [¹¹C]CH₃I.

For the conventional SA, 1.4–2.8 GBq of [¹¹C]ITMM was produced with $27 \pm 5\%$ radiochemical yield at 27 ± 3 min after the end of bombardment (EOB) starting from 14–20 GBq of [¹¹C]CO₂. The radiochemical purity was higher than 99% and SA was 121 ± 17 GBq/μmol at the end of synthesis (EOS).

For the ultra-high SA, [¹¹C]CH₃I was obtained using the single-pass I₂ method by iodination of [¹¹C]CH₄ which was formed in the target chamber in situ. Starting from 27 GBq of [¹¹C]CH₄, 0.7–1.5 GBq of [¹¹C]ITMM was acquired with $6 \pm 1\%$ radiochemical yield within 32 min from EOB. The radio chemical purity was higher than 99% and SA was $5,794 \pm 1,022$ GBq/μmol at EOS.

2. Small-animal PET study: Amount of nonradioactive carrier contained in [¹¹C]ITDM with conventional or ultra-high SA was 513.1 ± 58.7 or 10.9 ± 1.6 pmol in the injected solutions for PET studies. In PET images of rat brain with [¹¹C]ITMM of either conventional and ultra-high SA, the highest radioactive accumulation was seen in the cerebellum and the moderates were detected in the thalamus, hippocampus, striatum, and cingulate cortex. The maximum uptake of radioactivity of [¹¹C]ITMM with the conventional and ultra-high SA was 3.0 and 3.4 in the cerebellum, 2.3 and 1.6 in

the thalamus, 2.0 and 2.2 in the hippocampus, 2.1 and 2.4 in the striatum, and 2.0 and 2.3 SUV in the cingulate cortex, respectively.

To ensure kinetic analysis in PET study, estimations of the equilibrium state of [^{11}C]ITMM with conventional and ultra-high SA in each brain region of interest were obtained using plasma input function and averaged tissue time-activity curves (tTAC). The estimated equilibrium times of [^{11}C]ITMM with conventional and ultra-high SA were 150 and 150 for the cerebellum, 120 and 140 for the thalamus, 120 and 130 for the hippocampus, 120 and 130 for the striatum, and 100 and 120 min for the cingulate cortex, respectively. The uptake of [^{11}C]ITMM with either conventional and ultra-high SA reached at more than 85% of equilibrium state during PET scanning for 90 min.

Taken together, uptake of [^{11}C]ITMM with ultra-high SA increased overall compared to the conventional SA, which reached at estimated equilibrium state 90 min after PET scan started.

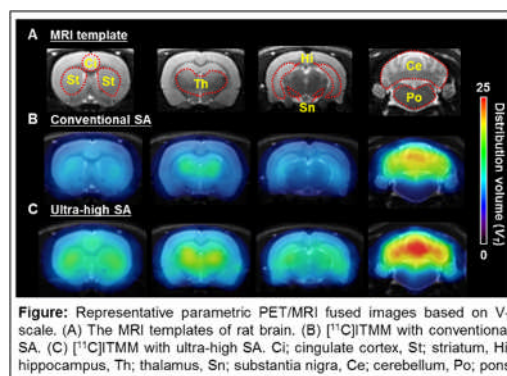
3. Kinetic analysis: Kinetic analysis of [^{11}C]ITMM was performed by two-tissue compartment model using plasma input and tTACs. Comparing kinetic parameters between the two SAs, there were no differences in K_1 of any brain regions. Meanwhile, k_2 and k_3 rate constants in the ultra-high SA tended to be faster compared with conventional SA. On the other hand, k_4 rate constant in ultra-high SA was slower than in the conventional SA. Correspondingly, distribution volume (V_T) and nondisplacable binding potential (BP_{ND}) in the ultra-high SA condition were higher than in the conventional SA.

The parametric images according to V_T scale for [^{11}C]ITMM with the ultra-high SA could be more visualize in mGluR1-rich regions than with the conventional SA and were also possible to identify in mGluR1-poor region, such as substantia nigra.

Conclusions: [^{11}C]ITMM with ultra-high SA demonstrated

improvement of specific binding for mGluR1 in brain regions. Hence, in vivo monitoring of mGluR1 by PET using [^{11}C]ITMM with ultra-high SA would help further understanding about CNS disorders involved in slight changes of not only mGluR1-rich but also mGluR1-poor regions.

Reference: Yamasaki T., et al. *PLoS ONE* 10: e0130006 (2015).



Development of a PET tracer for imaging of redox status in the brain

T. Okamura, M. Okada, T. Kikuchi, H. Wakizaka and MR. Zhang.

Molecular Imaging Center, National Institute of Radiological Sciences, 4-9-1 Anagawa, Inage-ku,
Chiba 263-8555, Japan.

Objectives

Reactive oxygen species (ROS) function as important signaling molecules at moderate concentrations, whereas high concentrations of ROS cause the disruption of redox homeostasis. This has been implicated in the pathogenesis of several brain diseases. *In vivo* imaging of brain redox status would therefore be useful for elucidating pathologic conditions and aiding in diagnoses of brain diseases. However, little has been reported on PET tracers for imaging of brain redox status. Here, we report the development of a PET tracer for redox status.¹

Figure 1 shows our approach for imaging of brain redox status. A lipophilic tracer (reduced form) enters the brain across the blood–brain barrier (BBB) after intravenous injection. A portion of the tracer is oxidized to a hydrophilic metabolite (oxidized form) depending on brain redox status, while the rest diffuses back into the blood. The metabolite is trapped or eliminated slowly because of its hydrophilicity. Hence, the brain radioactivity increases when oxidative stress occurs. By contrast, enhancement of antioxidant defense systems or inhibition of oxidases involved in oxidative stress results in the decrease in brain radioactivity. In this study, we designed a ¹¹C-labeled dihydroquinoline derivative (¹¹C]Q_{red}) and evaluated as a PET tracer for imaging of redox status in the brain.

Results and Discussion

The stability of [¹¹C]Q_{red} was examined in phosphate-buffered saline and mouse brain homogenate. The PET tracer [¹¹C]Q_{red} was stable in phosphate buffered saline; however, it was rapidly converted to its oxidized form ([¹¹C]Q_{oxi}) in the mouse brain homogenate. To confirm whether [¹¹C]Q_{red} can respond to the alteration of redox status, we employed diphenyleneiodonium and apocynin to modulate redox status and examined their effect on the oxidation of [¹¹C]Q_{red}. Diphenyleneiodonium and apocynin significantly decreased the initial velocity of [¹¹C]Q_{red} oxidation. Moreover, apocynin (0.01 to 10 mmol/L) caused the reduction of the initial velocity in a concentration dependent fashion. Thus, [¹¹C]Q_{red} was found to respond to the changes of redox status in mouse brain homogenate.

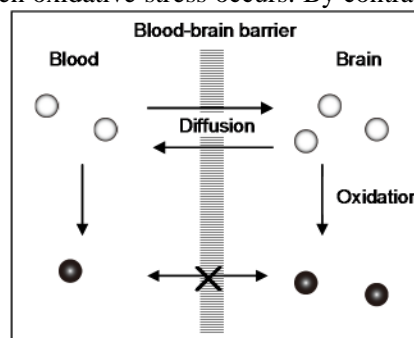


Figure 1. ○: a lipophilic tracer (reduced form)
●: a hydrophilic metabolite (oxidized form)

For imaging of brain redox status by the metabolic trapping, the reduced form [^{11}C] Q_{red} in blood must enter the brain across the BBB, whereas the oxidized form [^{11}C] Q_{oxi} in blood should not. The BBB permeability of [^{11}C] Q_{red} and [^{11}C] Q_{oxi} was examined by PET. The PET tracer [^{11}C] Q_{red} exhibited high uptake in the brain 1 min after administration, whereas the brain radioactivity of hydrophilic [^{11}C] Q_{oxi} was much lower than that of [^{11}C] Q_{red} for 60 minutes. The result indicates that [^{11}C] Q_{red} can readily diffuse into the brain but [^{11}C] Q_{oxi} formed in peripheral tissues cannot enter the brain from blood.

We investigated whether [^{11}C] Q_{red} can respond to the brain redox status altered by apocynin *in vivo*. Radioactivity in the brain of control mice reached a maximum level after injection of [^{11}C] Q_{red} and then slowly decreased, whereas the apocynin treatment caused a rapid decrease in brain radioactivity compared with control mice. We also analyzed the chemical form of radioactive compounds in the brain after intravenous administration of [^{11}C] Q_{red} . The reduced form [^{11}C] Q_{red} disappeared from the brain tissue of control mice, and the main radioactive compound in the brain was the oxidized form [^{11}C] Q_{oxi} . By contrast, [^{11}C] Q_{red} remained largely intact in the brain of the apocynin-treated mice. The rapid clearance of radioactivity for the apocynin group would therefore be due to the inhibition of the oxidation of [^{11}C] Q_{red} to hydrophilic [^{11}C] Q_{oxi} in the brain followed by the rapid diffusion of lipophilic [^{11}C] Q_{red} out of the brain. Thus, the difference in the [^{11}C] Q_{red} kinetics reflects the change in redox status caused by apocynin.

Conclusion

This study shows that [^{11}C] Q_{red} is a potential PET tracer for imaging of redox status in the living brain, and this tracer might be useful for studying the relationship between the development or pathogenesis of brain diseases and redox status.

Reference

1. T. Okamura et al. *J Cereb Blood Flow Metab* 2015; in press

Proposal of (*R*)-[¹¹C]Emopamil as a novel tracer for imaging enhanced P-glycoprotein function

J. Toyohara^{1,*}, H. Aramaki², Y. Zaitzu², M. Okamoto^{1,3}, S. Hosokawa², I. Shimizu²,
K. Ishiwata¹

¹Research Team for Neuroimaging, Tokyo Metropolitan Institute of Gerontology, Tokyo 173-0015, Japan; ²School of Advanced Science and Engineering, Waseda University, Tokyo 169-8555, Japan;

³Research Institute for Science and Engineering, Waseda University, Tokyo 169-8555, Japan.

Objectives: A number of substrate for P-glycoprotein (P-gp), such as [¹¹C]Verapamil, was developed for imaging P-gp function with positron emission tomography (PET). These substrates can measure decreased function of P-gp as an increased uptake of tissue radioactivity. However, this method would be unlikely to be able to measure enhanced P-gp function, because base-line tissue radioactivity is already below the limit of detection. 2-Isopropyl-5-[methyl-(2-phenylethyl)amino]-2-phenylpentanenitrile (Emopamil) is a calcium channel blocker of the phenylalkylamine class, having high blood-brain barrier (BBB) permeability and weak substrate for P-gp. These properties would be suitable for measuring enhanced P-gp function in the brain. The purpose of this study is to synthesize (*R*)- and (*S*)-[¹¹C]Emopamil and characterize their properties as P-gp tracers.

Materials and Methods: The Emopamil includes a chiral quaternary carbon centre, and a previous research has indicated that the optical isomers differ significantly in their biological effects. Therefore, we first synthesized (*R*)- and (*S*)-[¹¹C]Emopamil and compared their biodistribution, peripheral metabolism, and effects of P-gp inhibitor cyclosporine A (CsA). Then, we compared the brain pharmacokinetics of (*R*)-[¹¹C]Emopamil and (*R*)-[¹¹C]Verapamil in base line and CsA pre-treatment with small animal PET.

Results and discussion: (*R*)- and (*S*)-[¹¹C]Emopamil were synthesized from (*R*)- and (*S*)-Noremopamil, respectively, by methylation with [¹¹C]methyl triflate in the presence of NaOH at room temperature. The yield of (*R*)- and (*S*)-[¹¹C]Emopamil was approximately 30%. The specific activity of (*R*)- and (*S*)-[¹¹C]Emopamil was >74 GBq/μmol and radiochemical purity was >99%. The biodistribution of (*R*)- and (*S*)-[¹¹C]Emopamil in ddY mice demonstrated a significantly higher uptake

of (*R*)-[¹¹C]Emopamil in the brain. The regional brain distribution of (*R*)- and (*S*)-[¹¹C]Emopamil was homogeneous and non-stereoselective. (*R*)- and (*S*)-[¹¹C]Emopamil were rapidly metabolized to hydrophilic metabolite. Unchanged form of (*S*)-[¹¹C]Emopamil (39%) was significantly lower than that of (*R*)-[¹¹C]Emopamil (46%) at 15 min after injection in plasma. In contrast, >88% of radioactivity in the brain was intact and non-stereoselective. CsA pre-treatment increased brain activity approximately 3-fold, however, non-stereoselective. Since (*R*)-[¹¹C]Emopamil was metabolized less than that of (*S*)-[¹¹C]Emopamil, (*R*)-enantiomer was further evaluated with small animal PET in Wistar rats. The base line area-under-the-curve (AUC) of brain radioactivity (0–60 min) of (*R*)-[¹¹C]Emopamil was 2-fold higher than that of (*R*)-[¹¹C]Verapamil, but its AUC after CsA pre-treatment was comparable to that of CsA pre-treated (*R*)-[¹¹C]Verapamil.

Conclusions: (*R*)-[¹¹C]Emopamil is definitely a substrate for P-gp efflux at the BBB. (*R*)-[¹¹C]Emopamil has properties superior to those of the compound with a similar structure, (*R*)-[¹¹C]Verapamil, because the former shows double the baseline brain uptake, which may allow functional imaging of up-regulation of P-gp with PET.

References: Toyohara J, et al. *Nucl Med Biol* (2015), doi: 10.1016/j.nucmedbio.2015.09.001

Development of 1-*N*-[¹¹C]-Methyl-L- and -D-Tryptophan for Pharmacokinetic Imaging of the Immune Checkpoint Inhibitor 1-Methyl-Tryptophan

L. Xie ¹, J. Maeda ¹, K. Kumata ¹, J. Yui ¹, Y. Zhang ¹, A. Hatori¹, N. Nengaki ^{1,2},

H. Wakizaka ¹, M. Fujinaga ¹, M.-R Zhang ¹

¹Molecular Imaging Center, National Institute of Radiological Sciences, Chiba 263-8555, Japan;

²SHI Accelerator Service Co Ltd., Tokyo 141-8686, Japan.

Objectives: 1-Methyl-tryptophan (1MTrp) is known as a specific inhibitor targeting the immune-checkpoint protein indoleamine-2,3-dioxygenase, in two stereoisomers of levorotary (L) and dextrorotary (D) (1). A long-standing debate exists in immunology and oncology: which stereoisomer has the potential of antitumor immunotherapy (2). As a first step to disentangle the potential and explore the possibility of pharmacokinetic imaging in immunotherapy, we here developed two novel radioprobes, 1-*N*-[¹¹C]methyl-L- and -D-tryptophan ([¹¹C]L-1MTrp and [¹¹C]D-1-MTrp), without modifying the chemical structures of the two isomers, and delineated their pharmacokinetic imaging in whole body.

Methods: [¹¹C]L-1MTrp and [¹¹C]D-1MTrp were synthesized by reaction of the corresponding Boc-Trp-OEt with [¹¹C]CH₃I at 80 °C for 5 min, followed by deprotection with 2 N HCl at 100 °C for 5 min. The pharmacokinetics of the L and D isomers were tracked using dynamic PET/CT scans and biodistribution study after the radioprobes injection.

Results: [¹¹C]L-1MTrp and [¹¹C]D-1MTrp were obtained with radiochemical yields of 47 ± 6.3% (decay-corrected, based on [¹¹C]CO₂), a radiochemical purity of > 98%, specific activity of 47–130 GBq/μmol, and high enantiomeric purity. PET/CT imaging in rats revealed that for [¹¹C]L-1MTrp, the highest distribution of radioactivity was observed in the pancreas, while for [¹¹C]D-1MTrp, it was observed in the kidney (Fig. 1). *Ex vivo* biodistribution confirmed the PET/CT results, indicating the differences in pharmacokinetics between the two isomers.

Conclusion: Both [^{11}C]L-1MTrp and [^{11}C]D-1MTrp are therefore useful PET probes for delineating the distribution and action of the checkpoint inhibitor 1MTrp *in vivo*. This study represents the first step toward using whole-body and real-time insight to disentangle the antitumor potential of the two stereoisomers of 1MTrp, and it can facilitate the development of 1MTrp immunotherapy.

References: 1). Uyttenhove C, et al. *Nat Med.* **9**: 1269-1274 (2003).

2). Lob S, et al. *Blood.* **111**: 2152-2154 (2008).

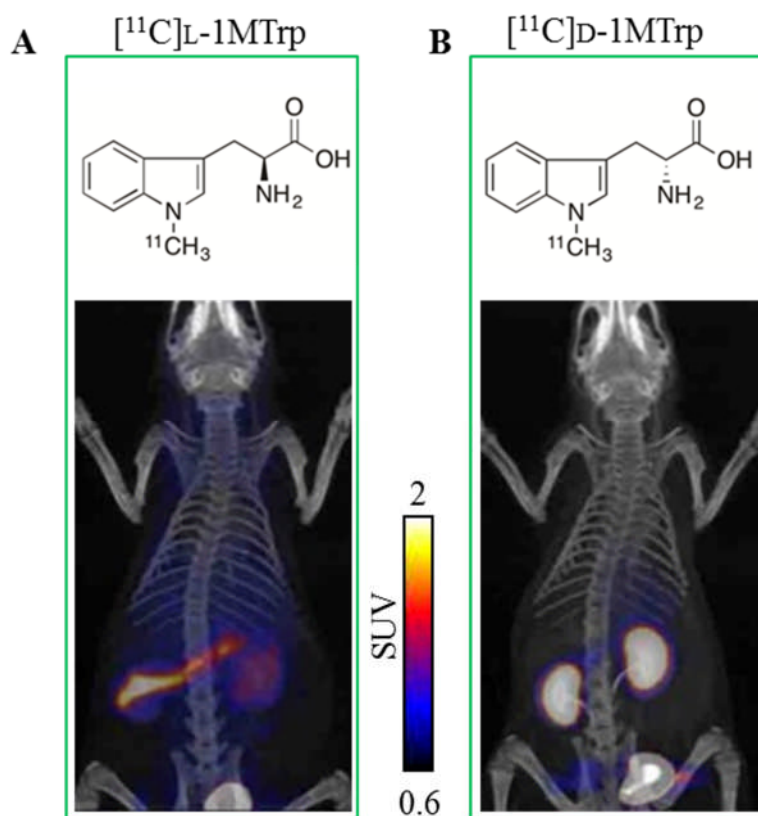


Figure 1. (A) Chemical scheme and representative pharmacokinetic images of [^{11}C] L-1MTrp (B) Chemical scheme and representative pharmacokinetic images of [^{11}C]D-1MTrp.

IN VIVO, IN VITRO, AND IN SILICO EVALUATION OF RADIOMETABOLITE OF [¹¹C]PBB3 AS A CLINICALLY USEFUL PET PROBE FOR IMAGING OF TAU PATHOLOGY.

H. Hashimoto¹, K. Kawamura^{1*}, M. Takei¹, N. Igarashi^{1,2}, T. Fujishiro^{1,2}, S. Shiomi^{1,2}, R. Watanabe^{1,2}, M. Muto^{1,2}, K. Furutsuka^{1,3}, T. Ito^{1,3}, T. Yamasaki¹, J. Yui¹, K. Nemoto¹, Y. Kimura¹, M. Higuchi¹, M.-R. Zhang¹

¹Molecular Imaging Center, National Institute of Radiological Sciences, Chiba 263-8555, Japan;

²Tokyo Nuclear Services Co., Ltd., Tokyo 110-0016, Japan; ³SHI Accelerator Service Ltd., Tokyo 141-0032, Japan.

Objectives: 2-((1*E*,3*E*)-4-(6-(¹¹C-methylamino)pyridin-3-yl)buta-1,3-dienyl)

benzo[*d*]thiazol-6-ol ([¹¹C]PBB3, Fig. 1) is a clinically useful PET probe for *in vivo* imaging of tau pathology in the brain. For the pharmacokinetic evaluation of [¹¹C]PBB3, it is important to elucidate the characteristics of radiometabolites. In this study, we evaluated radiometabolite after injection of [¹¹C]PBB3 in mice brain and plasma, identified the chemical structure of a major radiometabolite of [¹¹C]PBB3, and proposed the metabolic pathway of [¹¹C]PBB3.

Methods: [¹¹C]PBB3 was synthesized by reaction of the tert-butyldimethylsilyl desmethyl precursor with [¹¹C]methyl iodide using potassium hydroxide as a base, followed by deprotection. [¹¹C]PBB3 or carrier-added [¹¹C]PBB3 was injected into a mouse for *in vivo* metabolite analysis. The chemical structure of a major radiometabolite was identified using radio-HPLC and LC-MS. Mouse and human liver microsomes and liver S9 samples were incubated with [¹¹C]PBB3 *in vitro*, and its radiometabolite was analyzed using radio-HPLC. *In silico* prediction software was used to assist in the determination of the metabolite and metabolic pathway of [¹¹C]PBB3.

Results and discussion: In *in vivo* metabolite study, more than 70% of total radioactivity in the mouse brain homogenate at 5 min after injection represented the parent [¹¹C]PBB3, despite its rapid metabolism in the plasma. Also, *in vivo* metabolite study using carrier-added [¹¹C]PBB3 showed that the molecular weight of a major radiometabolite of [¹¹C]PBB3, which was called as [¹¹C]M2 (Fig. 1), was *m/z* 390 [*M*+*H*⁺]. *In vitro* metabolite study assisted by *in silico* prediction showed that [¹¹C]M2, which was not generated by cytochrome P450 enzymes (CYPs), was generated by sulfated conjugation mediated by a sulfotransferase. Our data demonstrated that [¹¹C]PBB3 was mainly metabolized to [¹¹C]M2 by sulfate conjugation mediated by sulfotransferases, and a minor radiometabolite, [¹¹C]M1 (Fig. 1), was yielded through oxidation mediated by CYPs. These results suggest that [¹¹C]M2 may be retained in the plasma, recirculated throughout the whole body, and may gradually enter the brain notwithstanding its relatively high polarity.

Conclusion: [¹¹C]PBB3 was rapidly decomposed to a polar radiolabeled metabolite in the plasma. The major radiometabolite, [¹¹C]M2, was identified as a sulfated conjugate of [¹¹C]PBB3. [¹¹C]PBB3 was metabolized mainly by a sulfotransferase and subsidiary by CYPs.

References: 1) Maruyama M, et al. *Neuron* 79:1094–108 (2013). 2) Hashimoto H, et al. *J Nucl Med* 55:1532–8 (2014). 3) Hashimoto H, et al. *Nucl Med Biol* (doi: 10.1016/j.nucmedbio.2015.08.006) in press.

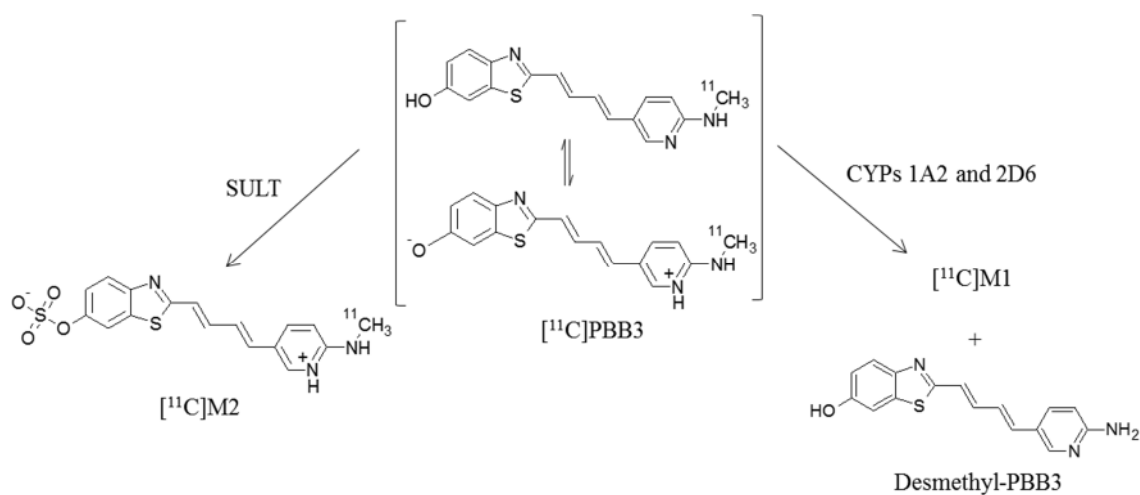


Fig. 1. Predicted major metabolic pathways for $[^{11}\text{C}]$ PBB3 and chemical structures of metabolites (SULT = sulfotransferase)

THE PRIMARY RESEARCH AND DEVELOPMENT OF IODINE-125 BRACHYTHERAPY SEEDS STRAND

Wen-Hui Zhang

HTA Co.,Ltd, P. O. Box 275(39), Beijing 102413, China

Objectives: It is reported that radioactive brachytherapy seed is an effective therapy since it is invented. However, there are some shortcomings of loose seeds therapy such as complexity of operation procedure, migrating or missing individual seed. Seed strand, which is combination of individual seeds with biocompatible materials, is designed for a simple seed implantation procedure, more stable location of individual seed and more reasonable radioactive dosage. This study uses the method of mold molding and sodium alginate as main moulding material, the seed strand manufacturing process parameters were optimized, the samples were tested and degraded in vitro.

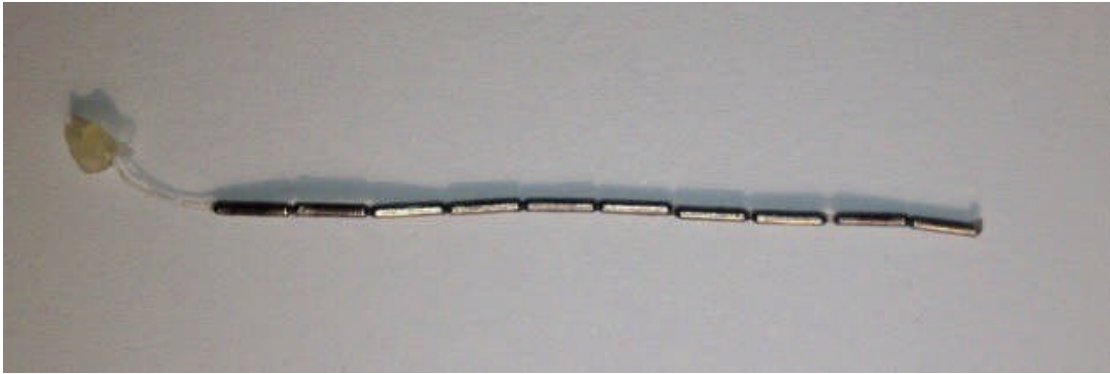
Results and discussion:

The optimized parameters of seed strand manufacturing process: Total concentration of sodium alginate is 5% (w/v). Among the mixed sodium alginate, the ratio of high viscosity vs super low viscosity is 1:15(w:w). The concentration of glycerol as plasticizer is 1% (w/v). The concentration of calcium ion in curing solution is 1%(w/v). The curing time is 4 hours. The temperature of drying is 50°C, Drying time is 2 hours.

Evaluation of the samples: The samples are line shaped well and mechanical stable after long time storage (one month), sterilization (100°C) for 1 hour and radioactive irradiation from itself. The samples are softened rapidly after immerge into physiological saline. The degradation time of the sample in physiological saline is about 60 days, and the degradation time change little after sealed storage (one month) or high temperature sterilization (100°C), but the radioactive irradiation from itself accelerate the degradation time of the samples slightly (degradation time is 50 days).

Conclusions:

The seed strand samples manufactured in this study are promising product for clinic usage.



References: 1) Daniel R. Reed, et al. Merrick. Brachytherapy, 2007, 6:129-134. 2) Wenhui Zhang, et al. Chinese patent publication number: CN103736201A. 3) Wenhui Zhang, et al. Chinese patent publication number: CN103736200A.

PREPARATION AND PRELIMINARY BIODISTRIBUTION OF NO-CARRIER-ADDED [^{125}I]MIBG

C.-Y. Fan, X.-R. Deng, Z.-H. Liu, F.-L. Li, B.-J. Chen, Z.-F. Luo*

(Department of Isotope, China Institute of Atomic Energy, Beijing, 102413, China)

Objective: Radioiodinated MIBG have been widely used as diagnostic agents for oncology, cardiology and PD, or as targeted radiotherapeutics for neuroendocrine tumors. Commercial carrier-added (c.a.) [$^{123/131}\text{I}$]MIBG have several disadvantages due to its low SA. There has been much interest in the preparation of high SA no-carrier-added (n.c.a.) [$^{123/131}\text{I}$]MIBG and its potential advantages over c.a. [$^{123/131}\text{I}$]MIBG in the last 20 years. A method without having to resort to HPLC would allow its wider application in clinic. The aim of this study was to prepare [^{125}I]MIBG and evaluate the effect of SA to tissue uptake. In the present study, we used a fluorous supported compound as the precursor for radioiodination. Then the biodistribution of n.c.a. [^{125}I]MIBG and c.a. [^{125}I]MIBG in normal mice were compared.

Results and Discussion:

1. Preparation of n.c.a. [^{125}I]MIBG:

The fluorous supported precursor (compound 1) for radioiodination was synthesized according to the literature with chemical purity of > 98%. This compound was radioiodinated by iodogen as the oxidant. The labeling yield was above 80% for ^{125}I . After purification with a fluorous solid phase extraction cartridge, n.c.a. [^{125}I]MIBG was obtained with radiochemical purity of > 95% and SA of 81.4 GBq/ μmol . The radiochemical yield was about 80%.

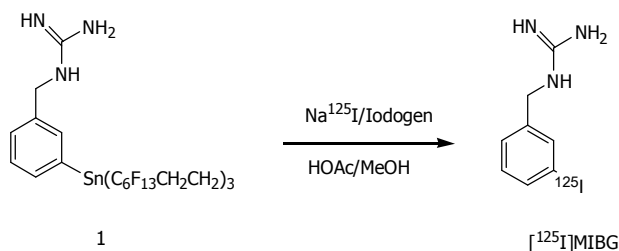


Figure 1 Preparation of n.c.a. [^{125}I]MIBG

The advantage of this method was that no HPLC was needed during the purification of the radiolabelled mixture. Thus preparation of n.c.a. [^{125}I]MIBG on a large scale for clinical application would be possible.

2. Biodistribution in normal mice:

Preliminary biodistribution of n.c.a. [^{125}I]MIBG and c.a. [^{125}I]MIBG in normal mice were performed to evaluate the effect of SA to tissue accumulation. The uptake of high SA n.c.a. [^{125}I]MIBG were significantly higher than that of low SA c.a.[^{125}I]MIBG in heart, spleen, lung and adrenals ($P < 0.05$). The heart/lung and heart/ liver ratios were also significantly higher for n.c.a.[^{125}I]MIBG (1.7-fold and 1.9-fold, respectively).

This showed that the high SA of n.c.a. [^{125}I]MIBG improved target accumulation and target/background ratio. When radiolabeled with ^{123}I or ^{131}I , theoretically, n.c.a. [^{123}I]MIBG could improve image quality, and n.c.a. [^{131}I]MIBG could enhance therapeutic effect as well as avoid the side effects of c.a. [^{131}I]MIBG.

Conclusions: The high SA of n.c.a. [^{125}I]MIBG contributed to target uptake and target/background ratio. After further evaluation of safety and effect, n.c.a.[$^{123/131}\text{I}$]MIBG may play an important role in the diagnostic or therapy of oncology, cardiology and PD.

Reference: Donovan A., et al. Nuclear Medicine and Biology 35:741-746 (2008).

PREPARATION OF [¹³¹I]-1H12 AND ITS BIOLOGICAL EFFECTS ON A549 NON-SMALL CELL LUNG CANCER

Minghua DU, MD

The Affiliated Hospital of Nanjing University of Traditional Chinese Medicine

No.155 Hanzhong Road, Nanjing, Jiangsu , CHINA 210029.

Objective:

- 1 Isotopic labeling: investigate the experimental conditions of radionuclide iodine [¹³¹I]labeling epidermal growth factor receptor (EGFR) monoclonal antibody (McAb) 1H12.
- 2 In vitro: observe the cell-binding function and biological effects of [¹³¹I]-1H12 to A549 human lung cancer cells.
- 3 In vivo: investigate the effectiveness and feasibility of ¹³¹I-epidermal growth factor receptor(EGFR) McAb on the proliferation of a heterologous graft in nude mice bearing A549 human lung cancer.

Methods:

- 1 Isotopic labeling: 1H12 was labeled with iodine [¹³¹I] by IODO-GEN method, its separation and purification was done by SephadexG-50 chromatography and its radiochemical purity was determined by NS paper chromatography.
- 2 In vitro: The immune competence of [¹³¹I]-1H12 was analyzed by cell-binding test. The cell apoptosis and cell cycles of A549 was analyzed by flow cytometry assay with various doses of [¹³¹I]-1H12(148, 74, 37kBq), free [¹³¹I] (148kBq), 1H12(80nmol/ml)and equivalent medium.
- 3 In vivo: A549 human lung cancer xenografts with positive EGFR expression were established in nude mice. 36 mice were randomly chosen and divided into 6 groups: high dose group(14.8MBq[¹³¹I]-1H12), medium dose group (7.4MBq[¹³¹I]-1H12), low dose group (3.7MBq[¹³¹I]-1H12) simple nuclides group (7.4MBq [¹³¹I]), simple McAb group (0.4ml 1H12), blank control group, for radioimmunotherapy studies. The tumor growth inhibition rate was determined by measurement of tumor volume; the side effects of [¹³¹I]-1H12 to normal tissue and organs was also observed. [¹³¹I]-1H12 uptakes in tumors would be detected by SPECT during treatment.

Results:

1 Isotopic labeling: The labeling rate of [^{131}I]-1H12 was 50.14%, its specific activity, radioactive concentration and radiochemical purity were 4.63MBq/ μg , 77.31MBq/ml and

96.92% separately.

2 In vitro: The specific binding rate of [^{131}I]-1H12 to A549 cells was 59.12%; The apoptosis rate and cycle blockage rate of A549 cell induced by [^{131}I]-1H12 were in a dose-effect relationship; The supreme apoptosis rate (44.35 ± 3.31)% and G2/M cell cycle blockage rate (51.17 ± 2.98)% were found in the A549 cells treated with 148kBq [^{131}I]-1H12.

3 In vivo: There was remarkable significant difference of tumor volumes at 32th day between high dose group, 7.4MBq group, 3.7MBq group and blank control group. The tumor growth inhibition rate of high dose group is 14.89%, medium dose is 20.14%, low dose group is 39.58%, simple nuclides group is 76.32%, simple McAb group is 88.76%, and blank control group is 99.73%. Compared with the blank control group, each radioimmunotherapy group remarkably suppressed the growth of tumor ($P < 0.01$). Irreversible destruction of tissues in radioimmunotherapy groups was observed under light microscope. There was no evidence of hepatotoxicity, renal toxicity and myelotoxicity in nude mice bearing A549 human lung cancer given [^{131}I]-1H12 over a 4wk observation period; SPECT imaging showed tumor could uptake [^{131}I]-1H12 well during treatment.

Conclusion:

1 Isotopic labeling: We successfully completed the labeling experiment, the method was simple and the compound was stable.

2 In vitro: [^{131}I]-1H12 can immunobinding with A549 cells and regulate cell cycle and induce apoptosis of A549 cells to inhibit its proliferation.

3 In vivo: [^{131}I]-1H12 has obvious dose-dependent anti-tumor effects on a heterologous graft in nude mice bearing A549 human lung cancer, with little obvious side effects. It might have some potential application prospect in biological targeted diagnosis and therapeutics.

Key words: non small cell lung cancer (NSCLC); epidermal growth factor (EGFR); radioimmunotherapy; isotopic labeling; monoclonal antibody (Mab)

Folic acid-conjugated BSA nanocapsule (n-BSA-FA) for cancer targeted radiotherapy and imaging

Yufei Ma, Sheng Liang, Jun Guo, Hui Wang*

Department of Nuclear Medicine, Xinhua Hospital, School of Medicine, Shanghai Jiaotong University, 1665 Kongjiang Rd., Shanghai 200092, China

Background:

The therapeutic efficiency of any agent highly depends on its adequate local delivery to the tumor site. Therefore, target-selective drug delivery with high efficiency, low toxicity and minimal side effects has been developed to improve the efficacy of radio-therapeutics. Capitalizing on recent achievements in the area of nanotechnology and nuclear medicine, we sought to develop a radiolabeled nano-drug that accumulated in tumors via tumor-selective targeted delivery system and treat the tumors with radionuclide.

Methods:

In this paper, we designed and synthesized a nano-capsule n-BSA-FA, and we radio-labelled it by $^{125/131}\text{I}$ using Iodogen method. Then we evaluated $^{125/131}\text{I}$ - n-BSA-FA using nuclear medical technology to test if it is potential as an imaging or therapy drug.

Results:

The successful construction was proved by agarose gel (figure1) .

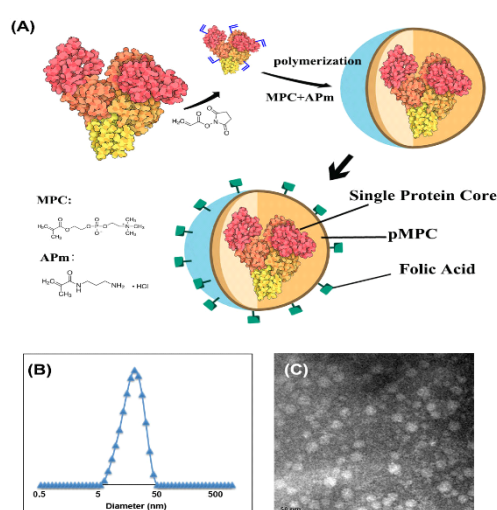


Figure 1. Cartoon illustration of n-BSA-FA. A) Synthesis route and structure sketch of n-BSA-FA B) hydrodynamic diameter of n-BSA-FA of around 20nm from DLS C) Transmission electron micrograph of n-BSA-FA with uniformed size distribution, negatively dyed by PTA

THE ESTABLISHMENT OF STERILE EXAMINATION METHODS FOR TECHNETIUM [^{99m}Tc] ALBUMIN AGGREGATED (^{99m}Tc -MAA) INJECTION

Jing-Jing Yu^{1, 2}, Jian-Dong Du¹, Xian Zhang¹, Hai-ping Cui^{1, 2,*}

¹ Atom High Tech Co. Ltd., Beijing 102413, China; ² China Institute of Atomic Energy, Beijing
102413, China

Objective: To establish the method of sterility test for Technetium [^{99m}Tc] Albumin Aggregated (^{99m}Tc -MAA) Injection, a sterility test of ^{99m}Tc -MAA was carried out using the technique of direct inoculation, and the validation test was accomplished according to Chinese pharmacopoeia (2010 edition). We validate the sterility test method of ^{99m}Tc -MAA sample that treats with direct inoculation procedure, which includes inhibition test for bacteria and fungi. It was illustrated that the establishment of sterility test must be reassured with validation test through bacteria solution, examination of culture medium, estimation of appropriate inoculation, and selection of positive control germs.

Results and Discussion:

1. We used direct inoculation method to control the bacteria in the sterility test for ^{99m}Tc -MAA injection. The inoculation dose was 0.2 mL per tube. All of positive strains and test strains revealed growth of microorganism, and the substance control and negative control gave no evidence of growth. The recovery rate was more than 90%.
2. ^{99m}Tc -MAA has a property of radioactivity. As the membrane filtration technique is unsuitable, the direct inoculation method under test for sterility of the product to be examined is introduced to reduce the radioactive waste and protect human health.
3. The content of microorganism test should be improved step by step, so that the general level of microorganism test in China could be elevated.

Conclusion: The method could be used to test for sterility test. The antimicrobial activity of ^{99m}Tc -MAA is able to remove through direct inoculation. The method is simple with less inoculation of radioactivity relatively. It is a suitable method for the sterility test of ^{99m}Tc -MAA injection.

References: 1) MA Shi-hong. Chin J Pharm Anal 27(6): 877-880(2007). 2) ChP. 2010. Vol: Appendix XI H.

Evaluation of the diagnostic value of 99mTc-MIBI SPECT positive tumor imaging and MRI in the recurrence or postoperative residual lesions of glioma

Weixiao Zhang, Yajie Liu*

Department of Nuclear Medicine, The Second Affiliated Hospital of Nanjing Medical University,
Nanjing, Jiangsu 210011, China

Objective: Gliomas are the most common of these, and comprise 1.35% of all cancers in the USA. One of the most difficult clinical dilemmas in the management of patients with glioma is the identification of tumor recurrence in patients who have undergone prior surgical resection and radiation therapy. Furthermore, an accurate diagnosis is crucial for patient management because therapy and prognosis are different for these lesions. Functional nuclear neuroimaging by positron emission tomography (PET) and single photon emission computed tomography (SPECT) have been applied to discriminate radiation necrosis from recurrent tumor over the last several decades. FDG-PET is limited by the high uptake of glucose in the normal brain cortex. Furthermore, PET imaging is relatively expensive and not widely available. Therefore brain SPECT has been proposed as a feasible alternative imaging technique. The main objective of this study was to evaluate the value of 99mTc-MIBI SPECT positive tumor imaging and MRI in the diagnosis of recurrence and postoperative residual of glioma.

Methods and Results:

1. Patients' characteristics : A total number of 30 patients (14 women and 16 men; median age of 49.2 years, range 35-69 years) were enrolled in this study. According to the Daumas-Dupont classification these patients had 13 grade II, 8 grade III and 7 grade IV. 23 patients were initially treated with surgery and radiotherapy, 5 with radiotherapy alone, and 2 with radiotherapy and concomitant chemotherapy. The study was approved by the ethics committee of the second Affiliated Hospital of Nanjing Medical University, and informed written consent was obtained from all the patients.

2. 99mTc-MIBI SPECT positive tumor imaging: Using MIBI started 30min after intravenous injection of 740 MBq of MIBI. MIBI preparation and quality control were according to the manufacturer's instructions. The SPECT scans were performed from the thorax to the pelvis. A dual-head γ camera (Infinia Hawkeye; GE Healthcare, Chalfont St. Giles, UK) equipped with a crystal 3/8ths of an inch thick and a low-energy, high-resolution collimator was used to acquire SPET/CT. The Dicom image files of each patient were saved in optic discs and transferred to a Xeleris 2.0 workstation (GE healthcare) for centralized reconstruction, reading and analysis.

3. MRI imaging: Written informed consent of the MR procedure was obtained from each patient. Imaging was performed at 1.5-T whole-body MR system (Magnetom SP 4000; Siemens, Erlangen, Germany). Contrast-enhanced T1-weighted (T1-Gd) and T2-weighted MRI were used to monitor the patients. All of the images were acquired with 4-mm slices, two signal averages, and a 22x16-cm field of view. T2-weighted MRI were acquired with a 256x128 matrix, TR=3000 ms, and TE=19/95 ms. T1-weighted MRIs were acquired with a 256x128 matrix, TR=500 ms, and TE=14.5 ms.

4. Results: Recurrences were identified in 21 out of the 30 patients (prevalence 70.0%), with altogether 26 lesions. All the lesions were confirmed by histopathological findings or clinical follow-up. The sensitivity of ^{99m}Tc -MIBI SPECT positive tumor imaging (80.1%) was lower than MRI (90.5%), While the specificity (88.9%) was much higher than MRI (77.8%). The accuracy between the two imaging has no significant difference. The sensitivity, specificity and accuracy were 95.2%、100%、93.3% when the two imaging methods combined. The result and the diagnosis value of ^{99m}Tc -MIBI SPECT positive tumor imaging and MRI of these patients are lined out in Table 1 and Table 2.

Table 1 The result of ^{99m}Tc -MIBI SPECT positive tumor imaging and MRI

Group	n	SPECT		MRI	
		Isotope concentration	No isotope concentration	Tumor	Non Tumor
postoperative residual	6	4	2	5	1
recurrence	15	13	2	14	1
No residual nor recurrence	9	1	8	2	7

Table 2 The diagnosis value of ^{99m}Tc -MIBI SPECT positive tumor imaging and MRI

Methods	Sensitivity (%)	Specificity (%)	Accuracy (%)
SPECT	80.1	88.9	80.6
MRI	90.5	77.8	86.7
Combined	95.2	100	93.3

Conclusions: ^{99m}Tc -MIBI brain SPECT is a non-invasive investigation technique available for routine clinical monitoring. It is sensitive and specific for the diagnosis of recurrence brain glioma. It is particularly useful to detect recurrence early, allowing timely adaptation of treatment. For these patients ^{99m}Tc -MIBI SPECT could be included in the follow-up with the neurological examination and neuromorphology imaging generally performed. The combination of ^{99m}Tc -MIBI SPECT positive tumor imaging and MRI has great clinical significance.

References:

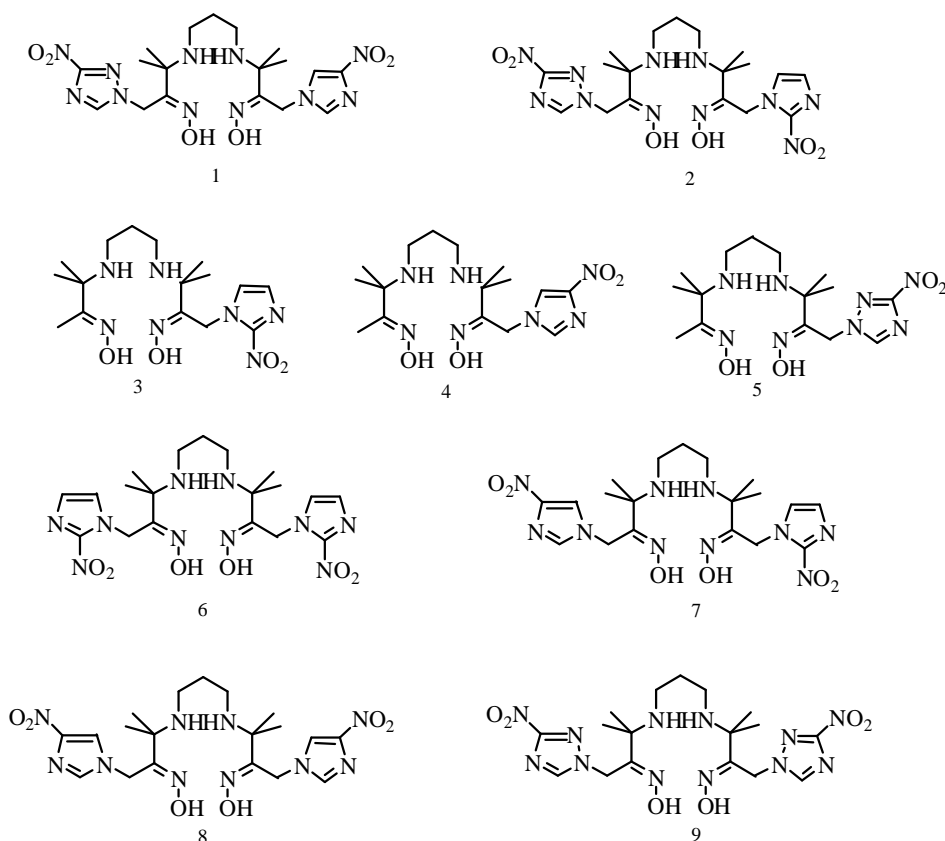
- [1] Kumar S, Arbab AS, Jain R, et al. Development of a novel animal model to differentiate radiation necrosis from tumor recurrence. *J Neurooncol.* 2012, 108(3):411-420.
- [2] Xu Cheng, Yongjun Li, Zhaoqiang Xu, Dianfu Li, Jie Wang. A meta-analysis of ^{99m}Tc -MIBI SPECT for detection of recurrent glioma after radiation therapy. *J Clin Neurosci.* 2011, 18(3):307-312.

IN VITRO AND IN VIVO EVALUATION OF TECHNETIUM-99M-LABELED PROPYLENE AMINE OXIME COMPLEXES CONTAINING NITROIMIDAZOLE AND NITROTRIAZOLE GROUPS AS HYPOXIA MARKERS

Q. Zhang, H.-F. Huang, T.-W. Chu*

Beijing National Laboratory for Molecular Sciences, Radiochemistry and Radiation Chemistry Key
Laboratory of Fundamental Science, College of Chemistry and Molecular Engineering, Peking
University, Beijing 100871, P. R. China

Objectives: Hypoxia markers have been the subject of intensive research in radiopharmaceuticals, but there is little work on markers with multi-redox centers. It is necessary to further develop and investigate the compounds containing multi-redox centers systematically. Thus two propylene amine oxime ligands, compound 1, containing 3-nitro-1,2,4-triazole and 4-nitroimidazole and compound 2, containing 3-nitro-1,2,4-triazole and 2-nitroimidazole were synthesized and radiolabeled with ^{99m}Tc , then these complexes were also evaluated in vitro and in vivo. Some comparisons were made with the other complexes of our previous work and some interesting conclusions were obtained.



Scheme 1. Chemical structures of PnAO compounds 1 and 2 and some similar compounds.

Results and Discussion:

1. In Vitro Experiments: *In vitro* experiments on ^{99m}Tc -1 and ^{99m}Tc -2 were carried out using murine sarcoma S180 cells. The difference between normoxic and hypoxic uptakes of ^{99m}Tc -1 and ^{99m}Tc -2 in S180 cells was significant. By comparing with other PnAO complexes containing one or two redox centers, the number and type of redox centers were found to play an important role. Firstly, for the complexes with one redox center, the highest to lowest hypoxic cellular uptake was 3-nitro-1,2,4-triazole > 2-nitroimidazole >> 4-nitroimidazole. Secondly, for the complexes with two redox centers, the effect of second redox center on hypoxic cellular uptake was 2-nitroimidazole > 3-nitro-1,2,4-triazole >> 4-nitroimidazole. Thirdly, difference in the octanol/water partition coefficient did not significantly influence cellular uptake for the ^{99m}Tc -PnAO complexes studied.

Table 1. *In vitro* biological evaluation of PnAO complexes (4 h)

Complexes	1	2	3	4	5	6	7	8	9
RC	4NI& NT	2NI& NT	2NI	4NI	NT	2NI&2NI	2NI&4NI	4NI&4NI	NT&NT
Number	2	2	1	1	1	2	2	2	2
Log P _{o/w}	0.45	0.70	1.59	1.54	1.74	1.10	1.29	1.23	1.42
Max uptake	36.8±0.6%	40.2±1.6%	24.4±3.9%	-	33.7±0.2%	59.0±0.9%	30.8±0.4%	-	35.0±0.7%
hypoxic/ normoxic uptake ratio	3.3	6.6	4.3	-	5.6	8.7	4.2	-	7.5

The data of complexes 3, 4, 6, 7, 8 are cited from the literature [1]; the data of complexes 5, 9 are cited from the literature [2].

2. Biodistribution study: The results again reinforce the importance of the type of redox center, where the complexes containing 2-nitroimidazole had relatively higher tumor uptake than their analogues. The partition coefficient also had an obvious influence on biodistribution result. The lower lipophilicity of ^{99m}Tc -1 and ^{99m}Tc -2 means lower uptake in the blood, lower background and higher T/B.

Table 2. The biodistribution of ^{99m}Tc -PnAO complexes in mice bearing S180 tumor (4 h)

Complexes	1	2	3	5	6	7	9
Tumor uptake (% ID/g)	0.48±0.14	0.74±0.13	0.75±0.16	0.35±0.03	0.86±0.22	0.38±0.16	0.25±0.06
T/B	2.24±0.81	1.71±0.41	0.62±0.43	0.39±0.19	0.81±0.34	0.83±0.13	0.31±0.08
T/M	4.22±0.62	2.78±1.05	4.15±1.17	3.79±0.59	3.24±0.65	2.05±0.37	4.58±0.76

The data of complexes 5, 9 are cited from the literature [2]

Conclusion: These complexes held moderate tumor-to-blood and tumor-to-muscle ratios, indicating they might serve as novel hypoxia markers. Some comparisons showed the *in vitro* evaluation may be connected with the number and the type of the redox centers and the biodistribution experiments may have relation with the hydrophilicity and the type of redox centers.

References: Huang H.F., et al. 1) Bioorg Med Chem Lett 2012; 22: 172-7. 2) Molecules 2012; 17: 6808-20.

EVIDENCE-BASED RADIONUCLIDE AND RADIOPHARMACEUTICAL APPROACHES OF FLOW PERFUSION IN HOLLOW-FIBER DIALYZERS.

Bimali Sanjeevani Weerakoon^{a,b}, Toshiaki Osuga^c

^aGraduate School of Advanced Integration Science, Chiba University, 1-33 Yayoi, Inage, Chiba, 263-8522, Japan., ^bDepartment of Radiography/Radiotherapy, Faculty of Allied Health Sciences, University of Peradeniya, Sri Lanka., ^cCenter for Frontier Medical Engineering, Chiba University, Yayoi, Inage, Chiba 263-8522, Japan.

Objective: The importance of optimum flow perfusion in an artificial kidney or hollow fiber dialyzer has long been a concern. Studying the functional behaviour of these hollow fiber dialyzers by means of functional imaging techniques is significant to develop these modules. Because of this various imaging techniques have been proposed using radionuclide and radiopharmaceutical agents. This article reviews the recent application of radionuclide and radiopharmaceutical agents for evaluating flow perfusion in hollow fiber dialyzers.

Results and Discussion: Scintigraphic images can provide information on radionuclide distribution in dialyzers that provides a useful tool in the evaluation of its functional status. In this review, both in vitro and in vivo experiments to evaluate the dialyzer performance are considered. Prediction of ultrafiltration rate in hollow fiber dialyzers was successfully possible with the application of a radioactive substance. In this, in vitro technique, the analysis of changes in the concentration of non-diffusible microaggregates albumin labelled with radioactive Technetium (Tc-99m) (5 mCi/1000ml) was recorded with a Gamma camera. This was considered to be more precise technique than the other methods, especially for the highly permeable dialyzers. The other interesting aspect of this method is the possibility of accurate measurement of the amount of backfiltration that couldn't be possible with simple calculations.

In vivo experiments on dialyzer performance are generally less compared to in vitro measurements. However, with the application of radiopharmaceutical into the blood of the hemodialysis patients, the dialyzer performance can be assessed indirectly. A continuous measurement of Tc-99m (150 to 200 mBq) with diethyltriaminepentaacetic acid (DTPA) and chromium-51-ethylenediaminetetraacetic acid (Cr-51-EDTA) (2 mBq) blood concentration was performed on patients undergoing routine hemodialysis in vivo. Here, the blood Tc-99m-DTPA activity was continuously monitored by a sodium iodide scintillation detector with promising results.

The verification of the performance of the pixel basis renal functional radionuclide image (RFRI) algorithm was performed with the Gamma camera renography system after a bolus input of 2 mCi/500ml Tc-99m into a dialyzer. In this process, the Tc-99m was filtered out from the blood while it was flowing through the hollow fibre, due to the negative pressure caused by the dialysate pressure pump. However, in this method, Tc-99m was not labelled with DTPA pharmaceutical because the molecular weight of Tc-99m DTPA radiopharmaceutical was greater than the size of the pores in the dialyser membrane.

Positron emission tomography (PET) were implemented as a non-invasive tool to evaluate the injected radioactive nuclide, 18-fluoro-deoxy-glucose (18FDG) (2.57 mCi) into a fluid circuit having a hollow-fiber membrane in dialyzer based bioreactor.

Conclusion: These approaches suggest that radionuclide can be successfully utilized to evaluate the performance of the hollow fiber dialyzers. Furthermore, these were revealed that radionuclide studies are providing a useful platform not only in vitro experiments but also in vivo experiments of dialyzer performance. It is also important to note down, for most of the utilized radionuclides in dialyzer performance was Tc-99m, Cr-51-EDTA and 18FDG. These radionuclides can be used in the evaluation process with or without application of a pharmaceutical. When applying the radiopharmaceutical, the pore size of the membrane should be taken into account and the molecular weight of the

radiopharmaceutical should be less than the pore size of the membrane. Another notable fact is Tc-99m-DTPA radiopharmaceutical can act as a useful agent in the continuous monitoring process of dialyzer function in vivo. This also provides the concept for the use of other radiopharmaceuticals of different molecular sizes which can be employed in an analogous fashion.

Reference: Ronco, Claudio, et al. A new scintigraphic method to characterize ultrafiltration in hollow fiber dialyzers. *Kidney Int* **41.5** (1992): 1383-1393.

IMAGING OF OSTEOLYTIC METASTASIS FROM BREAST CANCER WITH NEW INTEGRIN $\alpha_v\beta_3$ RECEPTOR TARGETED RADIOTRACER:[^{68}Ga]-DOTA-RGD₂

G-Q. SHAO¹, C. CUI¹, X-C. YAO¹, R. LUO¹, Y. ZHOU², S. LIU², F. Wang^{1,*}

¹Department of Nuclear Medicine, Nanjing Medical University Affiliated Nanjing Hospital, Nanjing, 210006, China; ² Department of Pharmacy, Purdue University, West Lafayette, 47907, USA.

Objective: Osteolytic metastasis brings about significant morbidity of intractable pain, spinal cord compression, pathologic fracture. Early diagnosis is definitely important and difficult through commonly used imaging methods. Integrin $\alpha_v\beta_3$, highly expressed on breast cancer cells, osteoclasts and specifically combined with radiolabelled arginine-glycine-aspartic acid (RGD) peptides, had attracted great attention for positive imaging of osteolytic metastasis. The aim of this study is to investigate the value of integrin $\alpha_v\beta_3$ targeted microPET/CT imaging with ^{68}Ga -DOTA-RGD₂ as radiotracer for the detection of breast cancer osteolytic bone metastases. We prepared ^{68}Ga -DOTA-RGD₂ and established animal model with Parathyroid hormone (PTH)-induced osteolysis in the calvarium (BP group). Biodistribution study and microPET imaging were performed in BP groups. Breast cancer osteolytic metastases animal model was established and ^{68}Ga -DOTA-RGD₂ microPET/CT imaging were performed for the detection of breast cancer osteolytic metastases.

Results and Discussion:

1. Synthesis of ^{68}Ga -DOTA-RGD₂: ^{68}Ga -DOTA-RGD₂ was prepared via one step method by adding 1 mL of $^{68}\text{GaCl}_3$ solution (185-370 MBq) into DOTA-RGD₂ vial and incubated in water at 100°C for 20 minutes. It was stable in vitro and its radiopurity was as high as (96.4±2.1)% 3h after its preparation.
2. Biodistribution study: Animal model with Parathyroid hormone (PTH)-induced osteolysis in the calvarium (PTH group) was established for biodistribution studies of ^{68}Ga -DOTA-RGD₂. Animals with injection of same volume of saline instead of PTH was served as Control group. Blood elimination of ^{68}Ga -DOTA-RGD₂ was fast while its uptake by the liver and kidneys were relatively low. It was discharged soon after its intravenous injection. In the PTH group, regional uptake of ^{68}Ga -DOTA-RGD₂ in osteolytic lesion of calvarium (%ID/g) reached peak (5.14±0.65) 60min after tail vein injection. It was significantly more than that in Control group (2.06±0.35, $t=7.81$, $P<0.05$). Binding specificity of osteolytic lesion with ^{68}Ga -DOTA-RGD₂ was confirmed via integrin receptor block study (pre-injection of high dose of DOTA-RGD₂).
3. MicroPET-CT imaging of PTH induced osteolytic lesions: ^{68}Ga -DOTA-RGD₂ and ^{18}F -NaF MicroPET-CT imaging was performed and radiotracer uptake ratio of osteolytic lesion to normal calvarium (T/N) was calculated. Bone T/N of ^{68}Ga -DOTA-RGD₂ was (6.1±0.97), significantly

higher than that of ^{18}F -NaF (1.2 ± 0.33 , $t=10.17$, $P < 0.05$). ^{18}F -NaF was mainly used for osteoblastic metastasis imaging with high diagnostic value than $^{99\text{m}}\text{Tc}$ -MDP and usually demonstrated "Cold area" in osteolytic metastasis. Osteolytic lesions, consisting of a great number of osteoblasts which are highly expressed integrin $\alpha_v\beta_3$ receptor, accumulated ^{68}Ga -DOTA-RGD₂ and displayed "hot area" on microPET-CT imaging. ^{68}Ga -DOTA-RGD₂ MicroPET-CT imaging offers one potential method for positive imaging of osteolytic lesions.

4. MicroPET-CT imaging of breast cancer osteolytic metastasis: Animal model with breast cancer osteolytic metastasis was established via intracardiac injection of breast cancer cells (MDA-MB-231). ^{68}Ga -DOTA-RGD₂ microPET/CT imaging was able to demonstrate the osteolytic metastasis in calvarium, thoracic vertebrae and lung metastasis. They were confirmed by pathology results.

Conclusion: ^{68}Ga -DOTA-RGD₂, as a new integrin $\alpha_v\beta_3$ receptor targeting radiotracer, was potential for positive imaging and early detection of osteolytic lesion or breast cancer osteolytic bone metastasis.

DEVELOPMENT OF RADIOGALLIUM COMPLEX-CONJUGATED MULTIFUNCTIONAL PEPTIDES FOR IMAGING OF CANCER

Kazuma Ogawa^{1,2,*}, Atsushi Ishizaki¹, Masaru Yokokawa¹, Akira Odani¹

¹*Graduate School of Medical Sciences, Kanazawa University, Kanazawa, 920-1192 Japan;* ²*Institute for Frontier Science Initiative, Kanazawa University, Kanazawa, 920-1192 Japan.*

Objectives: ⁶⁸Ga ($T_{1/2}$ = 68 min, a generator-produced nuclide) is an interesting radionuclide for clinical positron emission tomography (PET) because ⁶⁸Ga is a generator-produced nuclide that can be eluted at any time on demand from an in-house generator; it does not require a cyclotron on site. We have reported that radiogallium-labeled 1,4,7,10-tetraazacyclododecane-1,4,7,10-tetraacetic acid (DOTA)-conjugated (Asp)_n peptide [Ga-DOTA-D_n] has great potential for bone metastases imaging. In this study, compounds containing aspartic acid peptides linker (D_n) (n = 8 or 11) as a carrier to bone metastases, an RGD peptide [c(RGDfK) peptide] as a carrier to the primary cancer, and Ga-DOTA as a stable radiometal complex for imaging in one molecule, Ga-DOTA-D_n-c(RGDfK) (n = 8 or 11), was designed, prepared, and evaluated to detect both the primary cancer and bone metastases simultaneously using ⁶⁷Ga, which is easy to handle.

Methods: After DOTA-D_n-c(RGDfK) (n = 0, 8 or 11) was synthesized using Fmoc-based solid-phase methodology, ⁶⁷Ga-DOTA-D_n-c(RGDfK) (n = 0, 8 or 11) was prepared by complexing DOTA-D_n-c(RGDfK) with ⁶⁷Ga. The $\alpha_v\beta_3$ integrin binding affinities of the Ga-DOTA complex-conjugated c(RGDfK) peptides were determined using purified human $\alpha_v\beta_3$ integrin in a competitive binding assay with ¹²⁵I-c(RGDfK), which was prepared by chloramine T method with c(RGDyK) peptide. *In vitro* hydroxyapatite binding assays and biodistribution experiments of ⁶⁷Ga-DOTA-D_n-c(RGDfK) (n = 0, 8 or 11) were performed. Single photon emission tomography (SPECT) imaging experiments using tumor-bearing mice after injection of ⁶⁷Ga-DOTA-D₁₁, ⁶⁷Ga-DOTA-c(RGDfK) and ⁶⁷Ga-DOTA-D₁₁-c(RGDfK) were performed.

Results: The overall yields of the gallium complexes precursors, DOTA-D₈-c(RGDfK), DOTA-D₁₁-c(RGDfK), and DOTA-c(RGDfK) were 2.3%, and 3.3%, and 6.5%, respectively. The radiochemical yields of ⁶⁷Ga-DOTA-D₈-c(RGDfK), ⁶⁷Ga-DOTA-D₁₁-c(RGDfK), and ⁶⁷Ga-DOTA-c(RGDfK) were 93.6%, 92.4%, and 90.0%, respectively. After purification using HPLC, the radiochemical purities were all >97%. Because Ga-DOTA-D_n-c(RGDfK) (n = 0, 8, or 11) and c(RGDfK) showed similar affinity for $\alpha_v\beta_3$ integrin, the Ga-DOTA complex and the aspartic acid peptide linker did not significantly impede the affinity of c(RGDfK) peptide for $\alpha_v\beta_3$ integrin. ⁶⁷Ga-

DOTA-D_n-c(RGDfK) (n = 8 or 11) highly bound to the hydroxyapatite. ⁶⁷Ga-DOTA-D₁₁-c(RGDfK), which possesses a longer aspartic acid peptide linker, exhibited a higher binding ratio to the hydroxyapatite than did ⁶⁷Ga-DOTA-D₈-c(RGDfK). The accumulation of ⁶⁷Ga-DOTA-D₁₁-c(RGDfK) in bone was significantly higher than that of ⁶⁷Ga-DOTA-D₈-c(RGDfK). ⁶⁷Ga-DOTA-c(RGDfK) did not accumulate in bone. ⁶⁷Ga-DOTA-D_n-c(RGDfK) (n = 0, 8, or 11) exhibited high uptake in tumor. The accumulation of ⁶⁷Ga-DOTA-D₁₁-c(RGDfK) in tumor decreased when it was co-injected with c(RGDfK) peptide. In SPECT images, ⁶⁷Ga-DOTA-D₁₁ exhibited a marked accumulation of radioactivity in bone. Very little accumulated radioactivity was observed in tissues other than bone. ⁶⁷Ga-DOTA-c(RGDfK) showed a high accumulation of radioactivity surrounding the site of tumor cell inoculation. ⁶⁷Ga-DOTA-D₁₁-c(RGDfK) exhibited high accumulation of radioactivity in both tumor and bone, which is consistent with the biodistribution experiments.

Conclusion: This study suggests that ⁶⁸Ga-DOTA-D₁₁-c(RGDfK), which contains ⁶⁸Ga instead of ⁶⁷Ga, has great potential as a PET tracer for the diagnosis of both the primary cancer and bone metastases simultaneously.

**Evaluation of *in vivo* dynamics of the polymeric micelle
by using two different radioisotope modification approaches**

Akira Makino^{1,2,*}, Ayaka Tomoike¹, Masahiro Ono¹, Yasushi Kiyono², Hidehiko Okazawa², Hideo Saji^{1,*}

¹ Department of Patho-Functional Bioanalysis, Graduate School of Pharmaceutical Sciences,
Kyoto University, Kyoto 606-8501, Japan; ² Biomedical Imaging Research Center (BIRC),
University of Fukui, Fukui 910-1193, Japan

Objectives: Application of the polymeric micelle as carriers for drug delivery systems (DDSs) is an active area of investigation. This is because polymeric micelle can encapsulate arbitrary hydrophobic compounds into the core region, and deliver them to targeted regions by various active or passive drug delivery methodologies. To elucidate *in vivo* dynamics of the micelle is therefore of utmost importance. However, *in vivo* dynamics of self-assembled polymeric materials are often complex, as both decomposition of the assembly and degradation of the constituent polymer occur in parallel, suggesting the need for novel characterization strategies.

Lactosome is a core-shell type polymeric micelle composed of the amphiphilic block polydepsipeptide poly(sarcosine)-*b*-poly(L-lactic acid) (poly(Sar)-*b*-PLLA). In this study, Lactosome was radiolabeled by two different methods, and their *in vivo* dynamics was discussed by comparison of the biodistribution data.

Results and Discussions: ¹²⁵I-labeled Lactosome (¹²⁵I-Lactosome) was prepared from a mixture of the amphiphilic polydepsipeptide and hydrophobic ¹²⁵I-labeled PLLA ([¹²⁵I]-IB-PLLA), while ³H-Lactosome was prepared from the amphiphilic polydepsipeptide [³H]-poly(Sar)-*b*-PLLA, whose poly(Sar) *N*-terminal end was directly radiolabeled with ³H. These two RI-labeled Lactosomes were intravenously injected to mice and their biodistribution was evaluated by organ harvesting method.

RI-labeled Lactosomes showed prolonged blood circulation behavior, which is a known characteristic of Lactosome (1, 2), and were found to accumulate in the liver and the spleen with 5–10% ID/g. However, soon after the administration, radioactivity of ^3H detected from blood plasma was lower than that of ^{125}I . These results suggest that an initial burst of Lactosome had occurred. After the initial burst, both RI-labeled Lactosomes were found to decompose with constant rates. Six hours after administration, Lactosome becomes unstable due to expulsion of the constituent polymer, and decomposition is accelerated. Additionally, levels of ^{125}I in all organs gradually decreased over time, while levels of ^3H remained stable for at least 48 h following injection.

Conclusions: Comparison of the biodistribution data allowed for precise evaluation of the *in vivo* dynamics of Lactosome, and revealed three distinct phases of Lactosome decomposition: 1) an initial burst phase soon after administration, in which part of the Lactosome is broken; 2) gradual collapse of the Lactosome during the first 6 h following administration; (3) accelerated decomposition. Moreover, the constituent amphiphilic polymer of Lactosome exhibits high retention characteristics upon accumulation at various organs.

References: 1) Yamamoto, F.; Yamahara, R.; Makino, A. et al. *Nucle. Med. Biol.* **2013**, *40*, 387-394.
2) Makino, A. et al. *Biomaterials* **2009**, *30*, 5156-5160.

Versatile Synthesis of *C*-Functionalized Polyaminocarboxylate Bifunctional Chelating Agent with Aromatic Carboxylate

H. Suzuki, A. Kanai, Y. Arano

Department of Molecular Imaging and Radiotherapy, Graduate School of Pharmaceutical Sciences,
Chiba University, Chiba, 260-8675, Japan

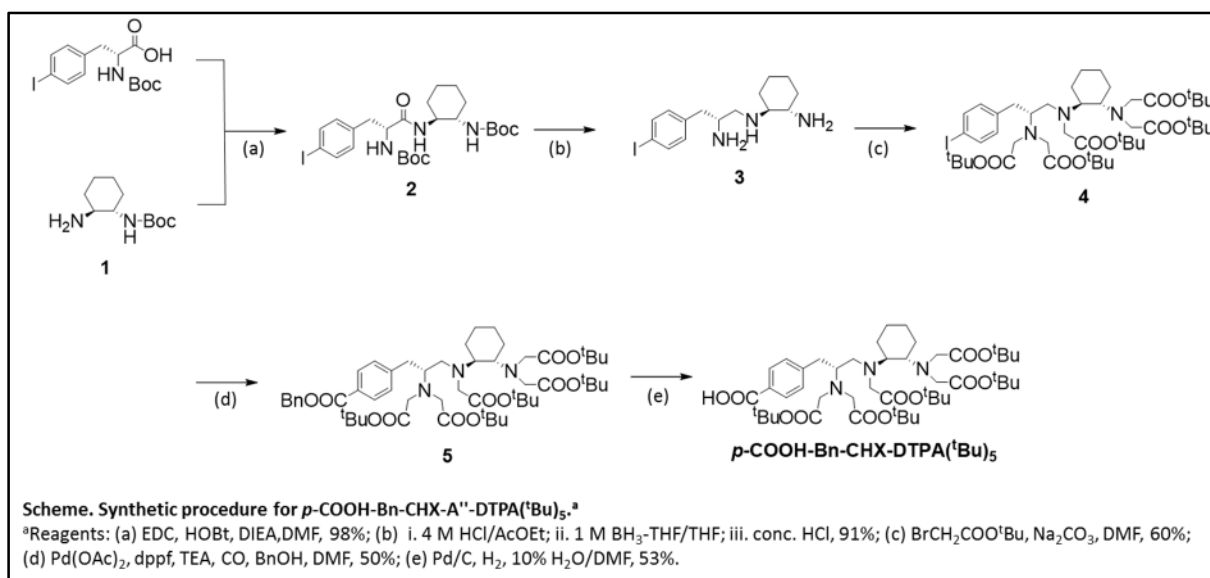
Objectives: The *C*-functionalized polyaminocarboxylate-based bifunctional chelating agents (BCAs) have an advantage over *N*-functionalized BCAs preserve for complexation reactions due to the preservation of their inherent chelating abilities. However, the biomolecule-coupling moieties of any *C*-functionalized polyaminocarboxylate-based BCAs are limited to amine or its derivatives, diazonium salt, isothiocyanate and bromoacetamide. In the course of our work on the reduction of hepatic or renal radioactivity levels of radiolabeled antibodies and their fragments, it was found that radiolabeled hippurate derivatives were preferentially excreted from the liver and kidney to urine when they were liberated from parental antibodies or their fragments in the organs.¹⁻³

The purpose of this study was to develop a general route to prepare *C*-functionalized polyaminocarboxylates with aromatic carboxylates. We selected cyclohexyl-DTPA derivative as the chelating moiety of choice, due to its ability to form inert metal complexes with a variety of metallic ions with rapid reaction kinetics and its well-established synthetic procedure.

Results and Discussion: The procedure employed for the synthesis of *p*-COOH-Bn-CHX-A"-DTPA(¹Bu)₅ is shown in the scheme. The compound **4** was synthesized according to the procedure of Clifford et al. using *p*-iodo-D-phenylalanine as the starting material.⁴ Briefly, the Boc-protected *p*-iodo-D-phenylalanine was condensed with Boc-protected (*S,S*)-1,2-cyclohexanediamine **1** to provide **2** in 98% yield. Deprotection of the Boc groups and subsequent reduction of the amides with BH₃-THF afforded **3** in about 91% yields. The backbone of Bn-CHX-A"-DTPA was then constructed by

alkylation of **3** with *tert*-butyl in 60% yields. The key compound **5** was obtained by palladium-catalyzed cross-coupling reaction of **4** in fair (50%) yields. After removing the benzyl group by the palladium-catalyzed hydrogenation, the final compound, *p*-COOH-Bn-CHX-A''-DTPA(¹Bu)₅, was obtained in overall yields of 14%. This compound is ready to use for solid-phase peptide synthesis. Since the present synthetic procedure involves the conversion of *p*-iodo group to *p*-carboxylate after construction of the backbone structure, this reaction would also be applicable to the synthesis of aromatic carboxylate derivatives of *C*-functionalized acyclic and cyclic polyaminocarboxylate compounds such as EDTA, DOTA and NOTA.

Conclusions: A synthetic procedure for preparing *p*-COOH-Bn-CHX-A''-DTPA(¹Bu)₅ was established. This compound would allow an additional molecular design to prepare radiolabeled antibodies and peptides of lower hepatic or renal radioactivity levels.



References: 1) *Nucl. Med. Biol.* **22**, 555-564 (1995). 2) *Cancer Res.* **59**, 128-134 (1999). 3) *Bioconjug Chem.* **18**, 190-198 (2007). 4) *J. Med. Chem.* **49**, 4297-4304 (2006).

Optically Pure Diphenoxy Derivatives as More Flexible Probes for β -Amyloid Plaques

Jianhua Jia, Mengchao Cui*, Boli Liu

Key Laboratory of Radiopharmaceuticals, Ministry of Education, Beijing Normal University, Beijing 100875, P. R. China

Objectives: The highly rigid and planar scaffold with π -conjugated systems has been widely considered to be indispensable for A β binding probes. However, our group recently reported a series of benzyloxybenzene derivatives with flexible structure as novel scaffold for the binding of A β plaques, and this new scaffold shared the same binding site with IMPY^[1]. In this study, two pairs of optically pure diphenoxy derivatives with a chiral center as novel A β binding probes were synthesized and evaluated (Figure 1).

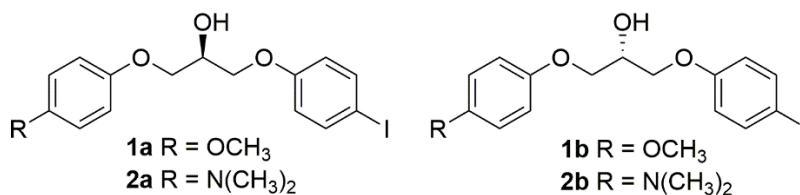


Figure 1. The structures of optically pure diphenoxy derivatives with a chiral center.

Methods: In vitro inhibition assay was carried out to evaluate the affinities of the two pairs of compounds for A β_{1-42} aggregates using [¹²⁵I]IMPY as the competing radioligand. Autoradiography in vitro on brain section of Tg mice (C57BL6, APP^{swe}/PSEN1, 22 months old, female) and AD patient (91 years old, male, temporal lobe) was performed to further confirm the high affinity of [¹²⁵I]**1a** and [¹²⁵I]**1b**. To study the biodistribution of different optical isomers [¹²⁵I]**1a** and [¹²⁵I]**1b**, the biodistribution experiment was implemented in normal mice (ICR, 5 weeks, male, n = 5).

Results: These compounds possessed high affinities that are comparable to or better than the affinity of IMPY, which implied these complexes also shared the same binding site with IMPY (Figure 2). Besides, [¹²⁵I]**1a** and [¹²⁵I]**1b** was successfully obtained with high radiochemical yield (RCY > 90% and RCP > 95%) and it could specifically label A β plaques on brain section of Tg mice and AD patient (Figure 2). In biodistribution experiment, [¹²⁵I]**1a** and [¹²⁵I]**1b** displayed no significant difference containing medium initial brain uptake (3.72 ± 0.31 and 4.37 ± 0.7 %ID/g, 2 min post-injection) and very fast clearance property ($\text{brain}_{2 \text{ min}}/\text{brain}_{60 \text{ min}} = 17.7$ and $\text{brain}_{2 \text{ min}}/\text{brain}_{60 \text{ min}} = 19.0$).

Conclusions: Two pairs of more flexible diphenoxy derivatives with a chiral center displayed high affinity for A β plaques. [^{125/123}I]**1a** and [^{125/123}I]**1b** could be potentially used as novel SPECT imaging agent for the detection of A β plaques in AD brains. Further studies of these radiolabeled probes were currently underway.

Acknowledgements: National Natural Science Foundation of China (No. 21201019).

References: [1] Yang Y, et al (2014) J Med Chem, 57, 6030–6042.

Corresponding Author: *Tel/Fax: +86-10-58808891. E-mail: cmc@bnu.edu.cn

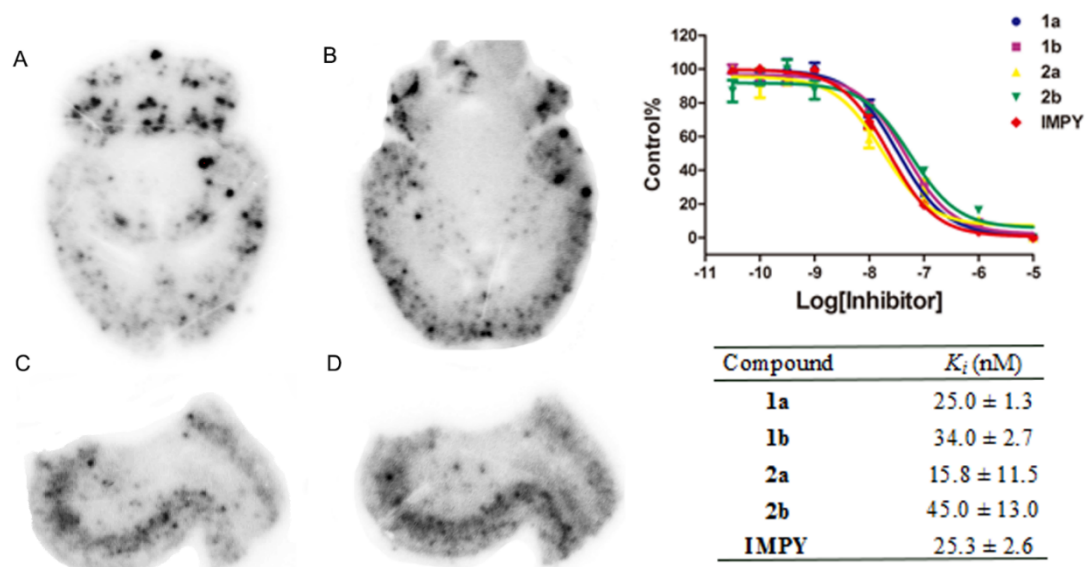


Figure 2. The ARG of $[^{125}\text{I}]\mathbf{1a}$ and $[^{125}\text{I}]\mathbf{1b}$ on brain sections of Tg mice (A, B) and AD patient (C, D); Inhibition data of **1a-2b** for the binding of $[^{125}\text{I}]\text{IMPY}$ to $\text{A}\beta_{1-42}$ aggregates.

Synthesis and evaluation of novel near-infrared probes with side PEG chains for in vivo detection of A β plaques

Kaixiang Zhou, Hualong Fu, Mengchao Cui*, Boli Liu

Key Laboratory of Radiopharmaceuticals, Ministry of Education, Beijing Normal University, Beijing 100875, P. R. China

Objectives: Recently, our group reported a series of smart A β probes for near-infrared (NIR) imaging based on the pull-push architecture with electron donating and withdrawing moieties bridged by the π -conjugated system consisting of polyenic chains. Among them, DANIR 2c^[1] and DANIR 3b^[2] displayed high affinity to A β aggregates and excellent *in vivo* NIR imaging in Tg mouse. However, these probes are restricted by high lipophilicity. In order to increase hydrophilicity, we have designed and synthesized a series of novel NIR probes containing different lengths of PEG chains in the electron withdrawing moieties.

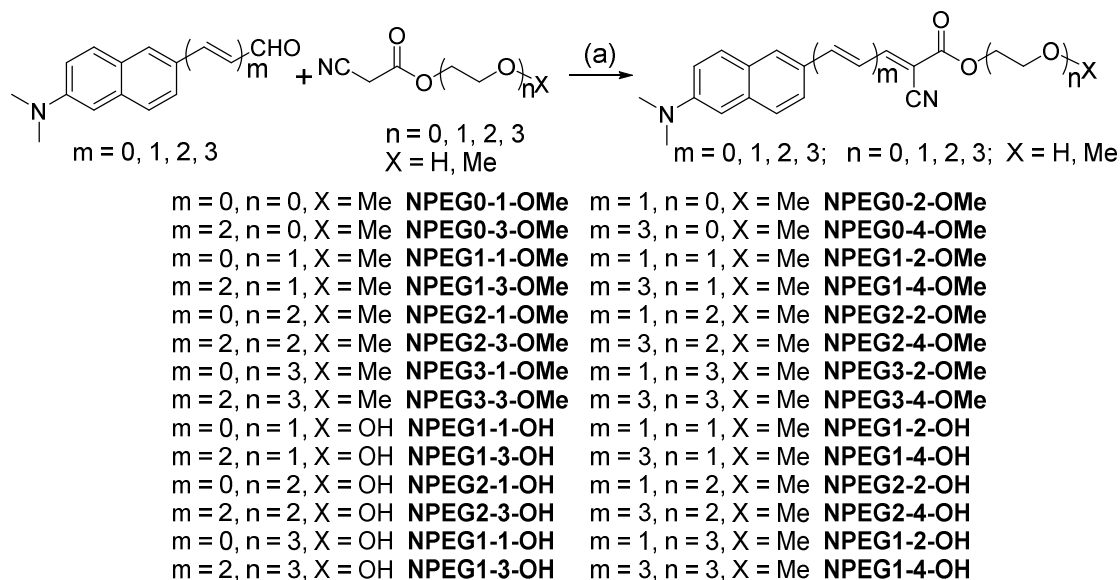


Figure 1. Synthesis of the designed NIR probes.

Methods: The chemical structures of the NIRFs were shown in Figure 1. First, the fluorescent properties, including fluorescent intensity, excitation and emission wavelength, upon interaction with A β aggregates or serum albumin in PBS were measured. *In vitro* neuropathological fluorescence staining was then performed on brain slices from Tg mice and AD patients to confirm the specific binding of these NIR probes to A β plaques. The quantification of the binding affinities of these NIRFs to A β aggregates was assessed by saturation binding assays. *In vivo* NIR imaging was performed in

Tg and age-matched WT mice. *Ex vivo* histology was conducted after *in vivo* imaging to confirm the binding of probes to A β plaques.

Results: Lengthening the polyenic chains leads to an obvious red shift of the emission maxima and apparent solvatochromism by increasing the polarity of solvent. Probes with longer polyenic chains ($n = 2, 3$) were successfully pushed into the NIR “window” in PBS (emission maxima > 650 nm) and displayed apparent fluorescence intensity increase and significant hypsochromic shift in the presence of A β_{1-42} aggregates. Distinctive staining of A β plaques was observed for all probes on sections from Tg mice and AD patients. High binding affinities of these probes were confirmed by saturation binding assay ($K_d < 50$ nM). Some probes could readily penetrate the blood-brain barrier with high initial brain uptake and fast to moderate washout from the brain. *In vivo* NIR imaging revealed that they could efficiently differentiate Tg and WT mice, and the presence and distribution of A β plaques in hippocampus, cortical and cerebellum regions were further confirmed by *ex vivo* histology.

Conclusions: In this study we reported on the design, synthesis, and assessment of an array of novel NIR A β plaque-specific fluorescence probes with PEG chains as NIR probe targeting A β plaques. Some of the probes displayed excellent fluorescent properties and high affinity to A β aggregates, which meets the prerequisites for noninvasively imaging A β plaques *in vivo*.

Acknowledgements: National Natural Science Foundation of China (No. 21201019).

References: [1] Cui M, et al (2014) J Am Chem Soc, 136 (9), 3388–3394.

[2] Fu H, et al (2015) J Med Chem, DOI: 10.1021/acs.jmedchem.5b00861. In press.

Corresponding Author: *Tel/Fax: +86-10-58808891. E-mail: cmc@bnu.edu.cn

Licochalcone A protect the heart from ischemia/reperfusion injury

W-H.GUO, P. JIA, X-F. FENG, S-L. XU, Z-J.JIA, J-T. SHEN, P. XU

Department of Nuclear Medicine Nanjing Drum Tower Hospital Affiliated to Nanjing University,
Nanjing, 210006, China

Objective: Myocardial ischemia (MI), which caused by a temporary lack of oxygen-rich blood to the heart, is a leading cause of high morbidity and mortality in the world. Myocardial ischemia (also known as angina) is a heart condition. Myocardial ischemia-reperfusion injuries in pathological disorders include reperfusion arrhythmias, transient mechanical dysfunction, myocardial stunning, and cell death. Oxidative stress caused by reactive oxygen species (ROS) has a considerable role in ischemia/reperfusion (I/R) injury, which impairs cardiac function. Licochalcone A, which belongs to the retrochalcone family, is isolated from the roots of Chinese licorice. Previous studies indicated that Licochalcone A have unique antioxidant properties and other pharmacological activities that may be relevant to protecting the heart from ischemia-reperfusion injury. Positron emission tomography (PET) imaging utilizing ^{18}F -FDG may provide a non-invasive means of evaluating the effect of treatment in MI. The aim of this study was to evaluate the cardioprotective effects of licochalcone A by microPET and TTC staining.

Results and Discussion: MI was induced in SD rats by the ligation of the left anterior descending (LAD) coronary artery. Rats were randomly assigned into five groups (n =5 per group): (1) control group, rats were treated with saline; (2) Diao xinxuekang capsules group (63mg/kg body weight); (3) Isosorbide Mononitrate group (3.2mg/kg); (4) Licochalcone A group (30mg/kg); (5) sham group (0.9% normal saline). All the rats were treated with drugs by oral administration for 7 days. Animals were then imaged using ^{18}F -FDG and a small-animal PET tomograph. Myocardial standard uptake values (MyoSUV) were systematically measured. At the end of experiment, the heart was excised and the infarct size was measured using 2,3, 5-triphenyltetrazolium chloride (TTC) staining to assess myocardial injury.

MicroPET results showed that the uptake of ^{18}F -FDG in the treatment groups was similar to those of the control group, with the radioactivity significantly lower than the sham group. The mean standard uptake value (SUV mean) in Isosorbide Mononitrate group and Licochalcone A group at 7 days post-injection was much higher than that in sham group ($p < 0.05$). After the treatment for seven days, SUV mean in day 7 in Diao xinxuekang capsules group, Isosorbide Mononitrate group and Licochalcone A group increased about 50% ($p < 0.05$). In addition, the infarct size decreased significantly ($p < 0.05$). Furthermore, TTC staining results were consistence with microPET results. Generally, both microPET and TTC results demonstrated that Licochalcone A protect the heart from ischemia/reperfusion (I/R) injury.

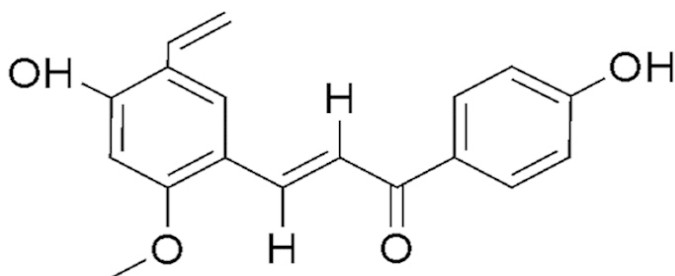


Fig 1 Chemical structure of licochalcone A

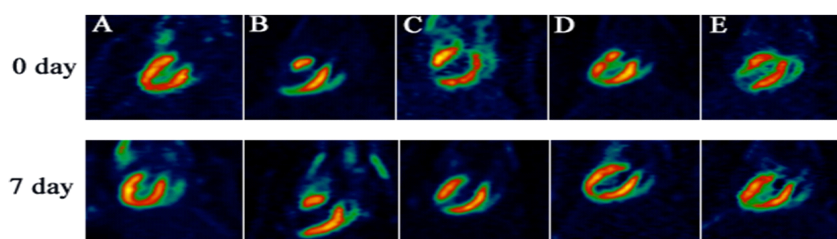


Fig 2 Licochalcone A protect the heart from ischemia/reperfusion injury by ^{18}F -FDG microPET. A. control; B. model; C. Diao Xinxuekang; D. Isosorbide Dinitrate; E. Licochalcone A

Table1. Infarct size of rats by Micro PET (Mean \pm SD, n=6)

Group	Dose (mg/kg)	Infarct size (%)	
		0day	7day
Control	---	---	---
Sham	---	24.64 \pm 1.06	25.04 \pm 1.12
Diao Xinxuekang	63	21.14 \pm 1.77	18.34 \pm 0.91
Isosorbide Dinitrate	3.2	24.70 \pm 2.07	17.60 \pm 2.19 ^{*##}
Licochalcone A	30	24.01 \pm 1.31	19.04 \pm 1.31 ^{*##}

^{*}P<0.05, ^{**} P<0.01 VS 0 day; [#]P<0.05, ^{##} P<0.01 VS sham

Conclusion:MicroPET and TTC staining results indicated that Licochalcone A exhibit cardioprotective effects during I/R injury. In this study, Diao Xinxuekang and Isosorbide Dinitrate were used as positive control. Licochalcone A may prevent production of oxidants, may inhibit oxidants from attacking cellular targets, may block propagation of oxidative reactions, and may reinforce cellular antioxidant capacity. The study clearly demonstrated that Licochalcone A protect the heart from ischemia/reperfusion injury.

Ninth Japan-China Joint Seminar on Radiopharmaceutical Chemistry

Date of Publishing: November 2015

Editing and Publication: Molecular Probe Program

Molecular Imaging Center

National Institute of Radiological Sciences

Anagawa 4-9-1, Inage-ku, Chiba, Japan 263-8555

Tel : +81-43-206-3709

Fax : +81-43-206-3261

E-mail : jcsrc@nirs.go.jp

Homepage : <http://www.nirs.go.jp>

Copyright ©2015 National Institute of Radiological Sciences
All Rights Reserved

Printed in Japan

NIRS-M-282